UC Berkeley
UC Berkeley Electronic Theses and Dissertations

Title
Fluidic Microvalve Digital Processors for Automated Biochemical Analysis

Permalink
https://escholarship.org/uc/item/3mg2x7gh

Author
Jensen, Erik Christian

Publication Date
2011

Peer reviewed|Thesis/dissertation

eScholarship.org Powered by the California Digital Library
University of California

Fluidic Microvalve Digital Processors for Automated Biochemical Analysis

by

Erik C. Jensen

A dissertation submitted in partial satisfaction of the

requirements for the degree of

Doctor of Philosophy

in

Biophysics

in the

GRADUATE DIVISION

of the

UNIVERSITY OF CALIFORNIA, BERKELEY

Committee in charge:

Professor Richard A. Mathies, Chair

Professor Lydia Sohn

Professor Jay Groves

Professor Bernhard Boser

Spring 2011

Fluidic Microvalve Digital Processors for Automated Biochemical Analysis

Copyright 2011

by

Erik C. Jensen

Abstract

Fluidic Microvalve Digital Processors for Automated Biochemical Analysis

by

Erik C. Jensen
Doctor of Philosophy in Biophysics
University of California, Berkeley
Professor Richard A. Mathies, Chair

The development of microfluidic sample processing and microvalve technology offers significant, thus far unmet opportunities for the miniaturization and large scale integration of automated laboratory systems. In this dissertation, the transistor-like nature of monolithic membrane valves for control of airflow and fluid flow is exploited to develop microfluidic processors for performing diverse bioassay procedures on a common programmable microchip format.

The transistor-nature of pneumatic microvalves is first exploited to fabricate devices that perform AND, OR, and NOT transistor-to-transistor logic operations. With this system, microvalves are used to control the actuation of other microvalves by regulating airflow. As a demonstration of computational universality, these operators are combined to perform more complex digital logic operations including binary addition. Integrated logical circuits such as demultiplexers and latching circuits are valuable because they reduce the power consumption and control equipment required for controlling large arrays of microvalves.

A digital microfluidic Automaton is demonstrated using 2-dimensional microvalve array technology. Digital transfer of fluids between microvalves enables precise and rapid metering of nanoliter scale sample volumes. Programs for reagent routing, mixing, rinsing, serial dilution, storage/retrieval and many other operations are demonstrated. Protocols for on-chip reagent mixing and serial dilution are optimized to achieve linearity over a 1000-fold dilution range. These optimized programs are combined to develop a rapid, quantitative assay for hydrogen peroxide, a biomarker of oxidative stress. A sub-micromolar limit of detection is demonstrated with an 8.5 min program runtime, thus establishing this platform as an effective tool for the miniaturization and automation of multi-step bioassays.

An extension of the Automaton platform to inhomogeneous immunoassays is presented. Capture antibody derivatized magnetic particles are utilized as a solid substrate. Effective procedures are developed for the transport, capture, rinsing, and delivery of reagents to magnetic particles in the digital microfluidic array. These procedures are used to demonstrate a model immunoassay for mouse IgG.

Automaton protocols are developed for processing and combinatorial mixing of a wide range of sample volumes. The ability to process large (μL scale) sample volumes enables the detection of low titer targets, and the modular coupling of the Automaton to a wide range of off-chip analytical detection instruments. The utility of these procedures is demonstrated for automated labeling of carboxylic acids for analysis with the Mars Organic Analyzer capillary electrophoresis instrument.

Optimized programs result in peak efficiencies that are within 1% of those for manually labeled samples. In addition, protocols for μL scale serial dilution are presented, and an effective programming language is developed for these operations.

The prospects for this technology are also presented including 1) demultiplexed control of the Automaton, 2) fully autonomous sample processing for the Mars Organic Analyzer, 3) nucleic acid amplification and analysis, and 4) high-sensitivity protein biomarker detection. The technology developed in this dissertation enables miniaturized and automated analysis of metabolic, protein, and nucleic acid biomarkers using a common, programmable microchip platform.

For my nephews,

Miles and Julian,

and in loving memory

of Ryan Cross

Table of Contents

Acknowledgements

This dissertation would not have been possible without the support of many brilliant minds and an emergent community of friends and family. First and foremost, I would like to thank my advisor, Professor Richard Mathies, for making this project possible and helping me stay focused on my goals. Thanks to Mary Hammond whose diligent efforts and advocacy paved a path forward for my project and this thesis. Throughout all of the challenges we faced, Rich and Mary's continual support created an environment in which new ideas could be formed and brought to life. I also want to thank Dr. Thomas Chiesl who has helped me design and coordinate my research with both creativity and intellectual rigor.

I have had the opportunity to work on several projects throughout the course of my research. Thanks to Dr. Yun Kyung Jung, Dr. Jungkyu Kim, and Dr. Avraham Bromerg for all of their hard work and collaborative spirit. I was also fortunate to have an opportunity to work with Dr. Amanda Stockton on the automation of sample analysis for the Mars Organic Analyzer. This work would not have been possible without Amanda's remarkable diligence and creativity. Our project was truly inspiring to me, and I believe that it created many new possibilities for portable biochemical analysis systems. Dr. Thomas Chiesl and Dr. Merwan Benhabib also played an important role in the evolution of this project. I am thankful to have been an honorary member of the Mars team.

When I first started this project I had the honor to work with Dr. William Grover. The genius of Will's accomplishments provided the framework for my project, and has broadly impacted the scientific community both academically and within the industry of molecular diagnostics. Will, I hope to have the opportunity to work with you again someday.

In my years before graduate school, several advisors and collaborators provided support and inspiration that helped push me towards my goals. I would like to thank Professor Ron Rusay of Diablo Valley College and Professor Veikko Keränen of the Rovaniemi University of Applied Sciences for a variety of exciting projects that we embarked upon. I would also like thank Professor David Deamer of the University of California, Santa Cruz. I conducted my undergraduate senior thesis research in Professor Deamer's lab. It was an inspiring and formative experience for me.

I would like to thank my parents, Lynette and Gary; and my step parents Pam, and Michael for all of their support and encouragement throughout the years. I feel very lucky to have had such devoted guidance in my life. I also want to thank my brother Jorgen and my nephews Julian and Miles for their love and support, and bringing joy to my life during difficult times.

Finally, I would like to thank Tanya Blanck and the rest of the Blanck family for their inspiration and support over the years.

Chapter 1: Introduction

In 1925, the first transistor was patented by Julius Edgar Lilienfeld. Thirty three years later, Jack Kilby demonstrated the first functional integrated circuit while working at Texas Instruments.[1] He described this invention as "a body of semiconductor material ... wherein all the components of the electronic circuit are completely integrated." Since this invention, the refinement of microfabrication techniques has enabled the integration of millions of transistors onto a common substrate and the development of modern microprocessors. The prospect of using microfabrication techniques to integrate fluidic control and bioanalysis structures onto a miniaturized substrate may offer similar revolutionary advancements in the fields of molecular diagnostics, clinical chemistry, and drug discovery.

Simplicity is the ultimate sophistication.

- Leonardo da Vinci

1.1 Molecular Diagnostics and the Need for Automated, Portable Analysis Systems

The completion of the sequencing of the human genome in early 2001 enabled the identification of approximately 23,000 genes encoding proteins. As the molecular mechanisms for disease are increasingly identified, *in vitro* diagnostics will begin to play a more significant role in the healthcare landscape. Molecular diagnostics is the measurement of DNA, RNA, proteins or metabolites to detect genotypes, mutations, or biochemical changes. These tests enable the detection and classification of existing disease, genetic profiling to determine the efficacy and safety of drug therapies, and predisposition diagnostic tests to determine the future risk of patients developing disease of monogenic or multigenic origins.[2] These capabilities allow healthcare professionals to more rapidly and effectively determine therapies for patients.

Molecular diagnostic testing requires robust and specific assays that are traditionally performed by specialized personnel in centralized laboratories.[3] A wide variety of equipment is typically necessary to perform these assays including centrifuges, vortexers, thermocyclers, and detection systems including microscopes and spectrometers. The development of robotic systems to automate molecular diagnostic tests has significantly increased the speed and throughput of centralized testing laboratories,[4] however, conventional laboratory automation systems have a large footprint and are often extremely expensive.

The development of point-of-care analysis platforms enables decentralized molecular testing and more rapid diagnosis of disease.[5] Rapid test results in critical care environments such as emergency rooms can potentially save lives. These capabilities can also be critical for the prevention of disease outbreaks or avoiding the buildup of resistance to drugs. Effective point-of-care testing systems require small footprints for ease of use and minimal manual sample preparation prior to analysis. Several point-of-care testing platforms are commercially available for a range of analytes. For instance, a broad range of blood metabolite levels can be determined using the Abbot ISTAT, a handheld detection system.[6] In addition, commercial platforms are currently being developed for point-of-care analysis of infectious disease and protein biomarkers.[7,8] However, progress has been limited for these biomarkers due to the complexity of operations required for immunoassays and nucleic acid analysis.

An additional advantage of portable analysis systems is the ability to perform molecular diagnostic tests in resource poor settings. The lack of accessibility and affordability of many commercial diagnostic tests is a significant cause of disease burden in developing countries.[5]

The development of low-cost, portable, low-power consumption, and automated molecular testing platforms would therefore significantly improve the quality of global healthcare. The ability to perform a broad range of assays using a single device would further improve the flexibility of healthcare management under these settings. Microfluidic control and analysis structures offer the unique ability to satisfy all of these requirements for portable and automated biomolecular testing.

1.2 Conventional Laboratory Automation

One of the first commercially available laboratory automation platforms was introduced in 1956 by Technicon Corporation.[9] (Figure 1.1A) The Autoanalyzer utilized Continuous Flow Analysis (CFA) in which a continuous stream of fluid is divided into segments by air bubbles. The presence of air bubbles assisted with mixing of reagents and samples by generating turbulent flow prior to transfer of the discrete reactions through a colorimeter. Furthermore, bubbles sweep fluid through tubing by using surface tension to avoid laminar flow dispersion of sample location. These platforms performed functions including sampling, mixing, dialysis, heating, detection, and data generation for hematological tests. The second generation Autoanalyzer II developed in 1974, utilized 2 millimeter glass tubing and had a throughput of 30 - 60 samples per hour. These systems were typically used for routine medical laboratory analyses including serum metabolite and protein quantification.[10] While these systems were a significant advancement in laboratory automation, the serial processing and analysis design limited throughput and frequently led to total system shutdown due to failure of individual components.

Common usage of microtiter plates began in the late 1950's and eventually had a significant impact on the standardization of laboratory automation. Microtiter plates enable parallel processing of clinical samples for high throughput anaylsis. Molecular diagnostic assays including ELISA and PCR are frequently performed in this format. Automated molecular diagnostics tests often utilize robotic sample handling systems compatible with 96-well plates.

These systems typically consist of robotic arms that can programmably dispense or withdraw reagents, control temperature, mix solutions (by shaking), and transport microtiter plates between locations. Figure 1.1B shows a picture of a conventional robotic sample handling platform, the Tecan Freedom EVO.[11] Highly accurate sample processing operations including serial dilution are possible using this and similar platforms.[12] While these systems dramatically increase throughput, they are expensive, consume large amounts of space, and require relatively large (μL-scale) sample volumes. Miniaturized devices with similar programmable sample processing capabilities would enable automation of a broad range of molecular diagnostic assays in a point-of-care or resource poor settings with minimal sample volume requirements.

1.3 Microfabrication and Microfluidic Integration

The integration of biomolecular assays into microfluidic devices offers both miniaturization and programmable sample processing capabilities for portable testing platforms. In addition, dense fabrication of microfluidic features enables the development of high-throughput analytical devices. A broad range of mechanisms have been demonstrated to automate transport of fluids within microchannels including electrokinetic,[13] electrowetting,[14] centrifugal forces,[15] and the use of microvalves and pumps.[16] The ability to process samples and concentrate biomarkers within microchannels enables testing applications requiring high sensitivity. Finally, the development of miniaturized biosensors and detection systems has

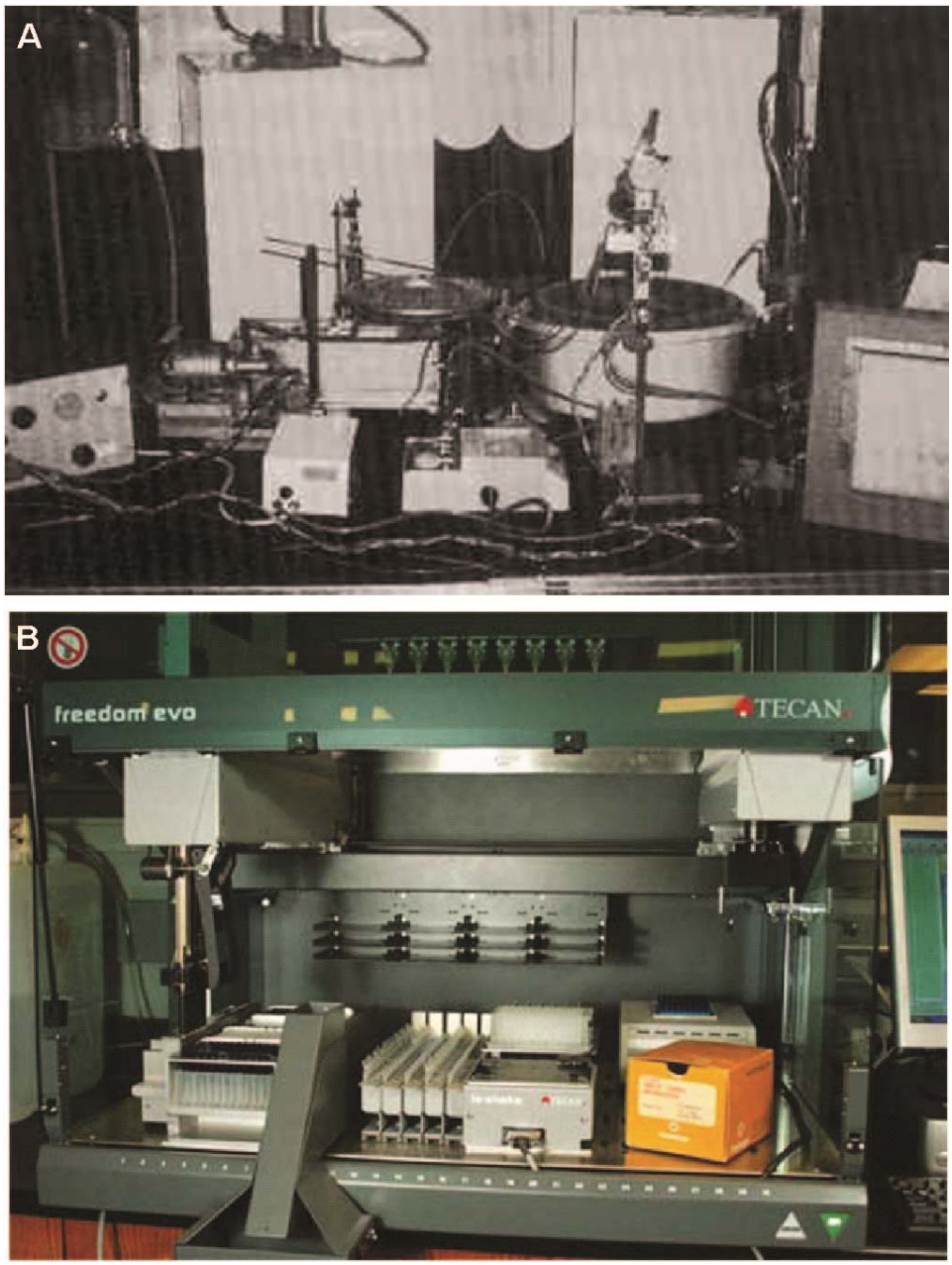

Figure 1.1. (A) Autoanalyzer platform introduced by the Technicon Corporation in 1947. (B) A modern sample processing platform for automating assays in microtiter plate format.

enabled fully integrated, miniaturized analysis platforms. While these capabilities represent significant advances toward automated, miniaturized molecular diagnostic systems, thousands of different microfluidic device designs have been proposed for different applications. Application specific devices require design changes to perform new procedures. In such devices, structures such as channels, pumps, reactors, storage cells, and mixers are integrated in series to follow the process flow of an assay procedure. In contrast, an effective programmable microfluidic system could utilize a common design architecture to achieve a broad range of operations. Since there are over 600 different clinical tests in Delmar's Guide to Laboratoy and Diagnostic Tests,[17] there is clearly a need for such programmability in microfluidic testing systems. The development of a truly programmable microfluidic processor would therefore significantly enhance the capabilities of systems for automated and portable molecular diagnostic applications.

Microfluidic devices have been demonstrated using several types of substrate materials including glass, polymers, and silicon. Glass substrates are compatible with a broad range of applications including electrophoresis and polymerase chain reaction. Additionally, glass has lower autofluorescence levels than many polymers and is therefore more suitable for applications requiring high-sensitivity fluorescence detection. Figure 1.2 illustrates the procedure for etching microchannels in glass wafers. Borofloat glass wafers are first coated with a 200 nm amorphous silicon (a-Si) sacrificial layer using a low-pressure chemical vapor deposition (LPCVD) furnace or plasma sputtering. Next, the wafer is spin-coated with positive photoresist (S1818, Shipley), soft-baked, and patterned by exposure to 365 nm UV light (Mercury i-line) through a contact aligner with a computer-generated chrome-photomask (Quintel Q4000, and/or Karl Suss MA6 mask aligners). The exposed photoresist is removed using 49 % buffered MicroDev developer and the a-Si is removed by SF_6 plasma etch (Plasma-Therm PK-12 RIE). Hydrofluoric acid (49 %) is used to isotropically etch the exposed features at a rate of ~7 μm/min. Slower etch rates can be achieved using buffered HF solutions. The remaining photoresist and a-Si is stripped from the wafer using PRS-3000 and SF_6 plasma, respectively. Access holes are drilled using a CNC-mill and diamond-tipped bits. Enclosed channels are formed either by thermally bonding to a glass backing wafer, or reversibly bonding the device to a flexible polymer such as polydimethylsiloxane (PDMS).

1.4 Microscale Fluid Dynamics

Fluids typically have laminar flow profiles in microchannels due to the low Reynolds numbers encountered at the microscale.[11] Reynolds number is defined as the ratio of inertial forces to viscous forces:

$$Re = \frac{\rho V L}{\mu}$$

where ρ is the fluid density, V is the velocity, L is the characteristic length, and μ is the dynamic viscosity of the fluid. Transition to turbulent flow occurs when the Reynolds number approaches 2000, whereas typical flows in microchannels result in Reynolds numbers less than one. The Schmidt number is defined as the ratio of momentum diffusivity (viscosity) and mass diffusivity:

$$Sc = \frac{\mu}{\rho D}$$

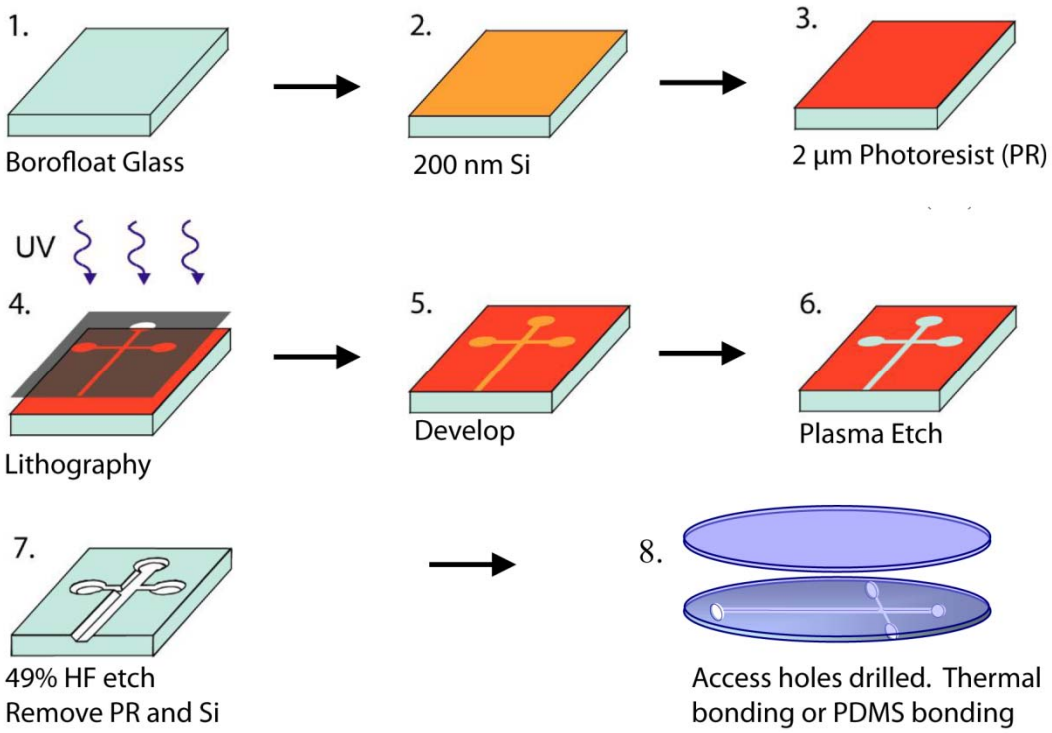

Figure 1.2 Steps in the fabrication of glass-based microdevices. A 1.1 mm wafer (1) is coated with a 200 nm amorphous Si layer (2) and a 2 µm layer of photoresist (PR, 3). Standard UV lithography is conducted (4) with development of photoresist (5) and plasma etch of a-Si (6). A wet etch of the glass is conducted (7) before PR is stripped and a-Si removed. Access holes are drilled and the wafer is thermally bonded to a blank wafer or reversibly bonded to PDMS (8) to complete the device.

where D is the mass diffusivity. High Schmidt numbers are encountered in microfluidic systems with analytes having a slow molecular diffusivity in comparison to their viscous momentum. Due to these properties, the corresponding mixing rates of fluids are determined by diffusion. In one dimension, the displacement due to diffusion is determined by the following equation:

$$< x^2 > = 2Dt$$

Where $< x^2 >$ is the mean square displacement, D is the diffusion coefficient, and t is time. For instance, it would take hemoglobin approximately 2 hours to diffuse 1 mm in a microchannel. Active mixing elements are therefore typically necessary to perform rapid sample processing and bioanalyses using microfluidic devices.

1.5 Microvalves and Pumps

Like transistors in electronic microprocessors, microfluidic valves can act as fundamental logic and control elements in microfluidic devices. Microvalves and pumps automate the transport of samples and reagents to various locations on a device for processing and analysis. Active mechanical microvalves employ moving parts to open and close microchannels. Several forms of active mechanical microvalves have been demonstrated using electrostatic, magnetic, piezoelectric, and pneumatic actation mechanisms.[16] Pneumatically actuated microvalves are the most commonly used and have been successfully applied to a broad range of applications due to the ease of fabrication and integration with other microfabricated analytical systems.[18]

The first micromechanical valves were fabricated using silicon microelectromechanical systems (MEMS) technology.[19] Among these demonstrations, thermo-pneumatic actuation systems were developed using integrated heaters to adjust the pressure inside of chambers and apply forces to elastic materials.[20,21] The fabrication of these structures was cumbersome, and highly integrated structures were not practical. A simpler fabrication approach was developed by Lagally et al. using manually placed latex membrane disks affixed to glass microchannel structures and an external vacuum source for actuation.[22] Although these structures were successfully used for controlled loading of nanoliter scale PCR reactors, the requirement for individual o-rings to hold the membranes in place prevented the development of densely integrated devices.

The most widely adopted microvalve technology was developed by Stephen Quake's group[23] in 2000 using soft lithography techniques developed by the Whitesides group in 1998.[24] Multilayer soft lithography uses an elastomeric polymer (PDMS) to form channel and microvalve features. A mold is typically prepared using SU8 photoresist and photolithography to form raised features. The PDMS is then poured over the mold and cured to transfer the features of the mold to the chip in the form of channels. Access holes are punched into the PDMS and the device is bonded to another layer to form enclosed channels. Microvalves are formed from orthogonal channels in stacked PDMS layers of the device. Application of a pneumatic pressure to one channel deforms the wall of the channel into the orthogonal channel and thereby blocks fluid flow. Removal of the pressure opens the orthogonal channel to fluid flow. Since fluid is displaced during valve actuation, a peristaltic pump can be achieved by using three valves in series for automated reagent and sample delivery.

Early demonstrations of this technology included a microfluidic memory device and comparator array each utilizing thousands of microvalves.[25] The parallelized control architecture

of these devices enabled independent delivery and pair-wise mixing of reagents within hundreds to thousands of reaction chambers. Since then, a variety of devices have been demonstrated using multilayer soft lithography for applications including protein crystallography,[26,27] genetic analysis,[28] chemical synthesis,[29,30] and single cell analysis.[31]

While the ease of fabrication and extremely small feature size enabled by multilayer soft lithography has enabled the development of a wide range of molecular testing devices, these systems are incompatible with a number of applications. PDMS surfaces are generally incompatible with capillary electrophoresis. Additionally, the diffusion and adsorption of nucleic acid oligonucleotides and proteins/enzymes on and into PDMS can alter concentrations and contaminate substrates. Furthermore, the swelling of PDMS in the presence of organic solvents prevents the automation of non-aqueous chemistries and analyses.[32]

The monolithic membrane valves developed by Grover et al. [33] address these limitations and enable further advancements in automated microfluidic sample processing and control. These devices utilize a featureless polymer membrane bonded between two glass wafers. Monolithic membrane valves have also been demonstrated using Poly(methyl methacrylate) (PMMA) wafers instead of glass to produce inexpensive, disposable devices.[34] Commercially available PDMS membranes are typically used, however a range of polymer types including Teflon can be used for applications requiring the processing of strong acids or organic solvents.[35] Figure 1.3 presents the structure and function of a normally-closed monolithic membrane valve. An etched displacement chamber in one glass wafer and a discontinuous channel structure in a second glass wafer are bonded together using a featureless, 250 micron thick PDMS membrane. Application of a vacuum to the displacement chamber through a microvalve control channel pulls the PDMS membrane away from the discontinuity, filling the valve with fluid and allowing fluid to flow across the discontinuity in the fluid channel.

Self-priming monolithic membrane pumps can also be formed by arraying three valves in series (referred to as input, manifold, and output valves). A common six-step pumping cycle is (1) open the input valve, (2) close the output valve, (3) open the manifold valve, (4) close the input valve, (5) open the output valve, and (6) close the manifold valve. The volume pumped per cycle is a function of the volume of the central manifold valve, and flow rates can be adjusted by changing the actuation times in the program. These microvalves and pumps have been used to automate reagent delivery and sample processing in a broad range of applications including pathogen detection,[36,37] single cell genetic analysis,[38] and integrated DNA sequencing.[39]

Bus valves are a variation of monolithic membrane valves that utilize three fluidic connections instead of two. Fluid is free to flow between two of the connections when the valve is closed, and between all three connections when the valve is open. In the design illustrated in Figure 1.4, a series of bus valves (A-E) are arrayed along a common bus channel. This design enables selectable reagent delivery to any output, and the entire bus channel can be rinsed between operations to prevent carryover or cross-contamination. Bus valves can also be used for pumping operations to route nanoliter to microliter scale volumes. These structures have been utilized in automated devices for ribozyme evolution,[40] amino acid analysis,[41,42] and genetic analysis.[43]

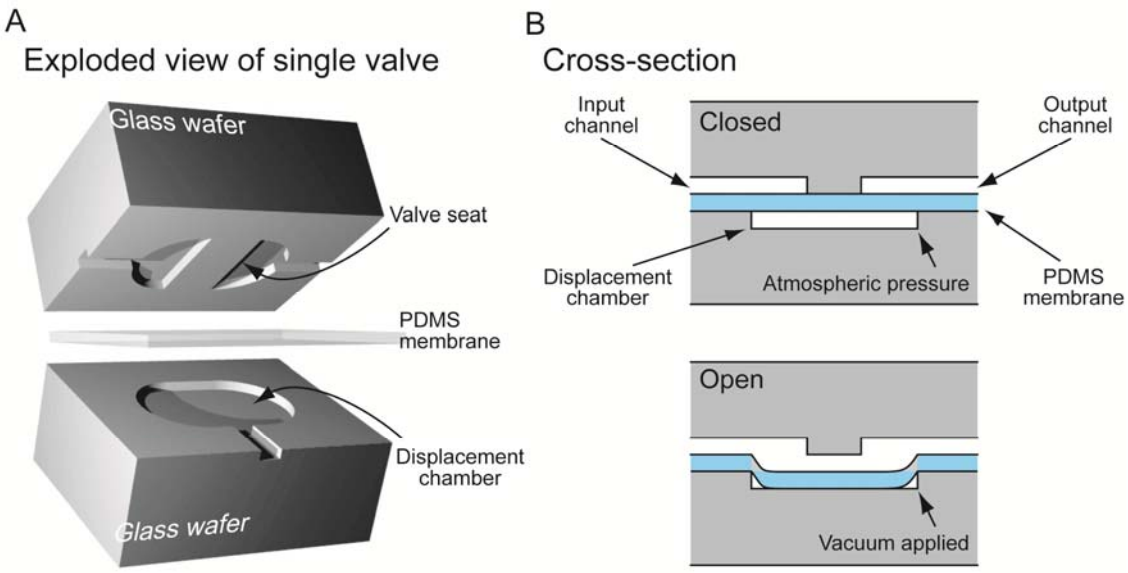

Figure 1.3 (A) Exploded view of monolithic membrane valve. (B) Cross sectional view of monolithic membrane valve. Application of a vacuum to the displacement chamber deforms the PDMS membrane and draws fluid into the valve through the fluidic connections.

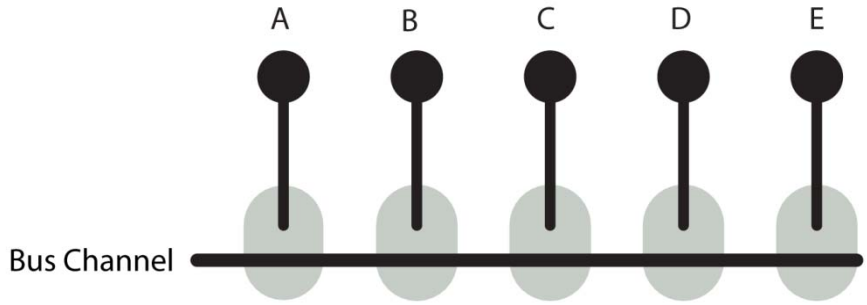

Figure 1.4 Device design with five monolithic membrane bus valves (A through E) sharing a bus channel. Fluidic channels are black and pneumatic features are gray. Black circles indicate drilled holes for fluidic inputs or outputs.

1.6 Programmable Microfluidic Processors

Although a variety of microvalve structures have been proposed for application specific testing devices, the development of multipurpose processors capable of diverse sample operations has been limited. A programmable microfluidic processing system must be able to perform a unique set of operations when provided with a new set of instructions. The monolithic membrane valves developed by our group are ideally suited for the development of these capabilities. Computer actuated solenoid valves are used to deliver vacuum and pressure pulses to the monolithic membrane valves, enabling the performance of complex actuation routines. Furthermore, the digital nature of microvalve actuation enables facile integration of logical processing operations for microfluidic device control.

Due to the laminar flow profiles encountered in microfluidic systems, the most basic operational requirement for a programmable microfluidic processor is active control of mixing reagents.[44] Passive mixing elements have been demonstrated that use serpentine channel geometries[45] or structured ridges within microchannels[46] to improve mixing speed. However, the outputs of these structures are hardwired and lack programmable control of mixing proportions. The most common approach to active mixing involves pumping two or more fluids through a circular channel path.[47] This results in the formation of concentric laminar shells that reduce the diffusive distance between the reagents and therefore enhance mixing rates.[21,48]

Another key requirement for biomolecular assays is the ability to serially process samples. For instance, a sequence of reactions or processing operations may be required starting from a single input sample. Figure 1.5 illustrates the structure of a microfluidic mixing loop used to automate serial dilution of nanoliter scale sample volumes.[49] After loading reagent and buffer into the loop, the reagents are mixed by the pumping valves, and then a portion of the loop is rinsed and then loaded with buffer. The mixing operation is performed again to generate a new dilution, and the entire process is iterated to perform serial dilutions. This illustrates the potential for microfluidic systems to perform serial processing operations, and replace key functionalities of conventional sample handling robotic systems. Although highly precise serial dilution operations are achieved with this system, the reagent proportions are limited by device geometry. A more programmable processing architecture would enable adjustable mixing proportions and the ability to process a range of sample volumes for various applications.

Grover et al. demonstrated a programmable microfluidic processor enabling the automated performance of DNA computations.[50] In this system, a series of reaction chambers were addressable by bus valves. Magnetic microspheres trapped within the reaction chambers captured specific DNA sequences. The microfluidic control architecture enabled transfer of the purified DNA sequences between a series of reaction chambers to determine the identity of multiple single nucleotide polymorphisms (SNPs). While this device is useful for programmable fluidic transfers operations, mixing proportions and sample volumes are also limited by device geometry. Electrowetting systems have also been used for programmable sample processing and analysis.[51,52] These systems exploit the change in surface-electrolyte contact angle due to an applied potential difference between the surface and the electrolyte. Using microfabricated arrays of electrodes, it is possible to manipulate aqueous droplets without the need for microvalves or channels. Basic procedures for droplet transport, mixing, and splitting operations have enabled automation of assay procedures including glucose determination,[53] immunoassays,[54] and pyrosequencing.[55] While basic automation operations are possible, droplet manipulations such

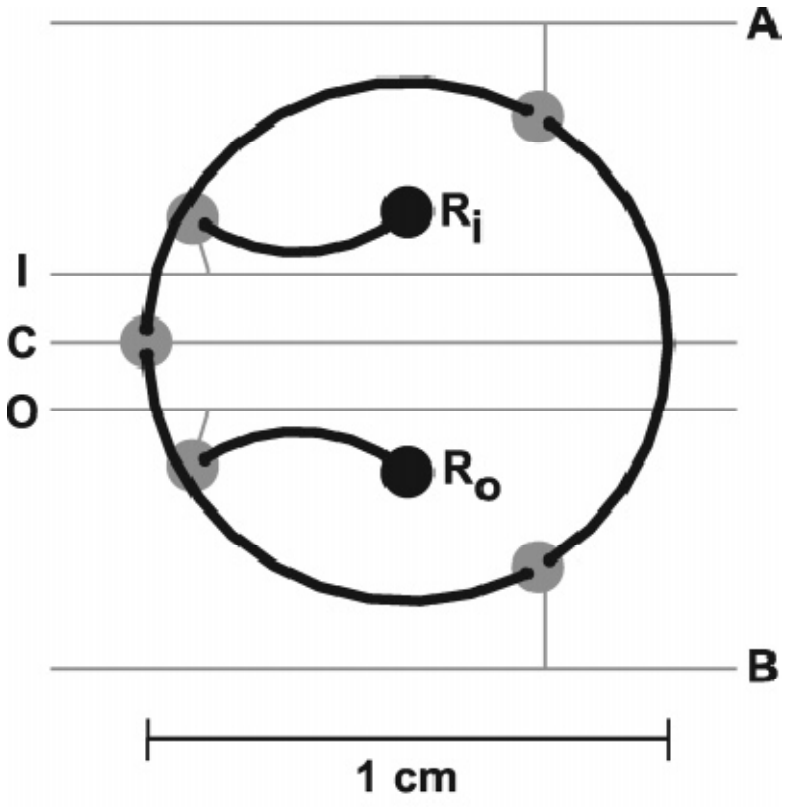

Figure 1.5 Design of a three-layer valve-based serial dilution circuit developed by Paegel et al.[49] Three conventional valves controlled by pneumatic inputs I, C, and O mix sample in the loop. Two bus valves controlled by inputs A and B pump sample and diluent into the loop and remove diluted sample. The carryover fraction between dilution steps is determined by the volume of the region between valves I and O.

as splitting operations typically suffer from significant imprecision, limiting quantitative analysis operations such as standard curve generation.[56] Furthermore the droplet format is incompatible with many downstream analysis methods such as capillary electrophoresis.

1.7 Integrated Logical Structures for Device Control

Most microfluidic assay platforms require off-chip control hardware including power supplies, computers, and solenoid valves that occupy more space and cost more than the devices themselves. It is therefore desirable to reduce the amount of off-chip control equipment in order to achieve greater miniaturization and reduce costs. One approach to reducing the number of off-chip solenoid valves necessary for microvalve actuation was demonstrated using a fluidic multiplexer[25] (Figure 1.6). With this system, a single input can be transferred to N outputs using $2\log_2 N$ pneumatic control lines. Alternative designs have been developed that prevent cross contamination of outputs, and improve scaling such that N!/(N/2)!2 outputs can be addressed using N control lines.[57] These structures can be implemented using both multilayer soft lithography and monolithic membrane valves. However, the additional pathways required for fluidic multiplexers significantly increase dead volumes of the device.

Grover et al. demonstrated demultiplexed control of latching microvalves enabling the control of 2^{n-1} independent microvalves with N off-chip controllers.[58] In principle, this system could control any configuration of pneumatic microvalves, pumps, and mixers. The key operating principle of this system is the use of microvalves to control airflow and perform pneumatic logical operations. Table 1 presents the expected results when various combinations of vacuum and pressure are applied to the input and control channels of a single microvalve. The transistor-like properties of microvalves presented in Table 1.1 enable the construction of pneumatic logical circuits that control the actuation of fluidic valves and perform specific on-chip tasks.

Table 1.1: "Truth table" for pneumatic logic

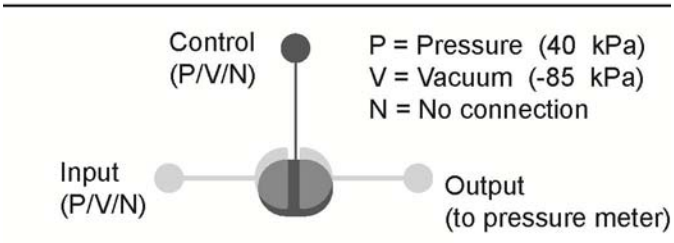

Rule	Maintained at input (kPa)	Maintained at control (kPa)	Measured at at output (kPa)
PP	40	40	0
PV	40	-85	40
PN	40	0	40
VP	0	40	0
VV	0	-85	-83
VN	0	0	0

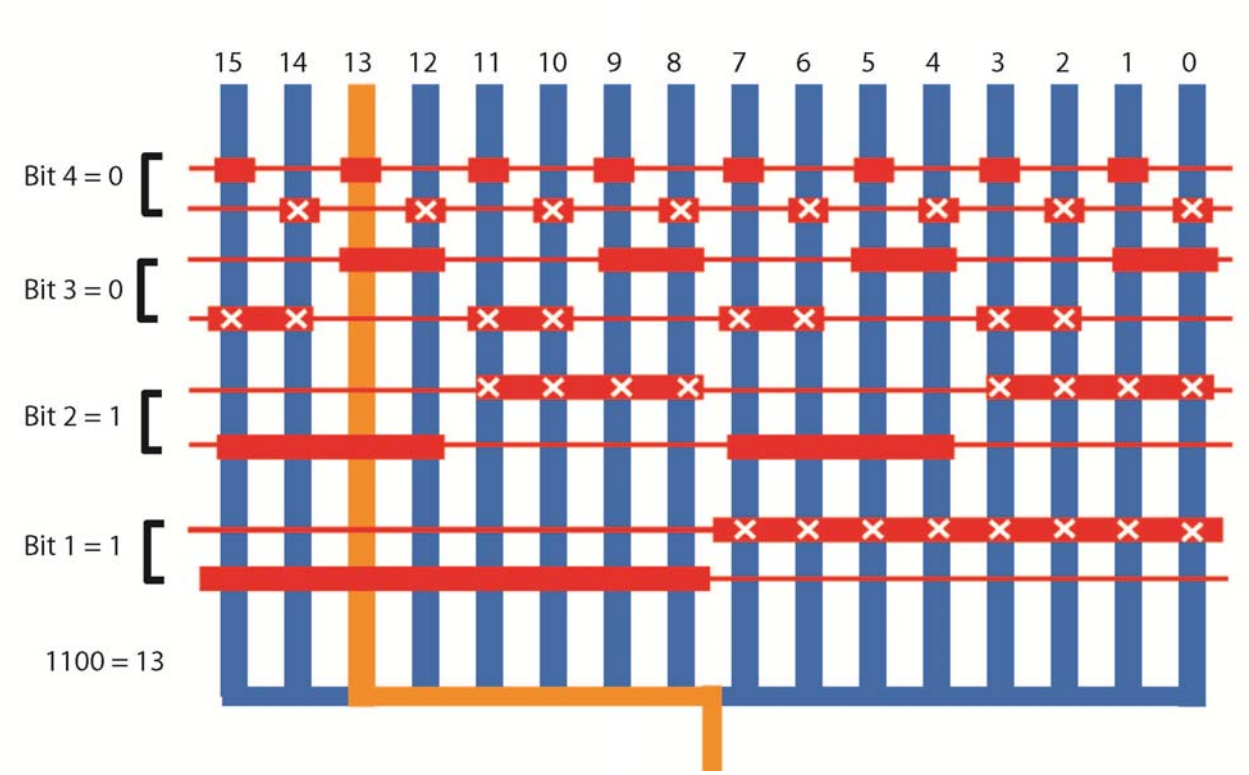

Figure 1.6 Microfluidic multiplexer developed by Thorsen et al.[25] in which N vertical flow channels are individually addressed using only $2\log_2 N$ horizontal control lines. Valves are formed by wide regions of the control channels (red) that intersect the fluidic channels (blue). Application of pressure to the control lines blocks fluid flow only in the widened regions. X's indicate closed microvalves. Each "bit" of the multiplexer can be controlled by a single off-chip solenoid valve. In this example, the binary values selected for each bit result in an open connection between a common input and output 13.

A particularly useful pneumatic logical circuit is the *vacuum-latching valve* circuit presented in Figure 1.7. Application of a brief pulse of vacuum to the two-valve circuit results in the latching of a third valve in the open state. Similarly, application of a brief pulse of pressure returns the third valve to the closed state. Rapid switching of states is possible since only 80 ms pressure and vacuum pulses are required. The feedback loops used to hold the latching valve open are closely analogous to NAND- and NOR- based latch circuits used as binary memories in digital electronics. A three valve *pressure/vacuum-latching valve* circuit was also demonstrated that latches a pressure in the closed state and holds the output valve closed against fluidic pressures as high as 17 kPa.

The demultiplexer circuit shown in Figure 1.8 can control sixteen independent latching valves using only five off-chip pneumatic controllers. The demultiplexer consists of a binary decision tree in which pressure or vacuum pulses are distributed by microvalves either to the left or right at each level of branching. The demultiplexer can route 120 ms pulses of pressure or vacuum to the connected latching valves, setting all sixteen output valves to any arbitrary pattern every 2 seconds. Using this approach, n off-chip pneumatic control lines can be used to control $2^{(n-1)}$ independent on-chip latching valves. Thus, the use of micropneumatic logical circuits should enable significant reduction of off-chip control equipment and further miniaturization of programmable microfluidic processors.

1.8 Development of a Portable Platform for Biochemical Analysis

The monolithic membrane valves developed by Grover et al. have enabled automation of basic sample processing operations for a portable biochemical analysis platform. The Mars Organic Analyzer (MOA) is a μCE-system designed to search for signs of extant or extinct life on Mars.[41] It is compact and portable (11" x 11" x 4" and 11 kg), and integrates high voltage power supplies, pneumatic controls, and fluorescence detection optics. A picture of the MOA instrument is presented in Figure 1.9A. The MOA uses capillary zone electrophoresis to separate and detect small molecule biomarkers including amines, amino acids,[41] carboxylic acids,[59] aldehydes and ketones,[60] and polycyclic aromatic hydrocarbons (PAHs).[61] With the exception of naturally fluorescent PAHs, these species are chemically derivatized with dyes prior to μCE separation with laser induced fluorescence detection. Chiral resolution of amino acids is achieved using cyclodextran-assisted CE, enabling determination of relative abundances of D- and L-enantiomers. The detection of a net excess of one enantiomer over the other on the surface of Mars would strongly suggest a biotic origin. The portability of this platform has enabled field testing of samples in a variety of environments including the jarositic Panoche Valley and the Atacama Desert in Chile. The MOA has also been used to analyze clinical samples for drugs of abuse, thus demonstrating its potential for point of care biomarker analysis.[62]

Figure 1.9B presents the layout of MOA microchip capillary electrophoresis device for autosampling of a pre-labeled sample for μCE analysis. A four-layer structure combines monolithic membrane valves with all-glass separation channels for capillary electrophoresis. These separations channels utilize a cross-injector structure for injection of a well-defined, repeatable sample plug. The network of monolithic membrane valves enables integration of a variety of sample processing operations on-chip. A typical MOA analysis begins by pumping buffer out of a peek tubing "sipper" attached to the chip. The buffer is deposited on a surface containing dye and amino acids extracted from a soil sample. The fluorescently labeled amino acids are then pumped into the sample reservoir of the CE channel. If necessary, the sample can

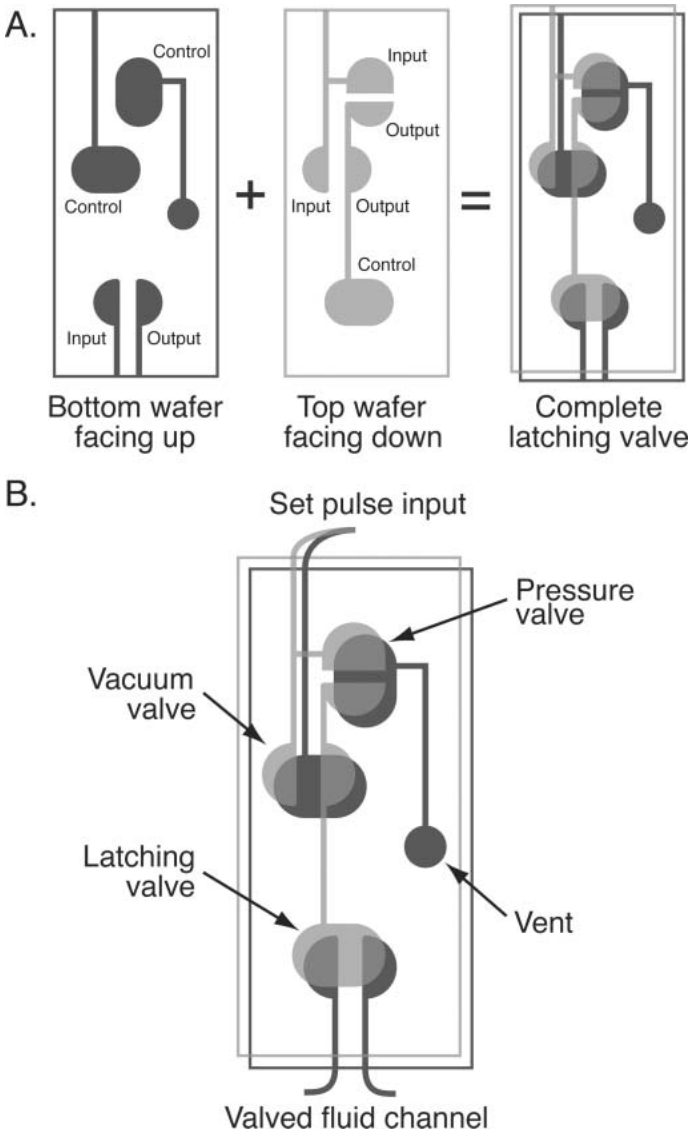

Figure 1.7 Latching valve structures developed by Grover et al.[58] (A) Three-layer device assembly (B) Design of a completed latching valve, including the vacuum and pressure valves that impart latching behavior to a fluidic valve. Application of a pulse of vacuum to the set pulse input traps vacuum in the circuit, and opens the latching valve. Application of pulse of pressure (40 kPa) to the set pulse input forces open the pressure valve and restores the latching valve to the closed state.

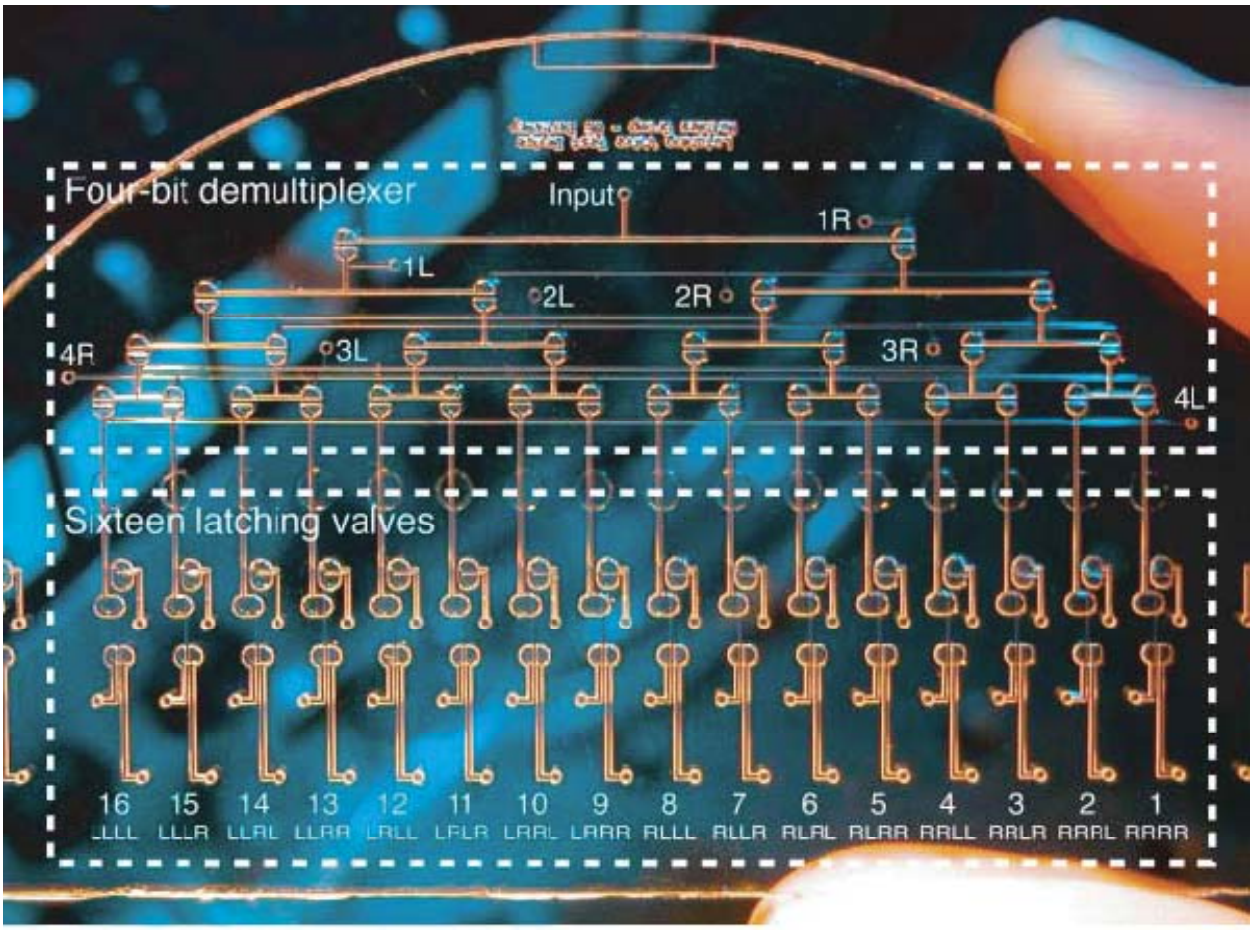

Figure 1.8 Photograph of a multiplexed latching valve test device.[58] A four-bit demultiplexer (top box) routes pressure and vacuum pulses from the single ‘‘input’’ connection to each of sixteen latching valves (bottom box).

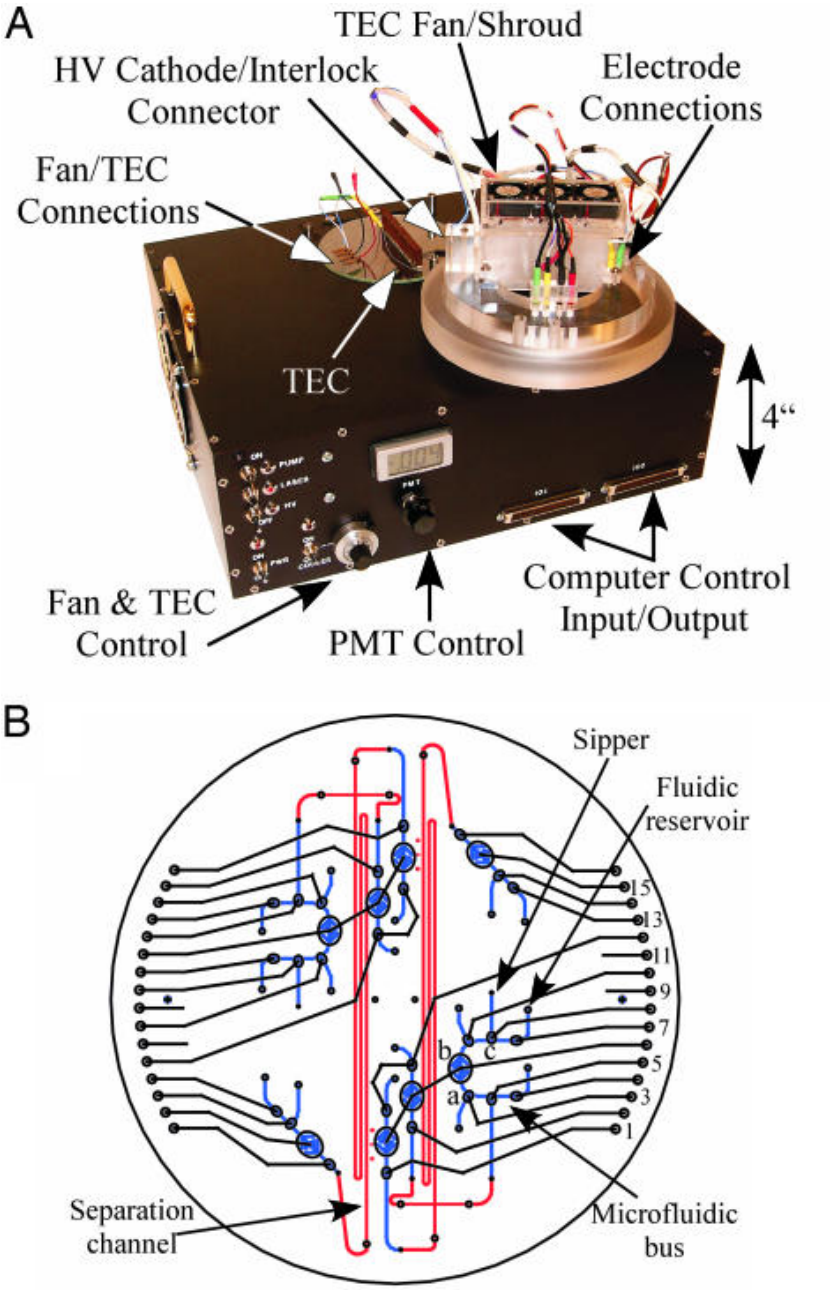

Figure 1.9 Portable MOA instrument developed by Skelley et al.[41] (A) Control system containing electronics, power supplies, pneumatic actuation solenoids, and optics necessary for CZE analysis and laser induced fluorescence detection. (B) Four-layer microfabricated device for amino acid analysis made of two separation channels (red), pneumatic manifold (black), and fluidic bus wafers (blue).

be diluted by pumping buffer into the sample reservoir. A portion of the sample can be archived for later use in an output reservoir.

While these microvalve networks represent a significant advancement toward automated sample preparation for automated CZE systems, a more general purpose sample processor would enable extension of this platform to a broad range of analyses. The previous sample processing architecture would require a variety of design changes for each new type of analyte including PAHs, aldehydes and keytones, and carboxylic acids. A programmable sample processor capable of implementing diverse protocols would clearly be a better solution for portable analysis systems. Labeling protocols for species such as carboxylic acids are more complex due to the need for activating agents, but could also be achieved with a more general purpose processing platform. Additionally, integrated capabilities for serial dilution and addition of standard would enable automated quantitative analysis. To achieve these diverse functionalities in an integrated device, a multipurpose sample processing architecture is required.

1.9 Digital Microfluidic Sample Processing Operations.

The pulsatile nature of fluid flow caused by monolithic membrane pumps results from the discrete transfer the contents of individual microvalves during opening and closing steps. During each cycle of a pumping program, the contents of a single microvalve are transferred in the forward direction, enabling precise metering of nanoliter scale volumes of sample. It should therefore be possible to perform digital fluidic operations in which the contents of a single microvalve are discretely transferred through a series of microvalves in a network. Such a system would enable the development microfluidic processing architectures in which a wide range of operations are enabled by the execution of different programs on the same device. Simple network designs such as a rectilinear array of microvalves should enable sufficient programmability to emulate other microfluidic processors with complex designs, thereby achieving a threshold of universality. Furthermore, the precise metering capabilities of monolithic membrane valves should enable the development of a digital microfluidic sample processing platform with sufficient precision for quantitative analysis applications. Such a system would enable automated sample processing for a broad range analytical testing systems for biomarker analysis.

In this dissertation, I describe the development of a programmable processor, or Automaton, that employs a 2-dimensional array of monolithic membrane microvalves for digital sample processing operations (Figure 1.10).[63] Sufficient programmability is achieved with this platform to automate diverse biomolecular assay protocols. Furthermore, the precise metering capabilities of the microvalves enable quantitative control over serial processing operations. This technology is a novel approach to digital microfluidic processing with greater operational precision and control over volumes than is possible with other approaches such as electrowetting arrays.

1.10 Scope of Thesis

The goal of the work presented in this dissertation is (1) the development and characterization of a universal micropneumatic digital logic architecture to enable integration of complex microvalve control operations on a microfluidic device. (2) The development and characterization of a microvalve-enabled digital microfluidic platform (Automaton) in which a broad

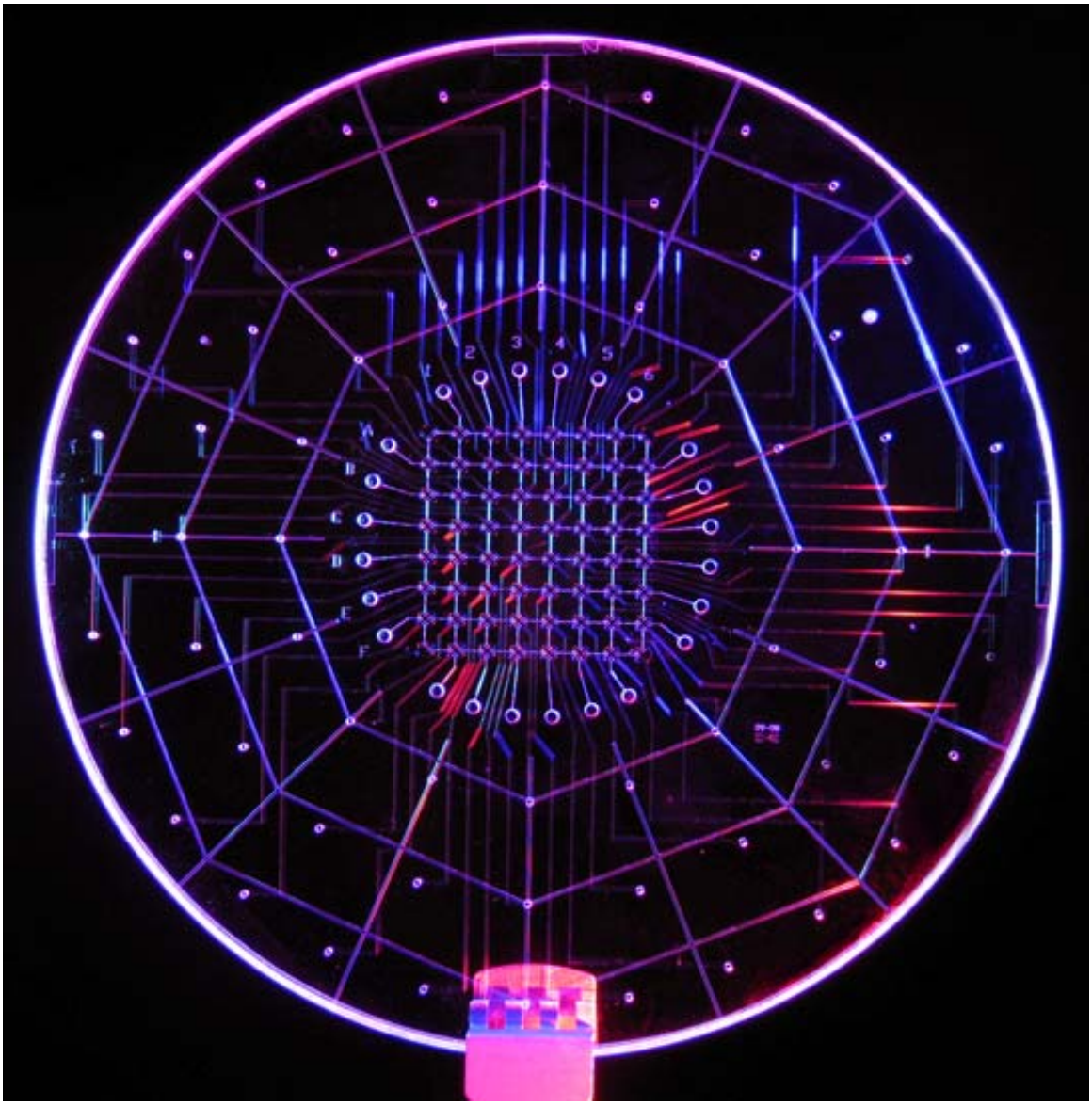

Figure 1.10 Photograph of the digital microfluidic Automaton developed by Jensen et al. The 8X8 array of microvalves in the center of the device enables performance of diverse assay procedures on a common microchip format.

range of sample processing operations can be achieved for assay automation. (3) The development of programs for the Automaton platform to automate quantitative homogeneous biomarker assays (4) The development of programs for the Automaton platform to automate heterogeneous biomarker assays including ELISA, and finally (5) The development of programs for the Automaton platform to automate sample processing operations for the Mars Organic Analyzer including on-chip labeling of a range of biomarkers.

Towards these ends, Chapter 2 presents the development of a universal micropneumatic digital logic system using the transistor like qualities of microvalves for the control of airflow. Boolean operators AND, OR, and NOT are developed and characterized. As a demonstration of computational universality, these operators are combined to perform more complex digital logic operations including XOR and binary addition. Finally, a pneumatic 8-bit ripple carry adder is demonstrated capable of performing over 65,000 unique computations on chip.

Chapter 3 presents the first demonstration of a digital microfluidic processor that utilizes the transistor-like properties of microvalves for compartmentalization and control of fluid flow. The discrete transfer of fluids in a two-dimensional array of microvalves is characterized, and basic operations are developed for reagent mixing, routing, storage, and serial dilution. These operations are combined to form an automated, quantitative assay for H_2O_2, a serum biomarker for oxidative stress using nanoliter scale sample volumes. Since the number of possible states in an N X N array is 2^N, complex assay automation procedures can be implemented on surprisingly small arrays.

Chapter 4 presents an extension of the Automaton platform to inhomogeneous immunoassays using capture antibody derivatized magnetic microspheres as a solid substrate. Effective procedures are developed for the transport, capture, rinsing, and delivery of reagents to magnetic microspheres in the digital microfluidic array. In addition, a basic combinatorial mixing program is presented using nanoliter scale sample volumes. Finally, the development of a microvalve controlled, high-throughput droplet generator for genetic analysis developed by Zheng et al. is reviewed.[38]

Chapter 5 presents the development of protocols on the Automaton for the processing and combinatorial mixing of a wide range of sample volumes. The utility of these procedures is demonstrated for automated labeling of carboxylic acids for analysis with the Mars Organic Analyzer. The ability to process large (μL scale) sample volumes enables the modular coupling of the Automaton to a wide range of off-chip analytical detection instruments. A programming language is also presented to effectively describe standardized processing operations.

Finally, Chapter 6 presents the prospects of this technology. Preliminary results are presented for demultiplexed control of the Automaton using novel latching circuits. Using this system, an 8X8 digital microfluidic array can be operated using only six off-chip solenoid valve controllers. In addition, plans for the use of the Automaton for the total integration of all MOA sample processing procedures are discussed. Additional prospects for biomarker labeling, purification, and analysis are presented, as well.

The transistor-like nature of monolithic membrane valves for controlling air flow and fluid flow has enabled the development of a highly programmable and miniaturized laboratory automation system. The digital microfluidic Automaton described herein enables the execution of complex sample processing operations using a simple microvalve network architecture. The programmability of this system can replace the complex, specialized microfluidic circuits used in application specific devices. With the current 64 bit Automaton processor, over 10^{19} states can be defined for each step of a program. This high level of programmability enables essentially unlimited possibilities for the

microfluidic automation and miniaturization of diverse molecular diagnostics assays for point-of-care analysis and field testing. The evolution of transistor logic and modern microprocessors led to extraordinary advances in our ability to process information and control our environment. The technologies described in this dissertation are a first step toward microfluidic computers that process and control chemical and biological reactions for analysis. The resulting advances in our ability to study and diagnose disease should have a transformative impact on the quality and accessibility of molecular evidence based global healthcare. Further development of these technologies for handheld molecular diagnostic systems could revolutionize personalized medicine in both industrialized societies and in resource poor settings.

Chapter 2: Micropneumatic Digital Logic Structures for Integrated Microdevice Computation and Control

This was reprinted with permission from "Micropneumatic Digital Logic Structures for Integrated Microdevice Computation and Control," by Erik C. Jensen, William H. Grover, and Richard A. Mathies (2007) *J. Microelectromech. Syst*., 16, 1378–1385. © IEEE.

2.1 Abstract

It is shown that microfabricated polydimethylsiloxane membrane valve structures can be configured to function as transistors in pneumatic digital logic circuits. Using the analogy with metal–oxide–semiconductor field-effect transistor circuits, networks of pneumatically actuated microvalves are designed to produce pneumatic digital logic gates (AND, OR, NOT, NAND, and XOR). These logic gates are combined to form 4- and 8-bit ripple-carry adders as a demonstration of their universal pneumatic computing capabilities. Signal propagation through these pneumatic circuits is characterized, and an amplifier circuit is demonstrated for improved signal transduction. Propagation of pneumatic carry information through the 8-bit adder is complete within 1.1 s, demonstrating the feasibility of integrated temporal control of pneumatic actuation systems. Integrated pneumatic logical systems reduce the number of off-chip controllers required for lab-on-a-chip and microelectromechanical system devices, allowing greater complexity and portability. This technology also enables the development of digital pneumatic computing and logic systems that are immune to electromagnetic interference.

2.2 Introduction

Microvalves are playing a critical role in the development of fully integrated microfluidic systems for lab-on-a-chip devices.[64,65] Active mechanical microvalves using thermal, magnetic, piezoelectric, and pneumatic actuation mechanisms have been demonstrated.[16] The dense fabrication and parallel control capabilities of pneumatically actuated microvalves have enabled the development of devices in which hundreds of microfluidic operations can be performed in parallel.[23,66] The normally closed monolithic polydimethylsiloxane (PDMS) membrane valves developed by our group[66] have enabled complex microfluidic control operations in lab-on-a-chip applications ranging from single nucleotide polymorphism-based DNA computing[50] to nanoliter-scale Sanger DNA sequencing.[39] The structure and function of these normally closed membrane valves are illustrated in Fig. 2.1A. An etched displacement chamber in one glass wafer and a discontinuous channel structure in a second glass wafer are bonded together using a featureless PDMS membrane. Application of a vacuum to the displacement chamber through a microvalve control channel pulls the PDMS membrane away from the discontinuity, allowing fluid to flow across the discontinuity in the fluid channel (Fig. 2.1B). The utility of these structures also extends far beyond basic valving applications in lab-on-a-chip devices.

Many emerging lab-on-a-chip devices require large numbers of independent on-chip valves to control complex fluidic operations. The large number of off-chip controllers required for such applications imposes a practical limit on the number of independent pneumatic microvalves in a microfluidic device. Several strategies for reducing the number of off-chip controllers have been presented, including valve-based fluidic demultiplexers used for addressable routing of fluid to arrays of on-chip chambers.[25,67] Recently, we demonstrated that addressable arrays of independent microvalves can be controlled using an on-chip pneumatic demultiplexer together with bistable valve-based latching circuits.[58] In this system, microvalves are used like transistors to control airflow within microchannels and, in turn, the actuation of "working" output valves for fluid routing operations. Since these valve-based logical structures employ basic digital logic operations used in electronics, it should be possible to form networks of valves that are capable of performing even more complex logic operations to enhance device capability.

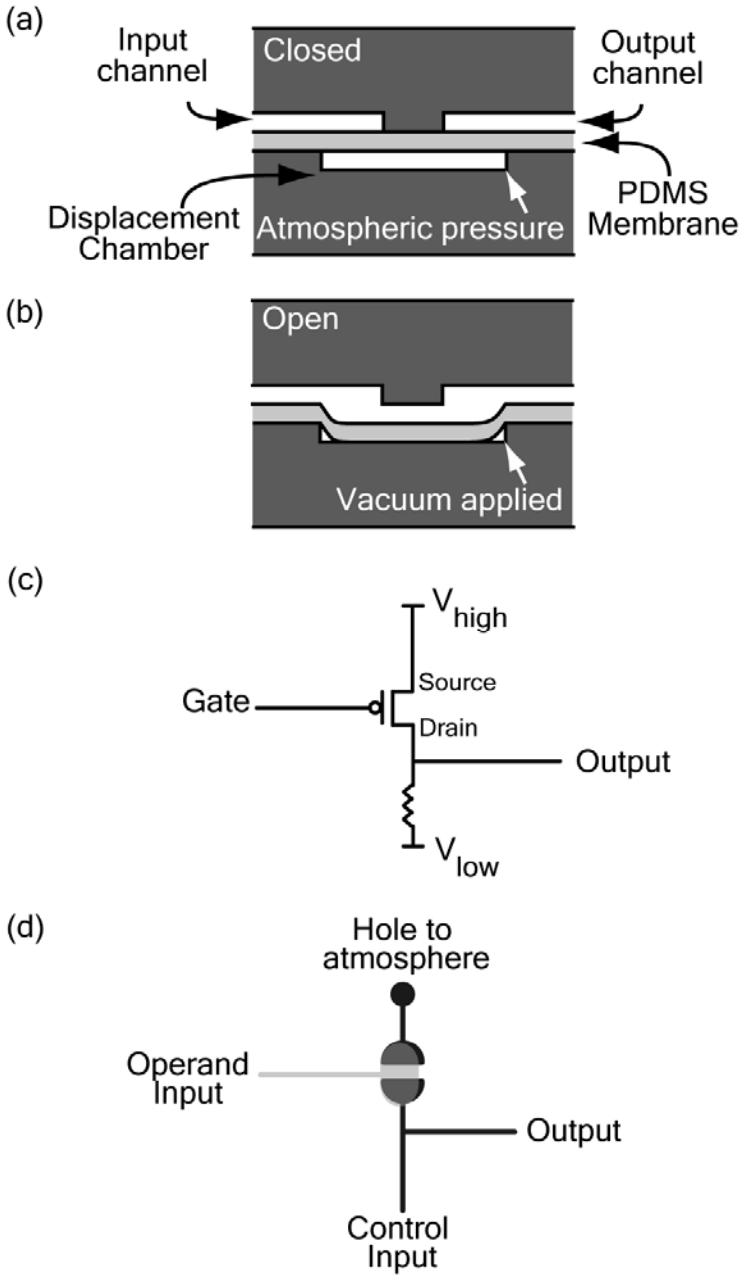

Figure 2.1 (a) Cross-sectional view through a monolithic membrane valve. The valves are normally closed with the PDMS membrane resting on the valve seat. (b) The PDMS membrane is pulled into the displacement chamber, opening the valve by the application of a vacuum through the control channel. Relationship between a (c) p-MOSFET inverter and a (d) pneumatic inverter showing that PDMS membrane valves can function as pneumatic transistors. Here, and in subsequent figures, light and dark gray represent etched channel features on the two different glass layers.

Macroscopic pneumatic logic devices were first developed in the 1960s,[68,69] and are still widely used in the automation of manufacturing processes.[70,71] Pneumatic logical control systems are particularly useful in environments in which electronic devices present a hazard or malfunction due to hostile interferences. Recently, analogies have been suggested between pneumatically actuated microvalves and p-channel MOSFETs (p-MOSFETs).[72] Basic logic gates such as pressure-amplifying inverters, AND gates, and OR gates have also been proposed and characterized using a variety of pneumatically actuated valves.[58,73,74] However, no system has been demonstrated for the large-scale integration of universal pneumatic logical structures in microfabricated devices. Analog computations such as solving the shortest path problem in mazes have been successfully performed using networks of microfluidic channels.[75]

In this paper, we design and fabricate networks of pneumatically actuated microvalves that function as logic gates and demonstrate integrated combinations of these gates that perform complex digital logic operations. Fig. 2.1C and 2.1D illustrates the relationship between a single-transistor p-MOSFET inverter and its implementation with a normally closed pneumatically actuated microvalve circuit. With the source potential defined as 0 V, application of a negative voltage to the gate of the p-MOSFET induces a current from the positive voltage power supply (V_{high}) to the negative supply (V_{low}), resulting in a significant increase in the output voltage. In the equivalent pneumatic circuit, high pressure and low pressure correspond to V_{high} and V_{low}, respectively. Application of a negative pressure of sufficient magnitude to the operand input of a pneumatic inverter opens the valve, resulting in a current of air from the drilled hole at atmospheric pressure (defined as 0 kPa or P_{high}) to the gate control input which is supplied with a vacuum (P_{low}). This increases the pressure in the output channel to a level that is insufficient for the actuation of downstream valves. In both systems, a static current (electrical or pneumatic) continuously flows when the output is high. More complex micropneumatic inverters that block this static current have been previously demonstrated.[73,74] However, it is unclear if this feature would result in improved integration and speed, as was the case with the development of complementary metal–oxide–semiconductor technology for digital electronics.

As a test of the capabilities of these pneumatic logical structures, we have developed a variety of standard digital logic gates and combined them to function as an 8-bit ripple-carry adder. The 8-bit adder is shown to add arbitrary 8-bit binary numbers in a fully integrated glass–PDMS hybrid structure. Furthermore, we characterize the mechanical principles that allow extension of the technology to even more complex logical operations, including the integrated control of microfluidic chemical and biological analysis devices.

2.3 Methods

Device Fabrication. Device features were etched into glass wafers using conventional photolithography and wet chemical etching.[76] Briefly, 1.1-mm-thick 100-mm-diameter borosilicate glass wafers were coated with 200 nm of polysilicon using low-pressure chemical vapor deposition. The wafers were then spincoated with positive photoresist, soft baked, and patterned with the device design using a contact aligner and a chrome mask. After development and removal of irradiated photoresist, the exposed polysilicon regions were removed by etching in SF6 plasma and the exposed regions of glass were isotropically etched in 49% hydrofluoric acid to a depth of 50 μm. After stripping the remaining photoresist and polysilicon layers, the wafers were diamond-drilled to produce 500-μm-diameter holes for pneumatic input

connections. The wafers were then bonded together using a 254-μm-thick PDMS elastomer membrane (HT-6240, Rogers Corporation, Binghamton, NY).

Experimental Setup. Pneumatic inputs were supplied by the actuation of computer-controlled solenoid valves for the evaluation of individual microvalves, logic gates, and the adder circuits. Separate pumps were used to supply logic high (−87 kPa) and logic low (6 kPa) pressures to the solenoid valves. Pneumatic signals were conducted from the solenoid valves to the drilled chip inputs using polyurethane tubing with a 1.6-mm internal diameter and lengths ranging from 15 to 30 cm. Pressure measurements reported for single valves, logic gates, and the full adder are relative to atmospheric and were measured using a strain gauge pressure transducer (PM 100D, World Precision Instruments). Digital videos of the operation of the 4- and 8-bit adders were recorded using a charge-coupled device (CCD) camera.

Pneumatic Logic Gates. Pneumatic logic gates are composed of networks of valves to which pneumatic signals are applied via gate input channels. Pressures greater than −20 kPa that are applied to microvalve control channels are consistently incapable of valve actuation[66] and, therefore, represent a logic low, or the "false" value of digital logic. This is due to the adhesion force between the PDMS and the valve seat. The threshold pressure for microvalve actuation depends on the magnitude of negative pressure applied to the input channel, with an upper bound of −32 kPa. Fig. 2.2 shows the layout of several pneumatic logic gates that operate like MOSFET logic gates. Each logic gate requires one or more gate control input channels to which constant vacuum is applied during digital logic operations. Operand gate input channels (A, B) are supplied with −87 kPa as a logic high and 6 kPa as a logic low. A pneumatic AND gate (Fig. 2.2A) is composed of two microvalves connected in series. Vacuum will only be transmitted from the control input to the output if both valves are simultaneously actuated by vacuum applied to the operand inputs. Similarly, a pneumatic OR gate (Fig. 2.2B) is composed of two microvalves connected in parallel. The pneumatic NAND gate shown in Fig. 2.2C is a universal logic gate (a gate from which any logical function may be built) that functions similarly to a NOT gate. For this logic gate, the output is false if both operand inputs are true, and the output is true in all other cases. Combinations of the AND, OR, and NOT gates are also capable of universal logic operations. For instance, the pneumatic XOR (Fig. 2.2D) is composed of a combination of NOT gates and OR gates. When only one of the operand inputs (A or B) is true, the Ctrl 1 input vacuum is transmitted to either X1e or X1f, resulting in a logic high output. When both operand inputs are true, the opening of valves X1a and X1d creates a direct connection between the Ctrl 1 input and two drilled holes to the atmosphere. In this case, neither X1e nor X1f is actuated, and no vacuum is transmitted to the output. The buffer amplifier circuit shown in Fig. 2.2E amplifies operand input vacuum signal and enables successful signal propagation in more complex pneumatic logic circuits. This pneumatic buffer circuit is based on the relation, NOT(NOT(A)) = A. With both control inputs held at −87 kPa, application of a weaker vacuum to the operand input (A) opens valve b1. The opened connection to atmospheric pressure decreases the vacuum induced by the Ctrl 2 input, resulting in the closure of the valve b2. When valve b2 is closed, the full magnitude of the Ctrl 1 input is transmitted to the output.

As previously demonstrated,[58] when the same vacuum magnitude (−87 kPa) is applied to the control and input channels of a single valve, the valve closes after the output channel has reached approximately 98% of the input and control vacuum. This feature was utilized for the

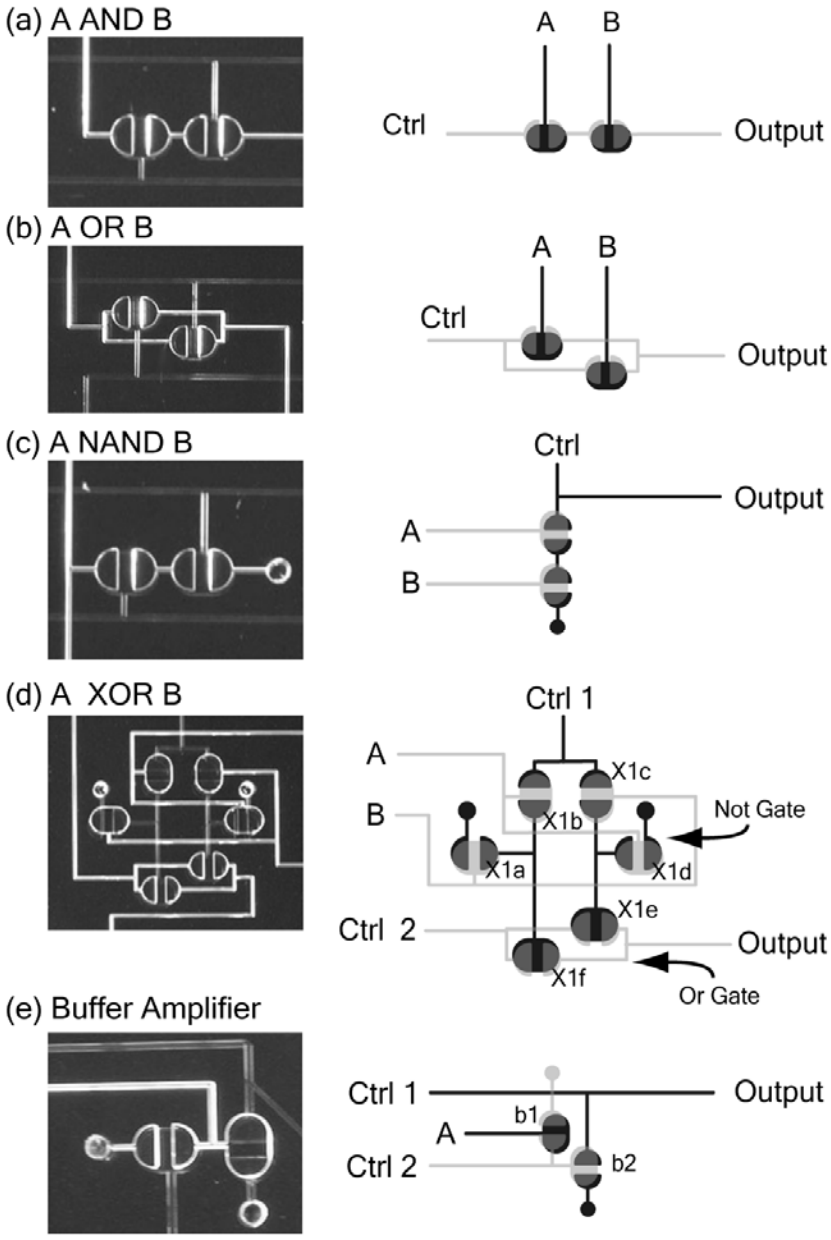

Figure 2.2 Photographs and schematics of pneumatic logic gates that function similarly to MOSFET (a) AND, (b) OR, (c) NAND, (d) XOR gates, and (e) a vacuum-amplifying buffer gate. (Solid circles) Drilled holes to the atmosphere serve as a source of air at atmospheric pressure (P_{high}) and vacuum applied to control channels (labeled "Ctrl") serves as a drain (P_{low}).

development of bistable latching valve circuits. To characterize the pneumatic signal transduction through microvalves as a function of control channel pressure, individual valve input channels were supplied with a constant pressure of −87 kPa, whereas the pressure in the control channels was varied using a separate vacuum pump. The input channel vacuum (−87 kPa) applies a force to the membrane that resists the force applied by vacuum in the control channel. This results in an increased threshold for actuation and causes the valve to close prior to the transmission of the full input pressure to the output. Fig. 2.3A shows a linear increase in equilibrium output vacuum magnitude with increasing control vacuum magnitude, with the *x*-intercept representing the actuation threshold. Since the slope of this curve (1.5) is greater than 1, a linear network in which the output of valve *n* is the control input of valve *n* + 1 will exhibit an exponential decrease in output vacuum magnitude with increasing *n* (Fig. 2.3B). This imposes a practical limit on the integration of pneumatic logical structures that do not employ a signal amplification mechanism such as the buffer circuit described above. The elevation of actuation threshold induced by vacuum in the input channel was confirmed by measuring airflow through a single valve with −87 kPa applied to the input channel (Fig. 2.3C).

Binary Addition Circuits. Since binary addition is used in a wide range of computing operations including subtraction and multiplication, it plays an important role in the operations performed by the central processing unit of a modern computer.[77] In this paper, we demonstrate the feasibility of pneumatic binary addition circuits as a proof of principle for universal computing capabilities. Fig. 2.4 shows the logic diagram and truth table of a binary full adder. The operand inputs (A, B, and Carry In) are processed by a circuit of AND, OR, and XOR gates, resulting in two outputs—Sum and Carry Out. The truth table shows the expected logical outputs for all possible combinations of input values. The pneumatic full adder (Fig. 2.5) is composed of two XOR gates and a hybrid OR gate in which two AND gates are aligned in parallel. Four gate control inputs (Ctrl X1, Ctrl X2, Ctrl X1X2, and Ctrl C) are required for the operation of this circuit. From the resting state in which each valve is closed, all of the operand and control gate inputs are simultaneously actuated with the exception of Ctrl X2 which is actuated after a 250-ms delay. This delay is necessary since the XOR2 gate processes the output of XOR1, which has a corresponding gate delay. In a ripple-carry adder, multiple full adders are chained together with the Carry Out of one adder connected to the Carry In of the next most significant adder. Fig. 2.6 shows the schematic layout of a pneumatic 4-bit ripple-carry adder.

During carry propagation, the pneumatic Carry Out of an adder passes through a 2-mm diameter via hole in the PDMS membrane before actuating valves in an adjacent adder as the carry input. Each X1X2 control input is connected on-chip through a channel network that leads to a single drilled input hole. A similar bus input system was designed for the Ctrl C inputs, whereas the X1 and X2 control inputs were separately combined using off-chip tubing. Since each of the full adder control inputs is supplied with pneumatic signals in parallel through bus channels or off-chip tubing, only four off-chip controllers are required to actuate all of the control inputs of multibit adders. The output channels for sums and the final Carry Out convey pneumatic signals to a linear array of valves used as a readout of the computed sum. Half adders were incorporated into the circuits for addition of the least significant bits in the multibit adders.

In the 8-bit pneumatic ripple-carry adder (Fig. 2.7), a similar bus architecture is used to actuate the control inputs of the adders in parallel. The adders are radially arrayed with output

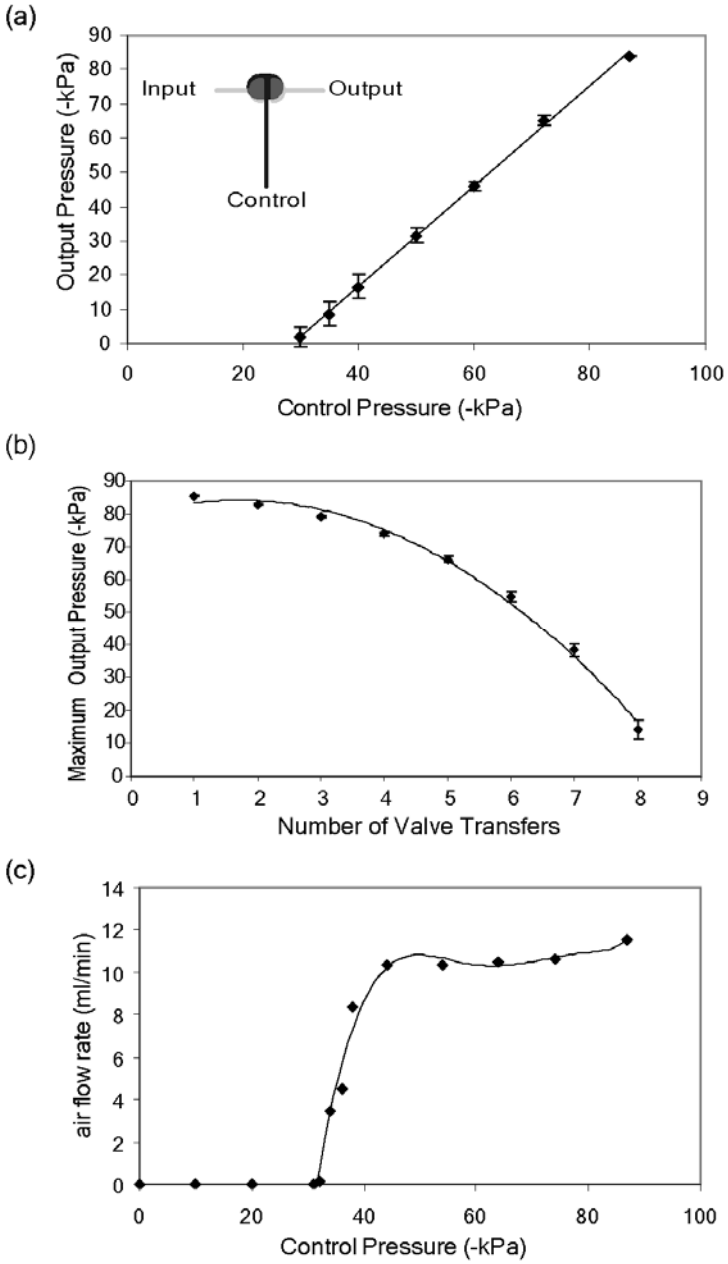

Figure 2.3 (a) Impact of valve control pressure on output pressure for single valves held at constant −87 kPa input pressure. Output vacuum magnitude linearly decreases with decreasing control vacuum. In (b), a linear regression was used to illustrate signal loss in a nested valve array. Without amplification, signal strength exponentially decays as a vacuum is transferred between the output and control channels of a series of valves with fixed input channel pressures (−87 kPa). In (c), output airflow rates as a function of control input pressure show a steep transition at −32 kPa, the threshold for valve actuation with a fixed −87 kPa input pressure.

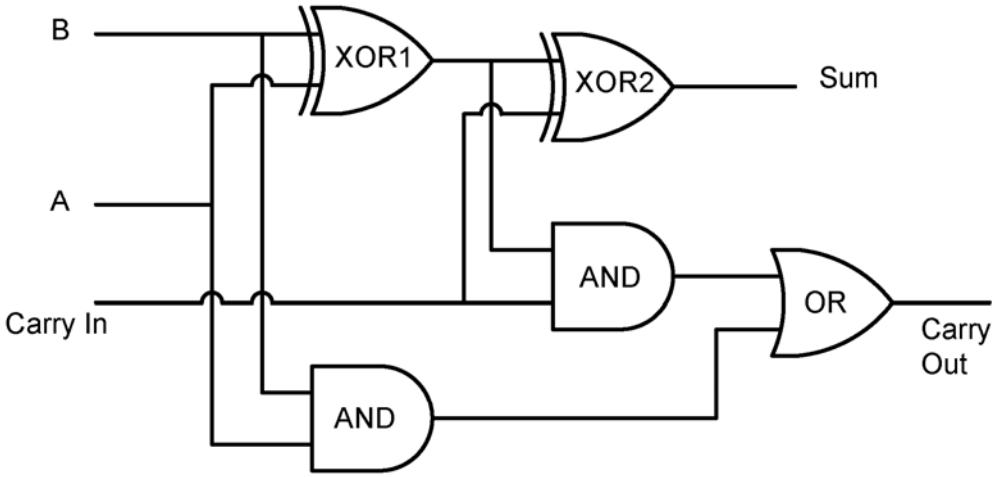

A	B	Carry In	Sum	Carry Out
0	0	0	0	0
1	0	0	1	0
0	1	0	1	0
1	1	0	0	1
0	0	1	1	0
1	0	1	0	1
0	1	1	0	1
1	1	1	1	1

Figure 2.4 Logic gate diagram and truth table for a full adder. A full adder processes a Carry In input along with two operand inputs (A and B) to generate a Sum and Carry Out.

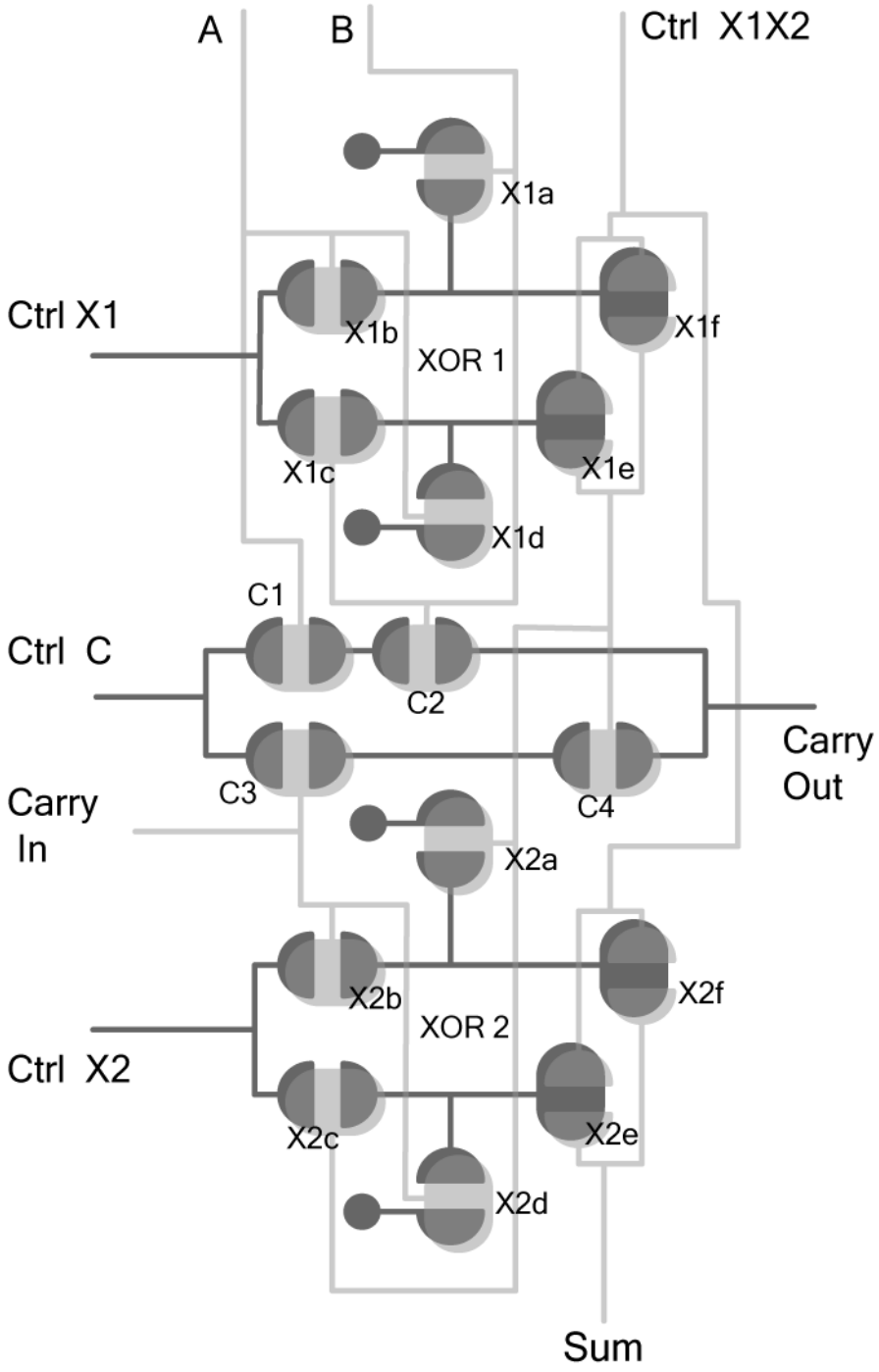

Figure 2.5 Layout of a pneumatic full adder. Four control inputs (Ctrl X1, Ctrl X2, Ctrl X1X2, and Ctrl C) for constant vacuum are required for the operation of the circuit. The pneumatic full adder processes a Carry In input along with two operand inputs (A and B) to generate a Sum and Carry Out. Valves X1a–X1f and X2a–X2f form the XOR1 and XOR2 gates, respectively, that are shown in Fig. 2.4.

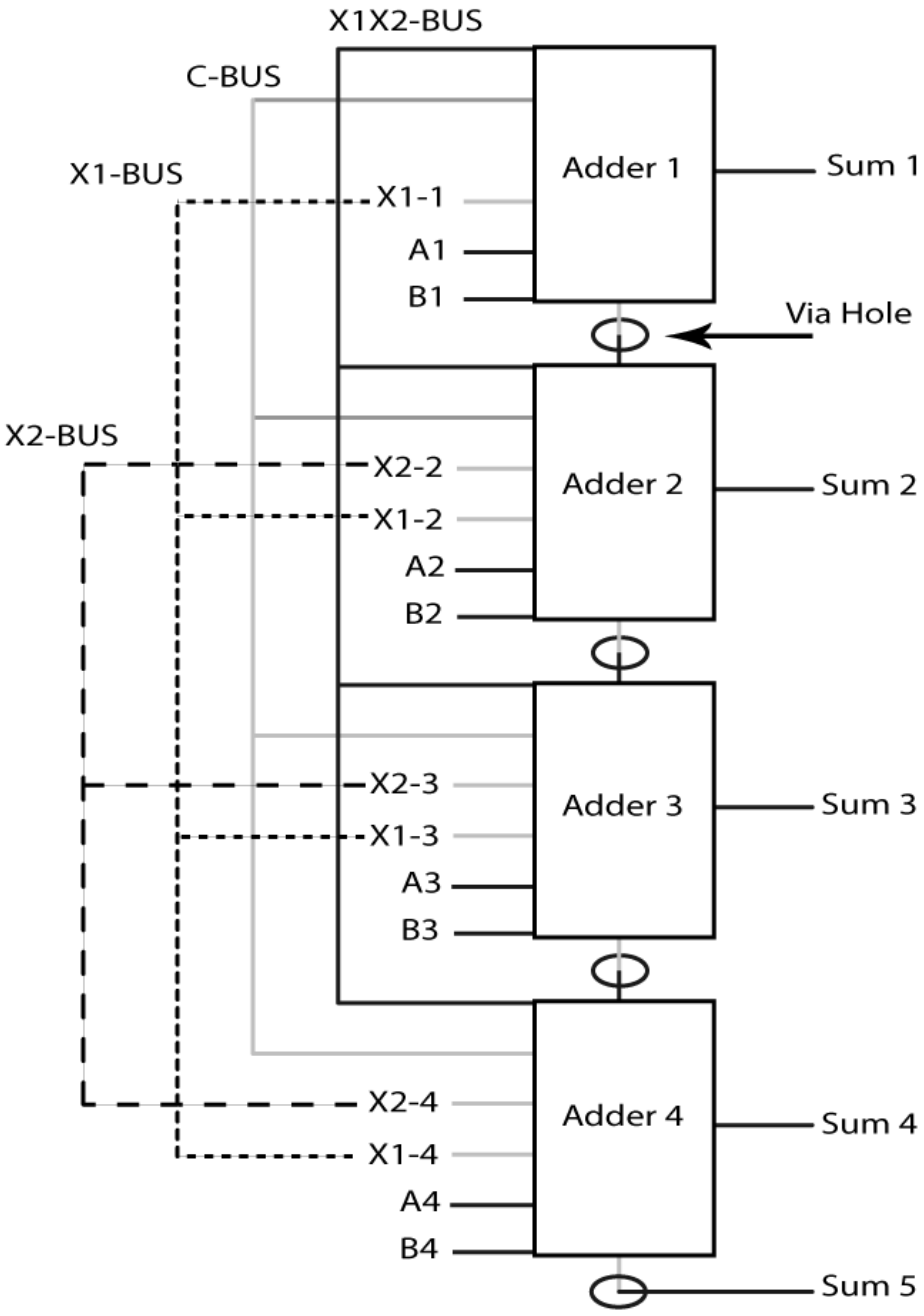

Figure 2.6 Schematic layout of a pneumatic 4-bit ripple-carry adder. Black and gray solid lines represent channels on opposite sides of the PDMS membrane, whereas dashed lines represent off-chip tubing connections. Carry propagation occurs in the direction from Adder 1 to Adder 4, passing through via holes in the PDMS membrane.

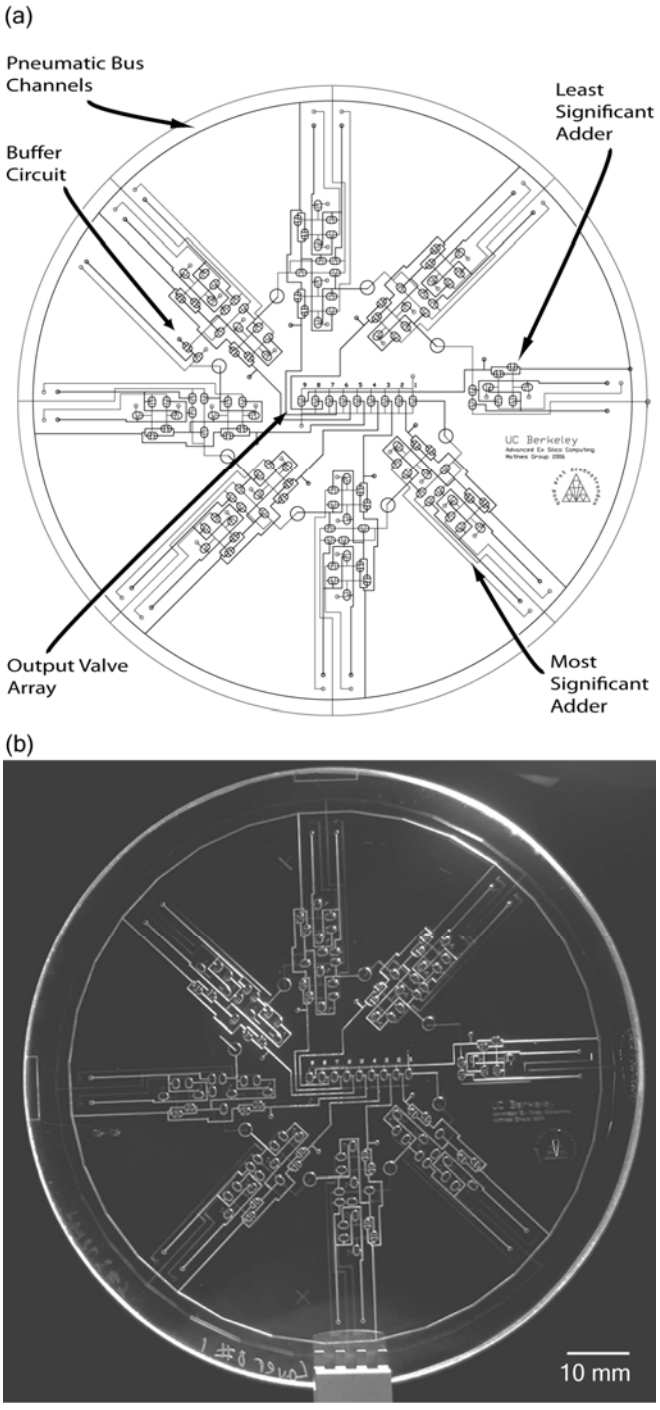

Figure 2.7 (a) Layout and (b) photograph of the 8-bit pneumatic ripple-carry adder. Circular channels along the perimeter are bus channels that supply pneumatic signals to each Ctrl C and Ctrl X1X2 gate input. The adders are radially arrayed with the least significant adder on the far right and carry propagation occurring in the counterclockwise direction. The Sum output of each adder and the final Carry Out actuate the output display valves in a linear array. A buffer circuit was added to amplify the pneumatic Carry Out signal of the fourth adder.

channels for sums and the final carry extending to a linear array of readout valves in the center of the chip. A buffer amplifier circuit was added to the Carry Out of the fourth adder to amplify the signal and ensure successful carry propagation through any number of the adders.

2.4 Results

Basic Logic Gates. The propagation times and output magnitudes of each individual logic gate in Fig. 2.2 were characterized on a single fabricated device (Appendix A). For each logic gate, operand and control inputs were simultaneously actuated. Each logic gate generated output vacuum magnitudes that fall into the correct ranges for logic high or logic low, as defined above. The lowest magnitude for a logic high output was observed for the XOR gate (−63 kPa) since it is composed of the most complex network of valves. Latching of the output vacuum occurs in the XOR gate if all of the inputs are simultaneously turned off. This latched volume would be eventually restored to atmospheric pressure due to the gas permeability of the PDMS membrane; however, the process can be expedited by actuating the operand inputs while the control inputs are closed. Dynamic response times were defined as the interval between the actuation of off-chip solenoid valves and the opening of an output microvalve due to a logic high output. Response times were determined using CCD camera videography. The longest response time (250 ms) was observed for the XOR gate. Since these response times include a delay due to the evacuation of tubing between the solenoid valves and the chip inputs, optimization of vacuum pump speed and the dimensions of off-chip tubing may significantly improve the speed of logical operations. Pressure transfer characteristics evaluated for the pneumatic inverter indicate sharp threshold transitions between high and low output for a wide range of gate control input pressures

Pneumatic Full Adder. Table 2.1 shows the output vacuum and pressure magnitudes of the pneumatic full adder for all possible combinations of inputs. As an example, the Carry Out is true when both XOR (A, B) and the Carry In are true. In these cases, the output of XOR1 is transferred to the control input of valve C4 (Fig. 2.5). The input of this valve is supplied with approximately −87 kPa signal via the Ctrl C gate input channel. Based on the −64 kPa logic high output of an individual XOR gate, and using the equation for the linear regression in Fig. 2.3A, a Carry Out vacuum of −54 kPa is predicted. This precisely agrees with the experimentally determined values from the pneumatic full adder. The operation of the full adder required a 250-ms delay for the actuation of the X2 control input. Delays less than 250 ms were insufficient for the transfer of output from XOR1 to the input of XOR2 and, therefore, resulted in incorrect

Table 2.1 Truth table for pneumatic full adder in kilopascals.

A	B	Carry In	Sum	Carry Out
6	6	6	0	0
-87	6	6	-46	0
6	-87	6	-48	0
-87	-87	6	0	-65
6	6	-87	-64	0
-87	6	-87	0	-55
6	-87	-87	0	-54
-87	-87	-87	-65	-65

output sums. To avoid latching of gates within the adder, an eight-step 2-s closing procedure is used to expedite a return to the resting state (see Appendix A). More complex closing procedures are not required for multibit adders since the closing program can be applied to each adder in parallel. No vacuum is transmitted to the Carry Out or Sum outputs during these closing procedures.

Multibit Adders. Fig. 2.8A shows selected outputs of the pneumatic 4-bit binary adder. Each row is a digital image of the output valve array taken after actuation with the indicated pattern of inputs. Open valves reflect more light and appear brighter than closed valves. Simultaneous actuation of all inputs except the X2 bus results in the automatic propagation of carry information throughout the system. The addition of 1111 and 0001 generates a carry in the least significant bit that is propagated through all of the other adders and results in the output sum of 10000. This represents a worst case scenario for the time required to compute a sum and was used to determine a reliable actuation delay for the XOR2 bus. Correct outputs were reliably Fig. 2.8B shows the output of several random inputs and worst case scenarios of carry propagation for the pneumatic 8-bit adder. The control inputs of the buffer circuit were powered by constant vacuum during the operation of the device, and a 1.1-s delay was used for the actuation of the X2 bus input. Previous designs that did not include the amplifier structure failed due to loss of signal during carry propagation. The need for signal amplification is due to the large number of serial valve transfers that occur during carry propagation and can be predicted based on the signal transduction data presented in Fig. 2.3. Particularly challenging cases arise when a weak carry signal must open a valve closed with a vacuum applied to its input channel. This is the case during the computation of 01111111 + 00000001 in which valve X2f is opened in the most significant adder by a propagated carry signal. Links to digital videos of the carry propagation through the 4- and 8-bit adders can be found in Appendix A.

2.5 Discussion and Conclusion

We have developed a technology for the design, fabrication, and testing of complex integrated digital logic structures using networks of normally closed pneumatically actuated microvalves. These microvalves were shown to function like the transistors in conventional transistor–transistor logic circuits. Here, we have demonstrated that these pneumatic "transistors" can be assembled into a variety of basic gate structures (AND, OR, NOT, NAND, and XOR) and shown that they can be combined using standard design principles to form computational circuits for binary addition. The development of an amplifying buffer circuit has allowed the extension of the technology to 8-bit binary adder circuits in which pneumatic signals must propagate through numerous gates. This result suggests that more complex logical circuits such as the significantly faster carry-lookahead adder[78] could be developed using the design principles demonstrated here. Future modeling of the mechanics of individual microvalves and further characterization of airflow through microvalve networks will allow precise optimization for improved response times. It has been noted that pneumatic logical devices are limited by the speed of sound in air.[68] Although this limitation has prevented any serious competition with digital electronics for computing speed, actuation frequencies in the millisecond scale are commonly used in lab-on-a-chip devices and should be attainable using micropneumatic logic. Furthermore, the miniaturization and integration of control systems may be particularly useful for the development of portable microelectromechanical system devices for pathogen detection[79,80] or extraterrestrial biomarker analysis.[41]

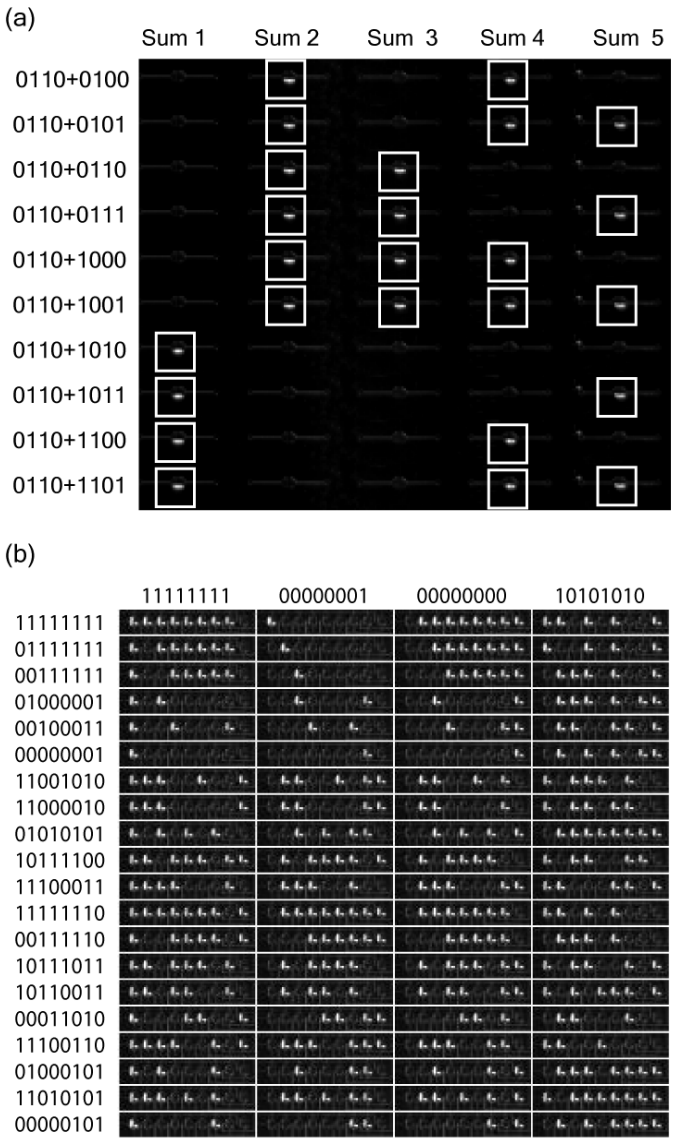

Figure 2.8 Video frames showing the linear output valve array (a) of the 4-bit pneumatic ripple-carry adder and (b) of the 8-bit pneumatic ripple-carry adder after computing the sums of the indicated inputs. Open valves reflect more light and appear brighter than closed valves. obtained for each of the 256 possible pneumatic input configurations using a 500-ms XOR2 actuation delay.

The timing of valve actuation can be integrated using micropneumatic logical structures. As the carry propagates through a multibit micropneumatic adder, an automatic series of valve actuations occur in a precise time sequence. Similarly, in digital electronics, delay circuits are often used to synchronize operational sequences in signal processing units.[81] As previously noted, the latching behavior of microvalve networks developed by our group resembles the function of simple memory circuits such as flip-flops.[58] These features could be exploited in future integrated systems that implement dynamic logical control. For situations in which latching behavior is disadvantageous, channels joining microvalves in a network can be modeled as an *RC* circuit with a capacitance and resistance to the ground (atmospheric pressure). Smaller microvalves and channels would decrease the network capacitance, and nanoscale leak channels or membranes with altered gas permeability may increase airflow to the latched volumes from the atmosphere without significantly decreasing output signals during a logical operation. Such a system for reducing the latching characteristics of microvalve networks will result in improved performance and obviate the closing procedures required here.

Integrated pneumatic logic structures have already proven useful for the development of latching structures and multiplexed control of valve arrays in complex lab-on-a-chip applications.[58] Further development in this area will catalyze progress toward the creation of multipurpose programmable microfluidic devices that can be utilized for diverse analyses. Miniaturized pneumatic logic structures may also allow integrated control in microassembly and microrobotic systems which often employ pneumatic actuation mechanisms.[82,83] Furthermore, this technology could be utilized to develop simple computing systems that are immune to radio frequency or pulsed electromagnetic interference.[84] Such computing devices may also be useful in extreme environments such as those of space missions with controlled pressure environments, where cosmic rays result in the malfunction or failure of electronic components.[85]

2.6 Acknowledgement

The device fabrication was performed by E. Chu at the Berkeley Microfabrication Laboratory, University of California.

Chapter 3: A Digital Microfluidic Platform for the Automation of Quantitative Biomolecular Assays

This was reprinted with permission from "A digital microfluidic platform for the automation of quantitative biomolecular assays," by Erik C. Jensen, Bharath P. Bhat, and Richard A. Mathies, (2010) *Lab Chip*, 10(6), 685–691. © The Royal Society of Chemistry.

3.1 Abstract

A digital microfluidic platform for the automation of quantitative, multi-step biomolecular assays is developed and optimized. The platform consists of a 2-dimensional array of microvalves that can be programmed to perform reagent routing, mixing, rinsing, serial dilution, and many other operations using nanoliter scale volumes of sample. Discrete transfer of fluid between microvalves is characterized using gravimetric flow analysis and optimized to achieve maximum efficiency. Protocols for on-chip reagent mixing and serial dilution are optimized to achieve linearity over a 1000-fold dilution range. These optimized programs are used to develop a rapid, quantitative assay for hydrogen peroxide, a biomarker of oxidative stress. A sub-micromolar limit of detection is demonstrated with an 8.5 min program runtime, thus establishing this platform as an effective tool for the automation of multi-step bioassays. The programmability of this system enables rapid development of diverse assay protocols on a common chip format.

3.2 Introduction

The integration of biomolecular assays into microfluidic platforms has numerous advantages including automated sample processing, nanoliter scale sample volume operations, and the potential for sample-in-answer-out analysis.[43] Furthermore, densely microfabricated features enable the development of devices in which hundreds to thousands of operations can be performed in parallel.[86,25] The microvalves developed by our group[66] have enabled compartmentalization and automation of fluid transport between mixers, reactors, and detection modules within a single chip. The programmable control of these microvalves has been exploited in the development of a wide range of microfluidic analysis systems from SNP-based DNA computing[50] to nanoliter scale Sanger DNA sequencing.[39] As the complexity of integrated operations continues to evolve and expand, the need for a microfluidic processor with more universal capabilities has become clear. Such a processor could replace many specialized microfluidic circuits that have limited, hardwired capabilities. A universal fluidic processing platform should enable combinatorial mixing, routing, addressing, washing, dilution, and other operations with inputs and outputs that are not limited by the microchannel geometry.

To address this challenge, we have developed and optimized a microfluidic Automaton with universal sample processing capabilities using a 3-layer glass–PDMS–glass hybrid structure (Fig. 3.1). In this system, discrete transfer of fluids between pneumatically actuated microvalves in a rectilinear array enables all of the desirable features described above. The basic operations are achieved by executing different programs of sequential valve actuations, and these operations can be combined to achieve high-level programs for the automation of multi-step biomolecular assays. The design of this system enables the precise metering of as little as 14 nL of fluid through circuits programmed for quantitative bioanalysis.

A variety of methods have previously been used for digital microfluidic manipulations. For instance, electrowetting enables the programmable transfer of aqueous droplets between an array of electrodes.[87] Basic operations such as droplet merging, mixing, and splitting have been performed. Applications have included enzymatic glucose determination,[88] clinical diagnostics on human serum samples,[53] and enzyme kinetic analysis.[89] However, these platforms still require significant off-chip sample preparation including standard curve generation for quantitative applications. Furthermore, these systems often suffer from significant imprecision in droplet splitting operations.[56] Two-phase, continuous flow microfluidic systems have also been

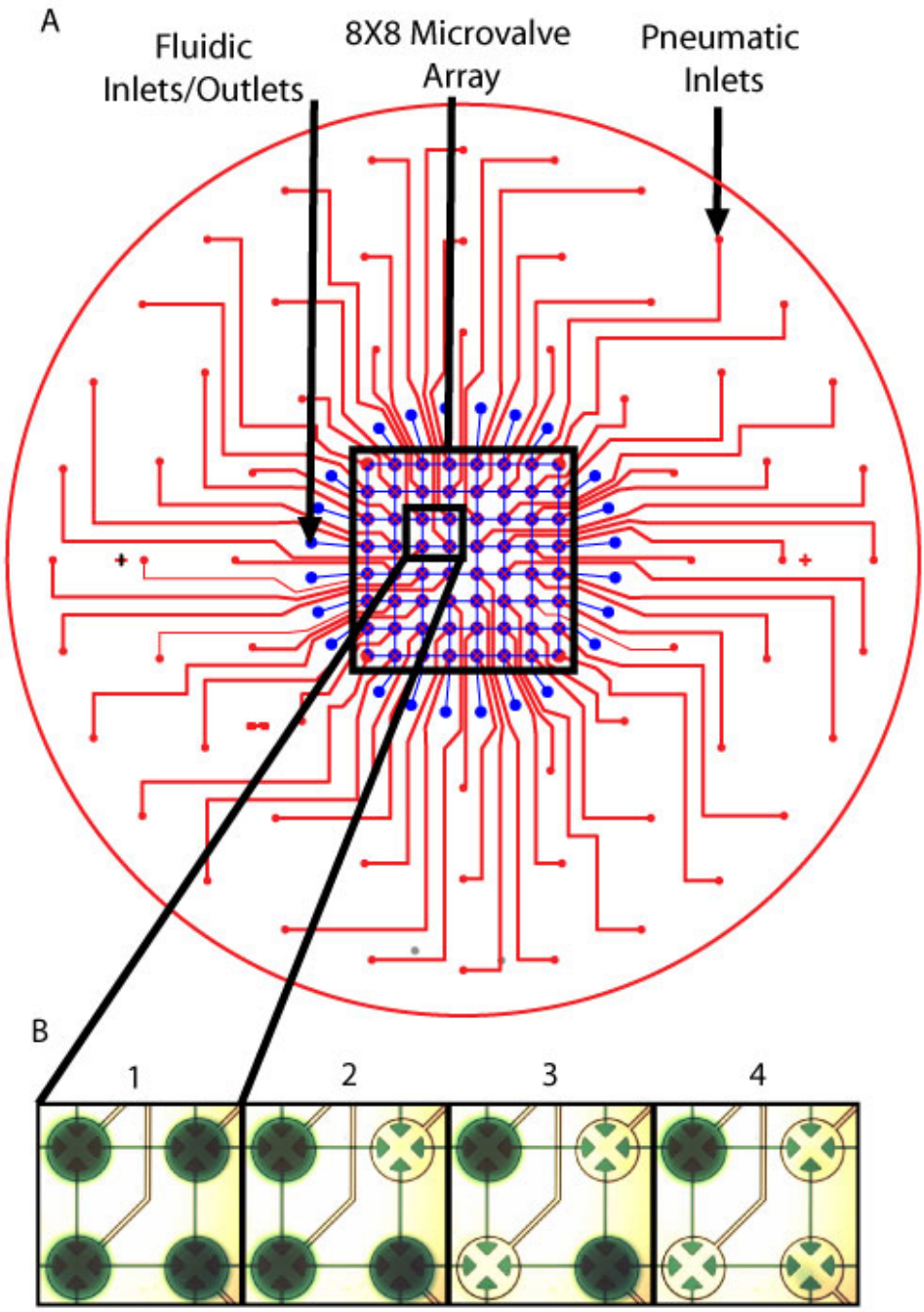

Figure 3.1 (A) Layout of the digital microfluidic platform or Automaton. Pneumatic channels (red) transmit pneumatic actuation signals to the central array of microvalves. The 4-way microvalves control fluid flow through a rectilinear grid of discontinuous fluidic channels (blue). Close up images of a portion of this array (B) show the programmable loading of a dye into actuated microvalves. The individual microvalves in this array serve as 120 nL reaction chambers as well as fluidic control mechanisms.

developed that enable reagent delivery and mixing within nanoliter scale aqueous droplet reactors.[90-92] In these systems, the specific protocols that can be performed are hardwired by device geometry, and multi-step processes such as serial reagent delivery require more complex device designs. Finally, multilayer soft lithography has been used for the development of large reactor arrays for parallelized bioanalysis and combinatorial mixing of reagents.[25,28,93] Although these systems can address a large number of reactors in parallel, they lack the serial sample processing capabilities that are critical for the automation of operations such as serial dilution.

Due to the laminar flow profiles of aqueous solutions and the corresponding lack of convective mixing in microchannels,[44] the most fundamental operational requirement for a programmable microfluidic platform is active reagent mixing. A wide range of reagent mixing schemes have been developed for microfluidic systems including fluidic loop mixers that pump multiple reagents through a circular channel path.[49,94] In these systems, the available mixing ratios are preset by the device geometry. The same functionality is achieved in our Automaton by cyclically transferring the contents of two or more microvalves connected in a loop. This enables variable, programmable mixing proportions that are defined at runtime by the number of valves in the circuit and the sequence of valve actuations.

Standard curve preparation is always a time consuming process, yet it is a critical step in a broad range of quantitative molecular assays including kinetic analysis, ELISA, and homogeneous assays for nucleic acids, proteins, metabolites, and other species. Specialized microvalve circuits have been developed that generate standard curves with fixed mixing ratios defined by microchannel geometry.[49,56,95] The programmability of the Automaton enables the generation of highly accurate standard curves with adjustable mixing ratios. Furthermore, the same microvalves that are used for standard curve generation can be used to achieve subsequent steps of an assay after a rapid rinsing cycle is performed. As a result, an entire quantitative assay can be integrated into a relatively small number of microvalves in the Automaton.

To demonstrate these high-level programming capabilities for biomolecular assay integration, we have developed an automated assay for the quantification of H_2O_2 using an enzymatic detection system. Elevated serum H_2O_2 is an indicator for oxidative cellular damage in conditions such as chronic allopathic neuropathy, the leading cause of kidney transplant failure.[96] The cell signaling characteristics of H_2O_2 have recently been investigated, as well.[97] Since a series of basic fluidic operations are combined to form the quantitative H_2O_2 assay program, the system can easily be adapted to the detection and analysis of other biomolecules; this technology is transferrable.

3.3 Methods

Design, Fabrication, and Control. Each monolithic membrane microvalve consists of an etched displacement chamber in one glass wafer and a discontinuous fluidic channel structure in a second glass wafer.[33] The wafers are reversibly bonded together using a featureless 254 μm thick PDMS elastomer membrane (HT-6240, Rogers Corp.). Application of a vacuum to the displacement chamber through a control channel pulls the PDMS membrane away from the discontinuity, allowing fluid to fill the chamber and/or flow across the discontinuity in the fluid channel. Device features were etched into 1.1 mm thick, 100 mm diameter borosilicate glass wafers using conventional photolithography and wet chemical etching as described previously.[76] The pneumatic layer was etched isotropically to a depth of 70 microns and the fluidic layer was

etched to depth of 30 microns. Each pneumatic channel addresses one of 64 fluidic valves connected in an 8 X 8 rectilinear array in the center of the chip. Pneumatic displacement chambers have a post-etch diameter of 1640 microns and were found to contain a maximum volume of 120 nL. Fluidic expansions[66] were designed to minimize dead volumes while still enabling facile and reproducible actuation. Pneumatic and fluidic channels have post-etch widths of 170 and 75 microns, respectively. The wafers were drilled with diamond-tipped bits to produce 500 and 1100 mm diameter holes for pneumatic and fluidic inputs, respectively.

An adjustable closing pressure was supplied to all unopened microvalves during the performance of programs. Individual microvalves were opened by application of an actuation pressure (-87 kPa) and held in that state for a specified opening time before proceeding to the next step. Similarly, microvalves were closed by switching to the closing pressure and holding for a specified closing time before proceeding. Opening and closing pressures were supplied to a 3/8" thick aluminium manifold by Labview-controlled actuation of solenoid valves (Teco Pneumatic, HV010E1-PSL). The manifold interfaces with each of the drilled pneumatic inputs via Viton O-rings (Parker, V747 5-197). A second 3/8" aluminum manifold is placed on the fluidic layer, with a central hole to allow access to the microvalve array and drilled fluidic inputs. The entire assembly is screwed together with six 3/8" bolts to ensure proper sealing of the O-rings and can be seen in Appendix B.1.

Device Characterization. Valve columns are designated A–H from left to right, and rows are designated 1–8 from top to bottom. A standard 3-valve pumping routine (valves B1, B2, and A2) was evaluated to determine the volume pumped per cycle in a 3-valve series as a function of valve closing pressure and actuation time. The time series of valve actuations for a 5-step, 3-valve pump can be represented as (100,110,010,011,001) where 1 represents an open valve and 0 represents a closed valve. The efficiency of pumping through 4- and 5-valve circuits was also evaluated. For a 4-valve series, the corresponding actuation sequence was (1000, 1100, 0100, 0110, 0010, 0011, 0001) with valves B1, B2, B3, and A3. The volume of one microvalve is sequentially transferred between the microvalves in the series. It is necessary to open an adjacent microvalve prior to closing a full microvalve for fluid transfer to occur. The closing pressure applied to microvalves not in use inhibits undesired fluid transfers to adjacent microvalves. Appendix Fig. B.2 shows a more detailed schematic of this program and the resulting direction of fluid flow in the microfluidic Automaton.

Prior to running assay procedures on the Automaton, the device was primed with the buffer used in each assay to fill all of the dead volumes within the fluidic array. When all of the valves are opened and buffer is loaded into the fluidic inputs, a slight vacuum is formed within the fluid channels due to the gas permeability of PDMS. This draws buffer into all of the fluidic channels and open valves. The process can be expedited by a series of cyclic valve actuations and typically requires several minutes to complete. After removal of air bubbles, microvalves are sequentially closed to leave only the dead volumes filled with buffer.

An 8-step mixing cycle and dilution program was developed that transfers the contents of two valves between a series of four valves connected in a loop (1100, 1110, 0110, 0111, 0011, 1011, 1001, 1101). The two initially filled valves can be loaded with different reagents and the program iterated to achieve a homogeneous mixture of the fluids. Much like the digital logic

circuits of electronic microprocessors, the output from a mixing circuit can be stored for future retrieval, or it can be used as the input for downstream processing operations. To automate the generation of standard curves, the above program is performed with buffer and sample, and then a portion of the resulting mixture is stored and used as the input for a subsequent dilution cycle. This dilution process is performed iteratively, resulting in a serially generated standard curve. The carry over fraction can be adjusted with the program to achieve a variety of dilution factors.

A program was developed to determine the dilution factors and the linearity of the automatically generated standard curves. After priming, 10 μM fluorescein and 1X TTE pH 8.3 were loaded into separate input wells. An automated program was used to load the appropriate microvalves with buffer and dye and then generate the standard curves as described above. Confocal fluorescence data were acquired using a Zeiss Axioplan microscope and a 200 mW, 488 nm laser excitation source (Novalux, Protera-488-15). The laser was reflected off of a FT510 dichroic beam splitter and focused through a 32X objective (LD Achroplan, 0.4 NA) onto a fluidic channel in the mixing circuit. Fluorescence emission was collected through the same objective, passed through a 515 nm long pass filter, and focused onto a 200 micron pinhole covering a PMT (Hamamatsu H9306-03).

Hydrogen Peroxide Assay. A program was developed to automate the quantification of H_2O_2 by generating a standard curve, mixing each level of the curve with enzymatic detection reagents, and then quantifying unknown samples (Fig. 3.2). A priming operation was performed as described previously using 0.1 M sodium phosphate buffer pH 7.4. Stabilized 3% H_2O_2 (Invitrogen, A22188) was used to prepare a 30 μM H_2O_2 standard in the same buffer. This standard is loaded into a microvalve in the standard dilution circuit and mixed with one microvalve containing buffer. One unit of the resulting mixture is stored for the next iteration, while another is mixed with aminophenyl fluorescein (APF, 40 μM, Invitrogen, A36003) and horseradish peroxidase (HRP, 50 units mL^{-1}, Sigma, P8375) in an adjacent mixing circuit.

During this mixing phase (25 cycles), confocal fluorescence data were collected as described above in a channel within the mixing circuit. After each standard level has been quantified and a final washing step has been performed, a sample containing H_2O_2 is then mixed with APF and HRP on-chip, and the resulting fluorescence is compared to the standard curve for quantification. A 25 kPa closing pressure and -87 kPa actuation pressure were used to control the microvalves throughout the program. For reagent and buffer delivery steps, valve opening and closing times were 500 ms and 1000 ms, respectively. Opening and closing times of 50 ms were used for each actuation during the mixing cycles. The entire assay, including standard curve generation and triplicate sample analysis, is completed in less than 14 min.

To determine the precise dilution factors at each of the mixing steps, 10 μM fluorescein was loaded into the well designated for H_2O_2 standard. 1X TTE buffer pH 8.3 was loaded into each of the other input wells. The entire quantitative H_2O_2 program was then executed while confocal fluorescence data were acquired with the laser focused on a channel within each of the mixing circuits. The standard dilution steps and APF–HRP–standard mixing steps had dilution factors of 2.1 and 1.8, respectively. A similar procedure was used to determine a dilution factor

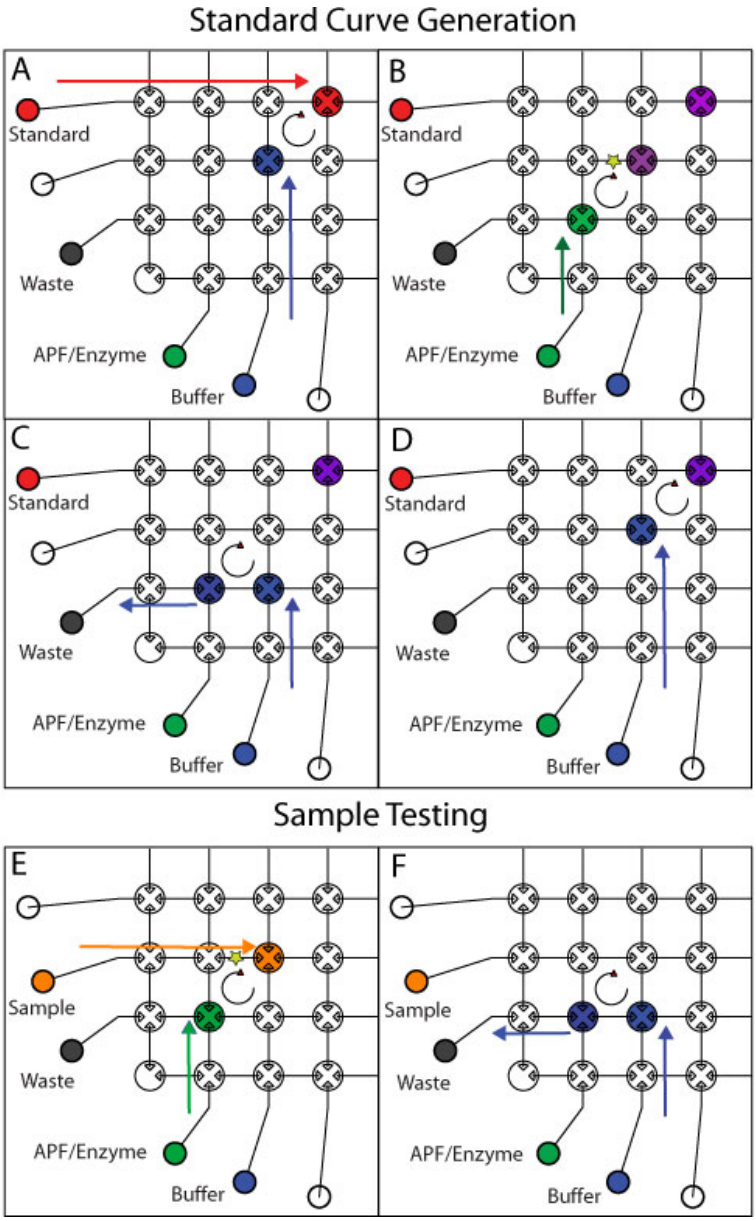

Figure 3.2 Illustration of the quantitative hydrogen peroxide assay program for the digital microfluidic platform. A hydrogen peroxide standard is diluted on-chip (A), and then mixed with aminophenyl fluorescein (APF) and horseradish peroxidase (HRP) while detecting fluorescence emission at 520 nM at the location indicated by the star (B). After washing (C), the cycle repeats itself as the next standard concentration is prepared for analysis (D). After a final washing step, a sample is loaded and mixed with APF and HRP (E), and the resulting increase in fluorescence is compared to the standard curve for quantification. After washing (F) the cycle repeats itself and the next sample is analyzed.

of 2.3 for the mixing of sample with APF–HRP by loading fluorescein into the input well designated for sample and executing the H_2O_2 assay program.

3.4 Results

Flow Rate Analysis. The maximum volume pumped per cycle in a 3-valve 5-step program was gravimetrically determined to be 120 nL at a pressure of 46 kPa and with a minimum valve actuation time of 200 ms (Fig. 3.3A). This corresponds to 84% of the displacement chamber volume which is in close agreement with previous results from linear 3-valve pumps.[66] Under these conditions, transfer of fluid between microvalves in the forward direction is maximal, and flow into closed microvalves is not observed. Low closing pressures and actuation times less than 200 ms tend to result in backflow in the pumping circuits which reduces the efficiency of transfer between valves in the forward direction. In both cases, the backflow is caused by the incomplete closure of microvalves prior to the closing of subsequent microvalves in the series. With 25 kPa closing pressures, the inclusion of additional valves in a pumping network does not significantly affect the volume pumped per cycle (Fig. 3.3B). The Automaton is therefore an effective platform for programmable movement of discrete volumes of reagents within a 2-dimensional array of microvalves.

Mixing and Dilution Programs. Fig. 3.4A shows the confocal fluorescence results of the circular mixing program. As the fluorescein is diluted with buffer, the data follow a dampened oscillatory curve during the initial mixing phase and rapidly (<5 s) reach equilibrium at an intermediate intensity value. The form of this curve is similar to data from microfluidic circular mixing circuits developed previously,[49] however, less reagents are consumed and mixing is achieved at least five times faster with the Automaton. The concentrations resulting from the mixing program are highly reproducible, as the %CV of multiple runs is less than 3.0%. Fig. 3.4B shows the result of three identical mixing programs run consecutively with intermediate washing steps. Washing was performed by pumping the results of the mixing program to a waste output, and then loading fresh buffer for a series of mixing cycles. The washing steps reduce the signal to background levels prior to the initiation of subsequent mixing programs. Fig. 3.5 shows epi-fluorescence video frames of the dilution of fluorescein and water. As the mixing program proceeds, the boundaries between buffer and dye are interdigitated, thereby reducing the effective diffusive distance for mixing. Non-laminar fluid flow during valve actuation may also contribute to this rapid convolution. Valve actuation times of 50–80 ms were found to achieve the fastest mixing times. This observation indicates that complete closure of the mixing circuit microvalves is not necessary for optimal mixing.

Fig. 3.6 presents the results from two different serial dilution programs with different dilution factors using a 4-valve circuit. In one instance, a 1.67 ± 0.04 dilution factor was achieved by utilizing the circuit dead volumes and one filled microvalve as a carryover fraction. At each iteration, the contents of one microvalve were sent to the waste, and one microvalve in the circuit was loaded with fresh buffer. Based on the isotropic etch dimensions of the dead volumes and experimentally determined volume of an open microvalve, a 1.65 dilution factor is predicted. This closely agrees with the experimentally determined dilution factor of 1.67. Starting from a 10 μM sample, this program iterates the dilution process 9 times resulting in a final concentration of 65 nM, which is indistinguishable from the background. Data from three separate runs indicate that the error increases roughly linearly with the iteration number (2.2%

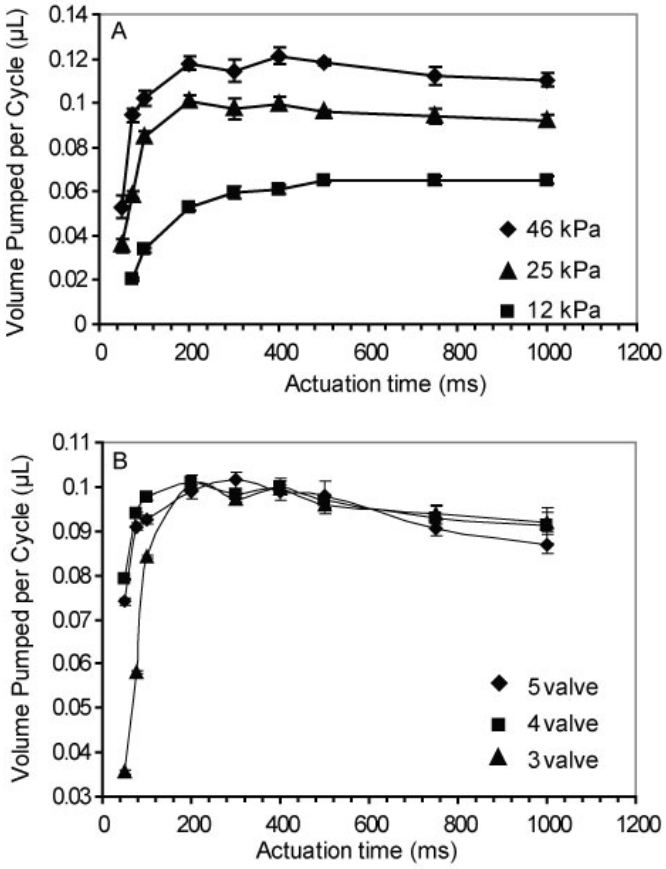

Figure 3.3 (A) A maximum volume pumped per cycle (120 nL) in a 3-valve pumping circuit was achieved using a 46 kPa closing pressure. Valve actuation times of 200 ms were sufficient to maintain this fluidic transfer efficiency. (B) The extension of conventional pumping programs to 4 and 5 valves does not significantly affect the fluid transfer efficiency.

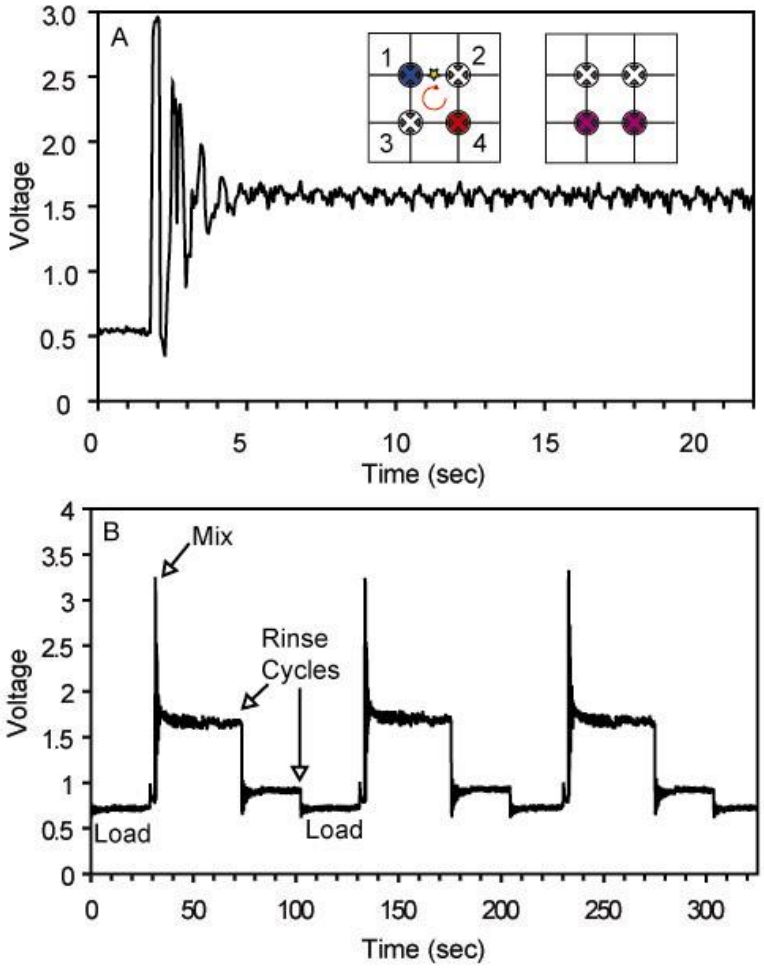

Figure 3.4 (A) Confocal fluorescence data from the reagent mixing/dilution program. Fluorescein (2.0 μM) was loaded into valve 4 and then diluted with buffer loaded into valve 1. These data were collected at the location indicated by the star. (B) Three consecutive mixing operations with intermediate washing steps.

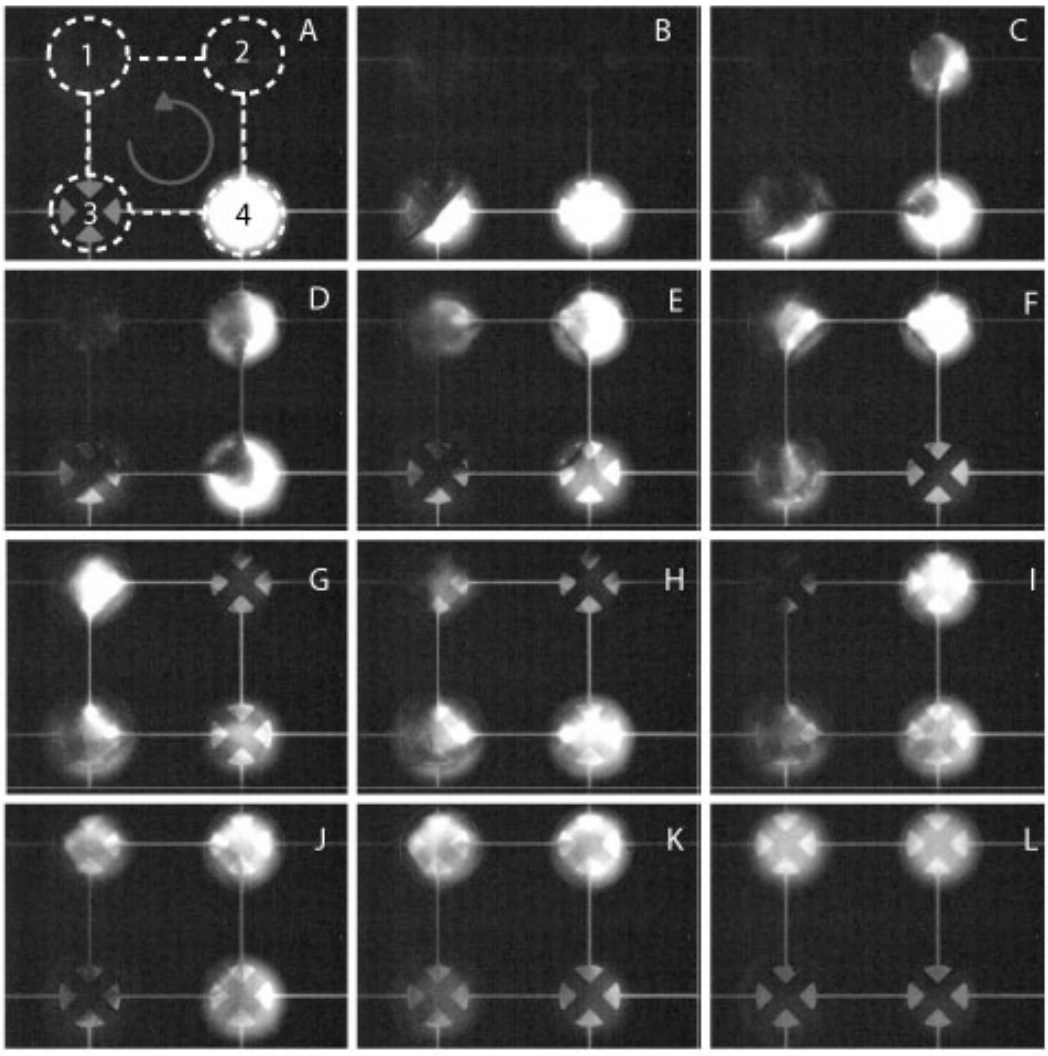

Figure 3.5 Video frames of the reagent mixing/dilution program using 80 ms valve actuations. Fluorescein was loaded into valve 4 and buffer was loaded into valve 1 (A). When valve 3 is opened, fluid enters from both valve 1 and valve 4 (B). Valve 1 is then closed and valve 2 is opened drawing fluid from valves 3 and 4 (C). Closing valve 3 completes the transfer of fluid to valves 2 and 4 (D). This transfer process is iterated in an 8-step/cycle 640 ms/cycle program (C K). After 5 cycles (3.2 sec), the contents of valves 1 and 2 appear completely homogeneous (L).

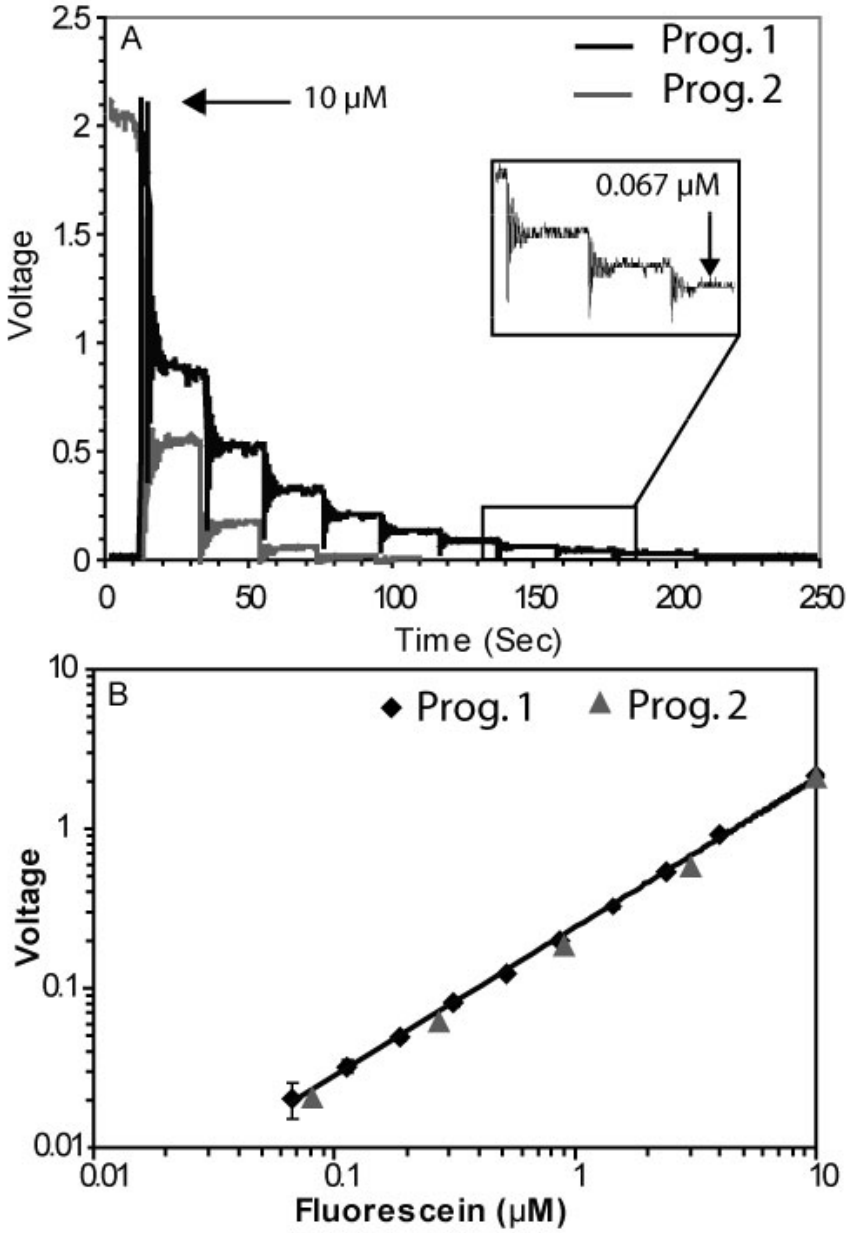

Figure 3.6 (A) Confocal fluorescence data from the standard curve generation programs. These programs iteratively dilute the contents of a 4-valve mixing circuit. A 1.67 dilution factor (Prog. 1) was achieved using dead volumes plus an open valve as the carry over fraction. A 3.33 factor (Prog. 2) was achieved by using only dead volumes as a carryover fraction. (B) Both curves are highly linear over a 1000-fold dilution range.

CV at the first dilution and 9.1% CV after the eighth dilution). In a separate program, a 3.33±0.07 dilution factor was achieved by using only the dead volumes as a carryover fraction. At each iteration, two microvalves in the circuit were loaded with buffer and the contents of two microvalves were removed to waste. For each program, the PMT voltage was plotted versus the fluorescein concentration on a logarithmic scale (Fig. 3.6B). Both of the resulting standard curves were highly linear over a 1000-fold dilution range ($R^2 > 0.99$). By using the residual contents of a single closed microvalve (14 nL) as a carryover fraction, a dilution factor of 12.6 (data not shown) is achieved (95% of predicted value). These results illustrate the versatility and programmability of the Automaton for fluidic operations involving the precise metering of nanoliter scale volumes of sample.

Fig. 3.7 shows the results from the H_2O_2 assay performed on the Automaton. HRP and APF are mixed with each standard H_2O_2 concentration during 25-cycle mixing routines. HRP catalyzes the irreversible reduction of H_2O_2 to hydroxyl radicals,[98] and the non-fluorescent APF reacts with reactive oxygen species to form a highly fluorescent product.[99] As the mixing program begins, an almost instantaneous increase in signal is observed due to the oxidation of APF. Within several seconds the signal stabilizes at a level that is proportional to theconcentration, with higher enzyme concentrations requiring fewer mixing cycles for signal saturation. After the recirculating mixing step, rinsing cycles are performed in which fresh buffer is loaded into the mixing circuit, recirculated, and then pumped to waste. Sequential decreases in signal can be observed during this phase. In the next phase of the program, samples are loaded into a mixing circuit, mixed with APF and HRP, and then the resulting signal is compared to the standard curve. Fig. 3.7 shows the results of this step using 5.0 μM H_2O_2 in buffer as a sample. A concentration of 5.0±0.2 μM is predicted based on quantification by the previously generated standard curve, thus demonstrating that the digital microfluidic platform enables a high degree of accuracy for quantitative biomolecular assays. The sample quantified in this example is within the normal range of human H_2O_2 serum levels.[96]

3.5 Discussion and Conclusion

The microfluidic Automaton presented here is a versatile platform for a broad range of sample processing operations enabling facile integration and automation of multi-step biomolecular assays. The system is capable of precise metering of nanoliter scale sample volumes and enables accurate quantitative analysis. Furthermore, the platform enables automated assay optimization by programmable adjustment of reagent concentrations.

The H_2O_2 assay demonstrated here serves as a model assay for a wide range of quantitative molecular assays that follow a program of (1) generating a standard curve, (2) combining standards with labeling reagents and (3) mixing samples with labeling reagents for quantification. For instance, the HRP– H_2O_2 system has been coupled with oxidases to detect a range of metabolites including glucose, uric acid, and acetylcholine. Assays for these analytes follow a similar procedure and can be automated by the Automaton.

The washing operations demonstrated here enable a large number of unique processes to occur serially within a limited number of cells in the array. This, in combination with the sample dilution capabilities, would be particularly useful in instances where the tested sample is outside of the dynamic range of the standard curve. In such a case, the mixing circuit could be washed to

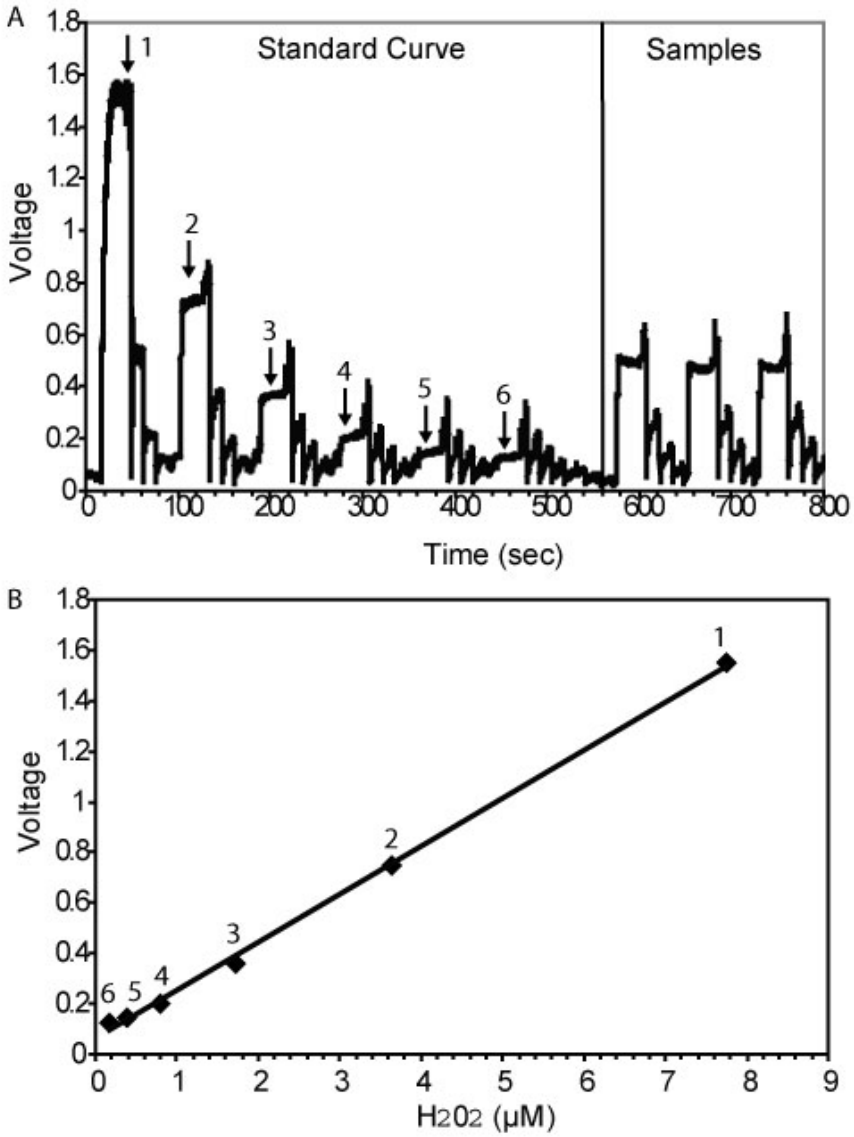

Figure 3.7 (A) Confocal fluorescence data from the quantitative hydrogen peroxide assay using the digital microfluidic Automaton. After each standard level is generated, continuous mixing with APF–HRP results in a rapid increase and then stabilization of fluorescence signal. Rinsing cycles are then performed to remove the reaction product from the array prior to the generation of the next standard concentration. After the standard curve is generated, triplicate samples are processed for quantification. (B) The relationship between hydrogen peroxide standard concentration and PMT signal.

remove saturated reaction products, and then reused for dilution by loading sample and buffer. This would be particularly useful for serum H_2O_2 assays since conditions of oxidative stress such as chronic allograft neuropathy may result in a wide range of elevated serum levels.[96]

Since a single 4-valve circuit can be loaded, mixed, and then effectively washed in less than 30 s, large scale combinatorial mixing operations can be implemented at practical timescales. For instance, all pairwise combinations of a set of 16 reagents could be evaluated within approximately 2 h using a single mixing circuit. The time scale of such a procedure can be further reduced by performing the mixing operations in parallel at different locations in the array. Mixing circuits can also be programmed to utilize a larger number of microvalves. This can be used to simultaneously mix larger sets of reagents, or to achieve different mixing ratios.

The number and complexity of possible operations grow exponentially with the number of microvalves controlled in the Automaton. With the current 64-bit processor, a total of $1.84 X10^{19}$ unique states can be defined for each step of a program. Using the current valve and channel design, a 20 X 20 array fits onto a 100 mm chip, however, an additional wafer layer would be necessary to accommodate all of the pneumatic addressing channels. The extra wafer can be added to the pneumatic side via thermal bonding such that each microvalve is addressed through a 500 micron via hole to its displacement chamber. Such a system would also enable a significant reduction of the channel lengths between microvalves and therefore dead volumes. Microvalves with as little as 5 nL displacement volumes have been demonstrated by our group,[39] and all of the fluidic features can be scaled down by reducing etch depth to as little as 4 microns.[100] These features should enable the precise metering of picolitre scale sample volumes within the Automaton.

We have previously shown that the power consumption and off-chip control equipment can be reduced by the use of binary demultiplexing pneumatic circuits connected to pneumatic latching valves.[58] In this pneumatic demultiplexing system, 2^{N-1} microfluidic valves are controlled by the actuation of N off-chip solenoid valves. We are currently investigating the feasibility of this system for microvalve actuation in the Automaton. A 6-bit demultiplexing system can address a 64-bit valve array within the space available on a 3-layer (glass–PDMS–glass) 100 mm diameter chip. In such a system, only 6 pneumatic control inputs are required to achieve the $1.84 X 10^{19}$ unique states.

The extension of this technology to inhomogeneous assays such as ELISA will be enabled by the use of methods to derivitize capture molecules either on a surface within a microvalve[101] or on the surface of microbeads that are held in the valves or channels. We have previously demonstrated the utility of derivitized magnetic particles for capturing both DNA[50] and cell[36] targets within microreactors. Magnetic particles can be immobilized within a reactor by the application of an external magnetic field during reagent delivery and washing steps of ELISA.[102] The programmability of the Automaton enables a wide range of fluidic processing operations on the same platform and offers significant advantages over other microfluidic systems such as electrowetting and conventional valve-controlled microchannel systems. The development of standardized mixing, washing, and transport operations that can be implemented combinatorially enables the performance of diverse protocols on the same device. Combined with the simplicity of device fabrication, these features will enable rapid prototyping of diverse

bioanalytical assays, synthetic biological, and synthetic chemical methods using such a universal automated microfluidic platform.

3.6 Acknowledgements

The Financial support for this work was provided by grant U54ES016115 from the U.S. National Institute for Environmental Health Sciences (NIEHS) through the trans-NIH Genes, Environment and Health Initiative. The content is solely the responsibility of the authors and does not necessarily represent the official view of the National Institute of Environmental Health Sciences or the National Institutes of Health. Additional funding was provided by Samsung Corporation. The Automaton was fabricated in the UC Berkeley Microlab with the assistance of Eric Chu. We gratefully acknowledge the initial conceptual idea of the Automaton by William Grover.

Chapter 4: Microvalve Enabled Digital Microfluidic Systems for High-Performance Biochemical and Genetic Analysis

This was reprinted with permission from "Microvalve Enabled Digital Microfluidic Systems for High-Performance Biochemical and Genetic Analysis," by Erik C. Jensen, Yong Zeng, Jungkyu Kim, and Richard A. Mathies, (2010) J. Assoc. Lab. Auto., 15, 455-463. © The Society for Laboratory Automation and Screening. Erik C. Jensen and Yong Zeng contributed equally to the article.

4.1 Abstract

Microfluidic devices offer unparalleled capability for digital microfluidic automation of sample processing and complex assay protocols in medical diagnostic and research applications. In our own work, monolithic membrane valves have enabled the creation of two platforms that precisely manipulate discrete, nanoliter-scale volumes of sample. The digital microfluidic Automaton uses two-dimensional microvalve arrays to combinatorially process nanoliter-scale sample volumes. This programmable system enables rapid integration of diverse assay protocols using a universal processing architecture. Microfluidic emulsion generator array (MEGA) devices integrate actively controlled three microvalve pumps to enable on-demand generation of uniform droplets for statistical encapsulation of microbeads and cells. A MEGA device containing 96 channels confers the capability of generating up to 3.4 X 10^6 nL volume droplets per hour for ultrahigh-throughput detection of rare mutations in a vast background of normal genotypes. These novel digital microfluidic platforms offer significant enhancements in throughput, sensitivity, and programmability for automated sample processing and analysis.

4.2 Introduction

The development of microfluidic sample processing and microvalve technology offers significant opportunities for the miniaturization and large-scale integration of automated laboratory systems. Integrated microvalve control enables precise metering of nanoliter-scale sample volumes through networks of microchannels.[16,43,66,77] Functions including on-chip pumping, reagent mixing, and droplet generation have been used to automate a wide range of biomolecular assays. The structure of the normally closed, monolithic membrane valves developed by our group is illustrated in Figure 4.1. These monolithic membrane valves have been used to automate a wide range of applications from single nucleotide polymorphism-based DNA computing[50] to nanoliter-scale Sanger DNA sequencing.[39] Here, we report on recent advances in the development of two digital microfluidic platforms enabled by microvalve technology that achieve massively parallel biomarker analysis, and an unprecedented level of programmability for assay automation.

4.3 Microfluidic Automaton

A digital microfluidic Automaton has been developed, based on two-dimensional microvalve array technology, for sample processing and analysis (Fig. 4.2). Digital transfer of fluids between microvalves enables precise and rapid metering of nanoliter-scale sample volumes through programmable valve networks within the array.[63] The basic program for the transfer of fluids between microvalves in a rectilinear array begins with a single open microvalve filled with fluid. An adjacent microvalve is opened, drawing fluid from the first valve. The first valve is then closed with an applied pneumatic pressure, forcing the remainder of the fluid into the second valve. A 120-nL bolus of fluid is transferred between the microvalves under optimal conditions. Programs for reagent routing, mixing, rinsing, serial dilution, storage/ retrieval, and many other operations have been developed. High-level device programming enables rapid automation of diverse assay protocols on a common chip format. Previous programmable digital microfluidic platforms have been demonstrated using electrowetting arrays;[87-89] however, these systems often suffer from significant imprecision in droplet splitting operations, thus limiting quantitative control.[56]

The pneumatically actuated microvalve array is composed of a three-layer glass polydimethylsiloxane (PDMS) hybrid structure,[66] and incorporates a rectilinear network of

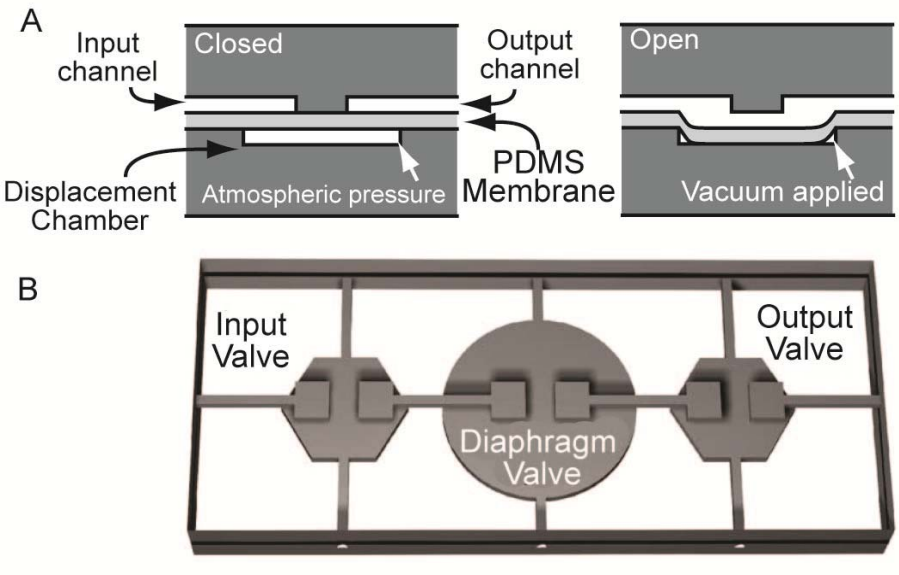

Figure 4.1 Cross-sectional view through a monolithic membrane valve. The microvalves are composed of a featureless polydimethylsiloxane (PDMS) membrane sandwiched between a discontinuous fluidic channel and a pneumatic displacement chamber. (A) The valves are normally closed with the PDMS membrane resting on the valve seat. Application of a vacuum to the displacement chamber through a control channel pulls the PDMS membrane away from the discontinuity, allowing fluid to fill the chamber and/or flow across the discontinuity in the fluid channel. (B) Three independently actuated microvalves in series form an integrated micropump for transport of samples and reagents.

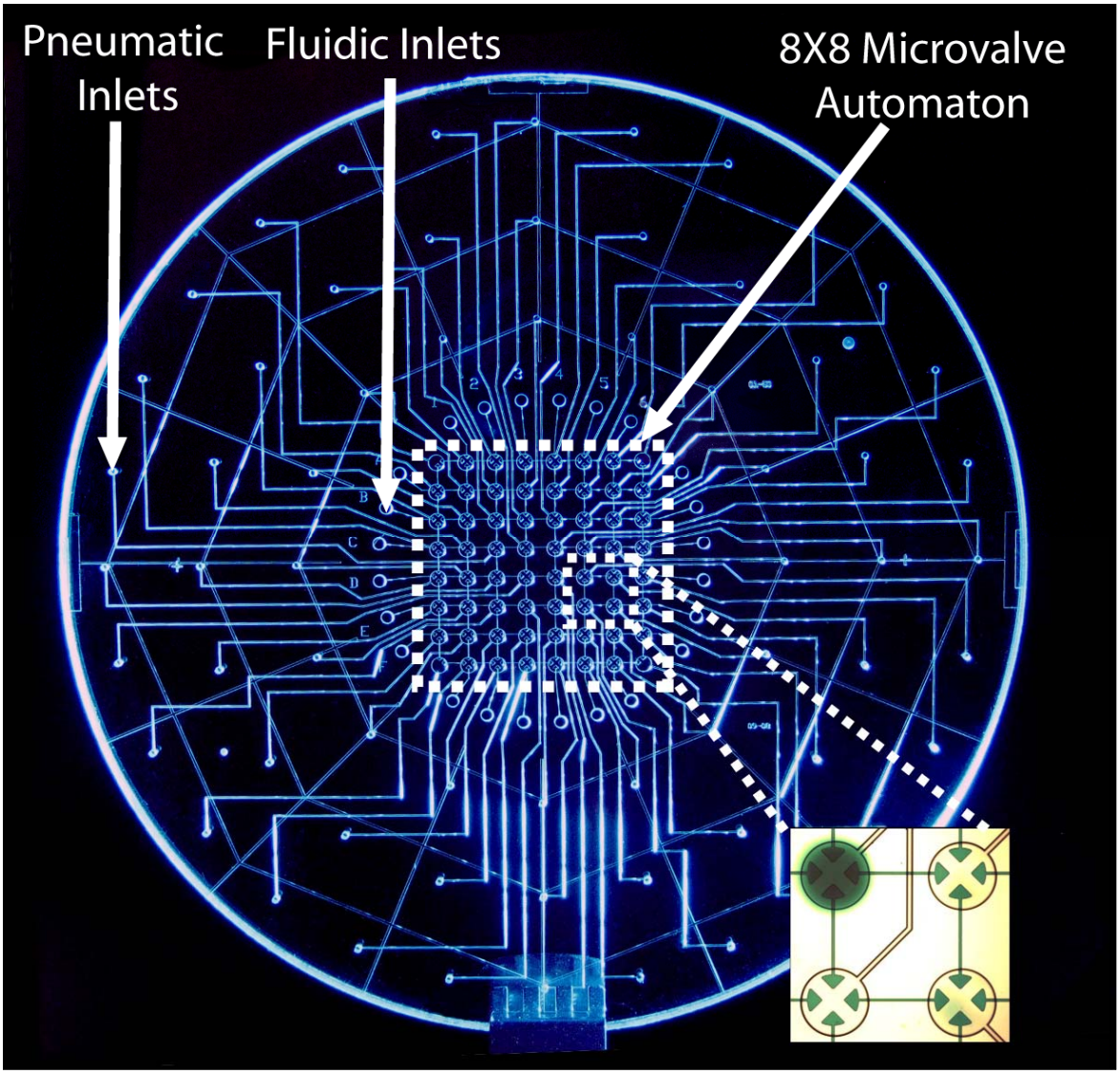

Figure 4.2 Photograph of the digital microfluidic Automaton. The four-way microvalves control fluid flow through a rectilinear grid of discontinuous fluidic channels. The inset shows a close-up portion of the array with a single microvalve storing dye in an automated program. The individual microvalves in this array serve as 120 nL reaction chambers and fluidic control mechanisms.

fluidic channels. Vacuum and pressure are supplied to the microvalves through drilled inputs on the pneumatic layer via computer-actuated solenoid valves. Samples and reagents can be loaded from drilled fluidic reservoirs to any subset of the microvalves by a programmed actuation sequence. The channels in the pneumatic layer are isotropically etched to a depth of 70 nm, whereas the fluidic features are etched to a depth of 30 nm to reduce dead volumes between the microvalves.

Programmable microfluidic systems for assay automation typically require active mixing mechanisms due to the laminar flow profile of fluids within microchannels.[44] Rapid reagent mixing is achieved with the Automaton by cyclically transferring the contents of two or more valves within a loop. For instance, an eight-step, 640 ms subroutine is iterated to cycle the contents of two microvalves through a four-valve loop. Dilution of fluorescein standards with buffer and analysis by fluorescence microscopy indicate this mixing is complete in less than 5 s (Fig. 4.3A). The digital fluidic transfers used in these programs result in mixing operations that are more than five times faster than traditional microfluidic mixing loops.[49]

Figure 4.3B shows data from three consecutive fluorescein dilution operations with intermediate valve rinsing steps. This serial processing program results in highly reproducible mixing proportions for nanoliter-scale sample volumes. Furthermore, rinsing programs enable reuse of valve networks for different operations at different time points in a program. The output from a mixing circuit can be stored for future retrieval, or it can be used as the input for downstream processing operations. Iteration of the mixing program enables rapid generation of precise serial dilutions with adjustable dilution factors. Because the dead volumes of an individual microvalve can be used as a carryover fraction, as little as 14 nL can be precisely metered and mixed using the current design, and subnanoliter volumes could be similarly controlled by reducing the etch depth of fluidic features.

More complex operations involving larger reagent sets can be achieved by using larger microvalve circuits for mixing. Figure 4.4 shows video frames of a program in which all possible combinations of a set of four reagents are prepared. The program is initialized by loading a subset of the four input reagents to the mixing loop. The same program can then be used to mix the reagents regardless of the size of the loaded subset. The scale of these operations can be increased by simply including more microvalves in the mixing circuit. Several of the basic operations described above were combined to develop a rapid, quantitative assay for H_2O_2, a biomarker of oxidative stress (Fig. 4.5). Elevated serum H_2O_2 is an indicator for oxidative cellular damage in conditions such as chronic allopathic neuropathy, the leading cause of kidney transplant failure.[96] In this program, a H_2O_2 standard was serially diluted, stored, mixed with horseradish peroxidase and aminophenyl fluorescein, and analyzed using laser-induced fluorescence to produce an on-chip calibration. After introduction of sample, this fully automated program achieves a submicromolar limit of detection with a 14-min runtime. Samples of H_2O_2 (5.0 μM) prepared at the normal human serum concentration are quantified with a high level of precision and less that 4% error. Furthermore, this program can be extended to a wide range of metabolic analytes without modification.

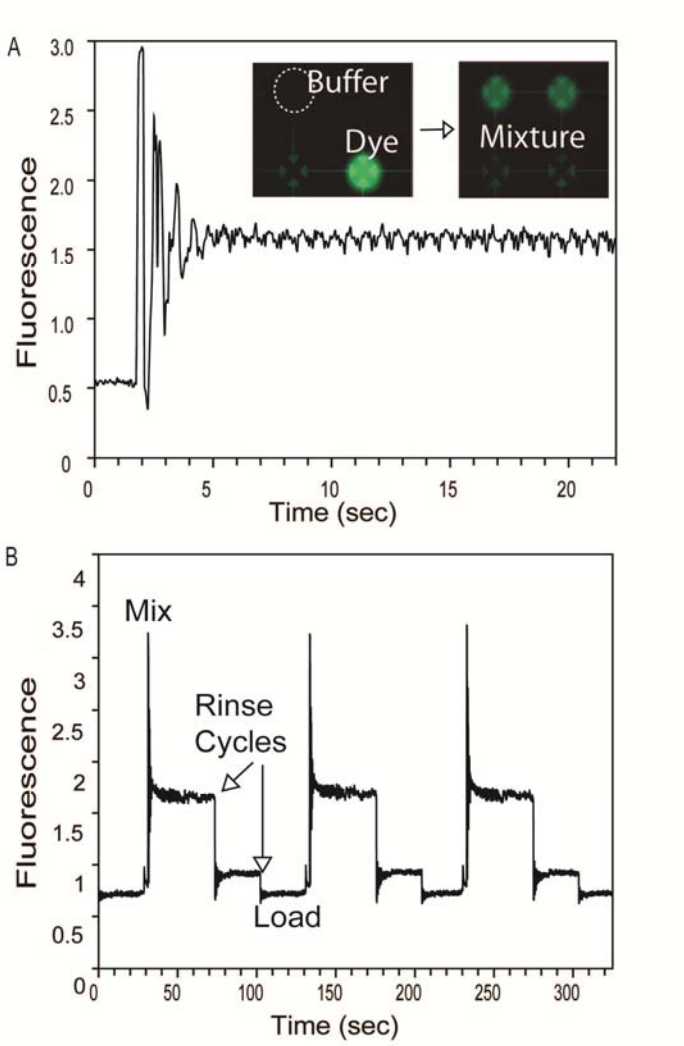

Figure 4.3 (A) Confocal fluorescence data and epifluorescent images from a reagent mixing/dilution program. Fluorescein and buffer were loaded into separate valves in a four-valve mixing circuit. Cyclic transfer of the volumes within the circuit results in rapid reagent mixing. As the fluorescein is diluted with buffer, the data follow a dampened oscillatory curve during the initial mixing phase and rapidly (< 5 s) reach equilibrium at an intermediate intensity value. (B) Three consecutive mixing operations with intermediate washing steps. These data demonstrate both the reproducibility of mixing operations and the efficiency of washing steps.

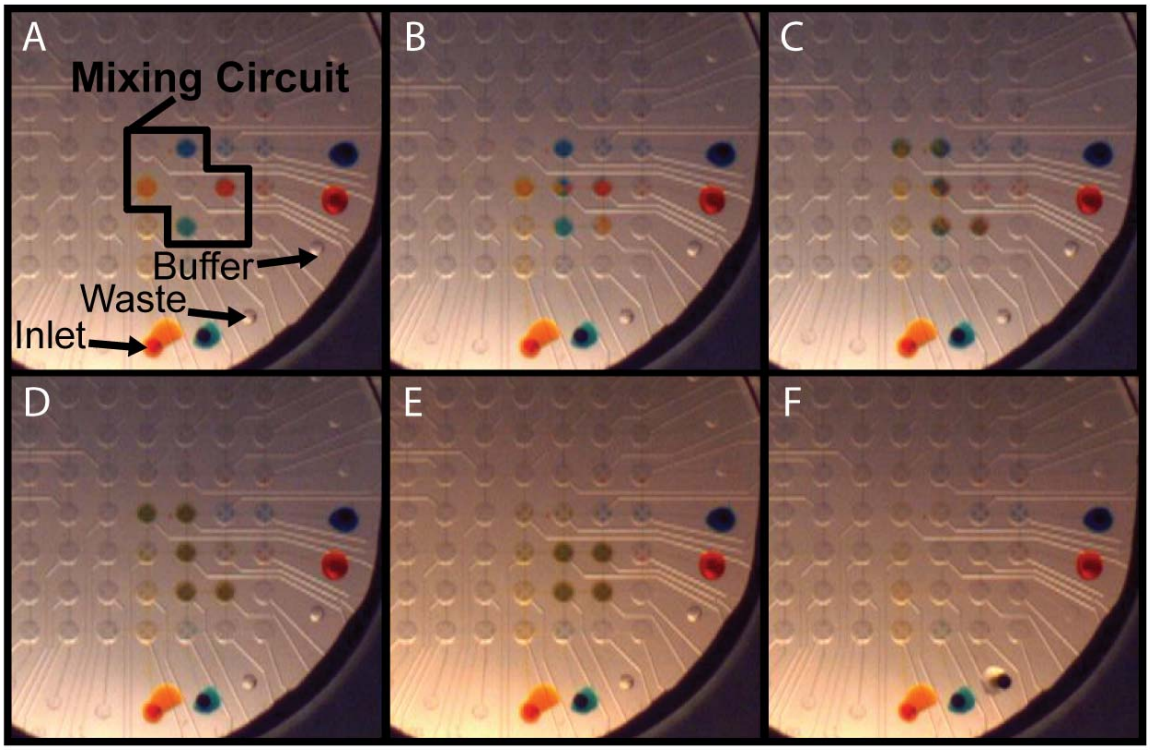

Figure 4.4 Combinatorial mixing program. (A) Any subset of four unique input samples can be loaded into a seven-valve mixing circuit. Reagents are partially mixed during the first cycle of recirculation (B, C) and completely mixed in subsequent cycles (D, E). Mixing circuit microvalves are cleared by a washing program (F).

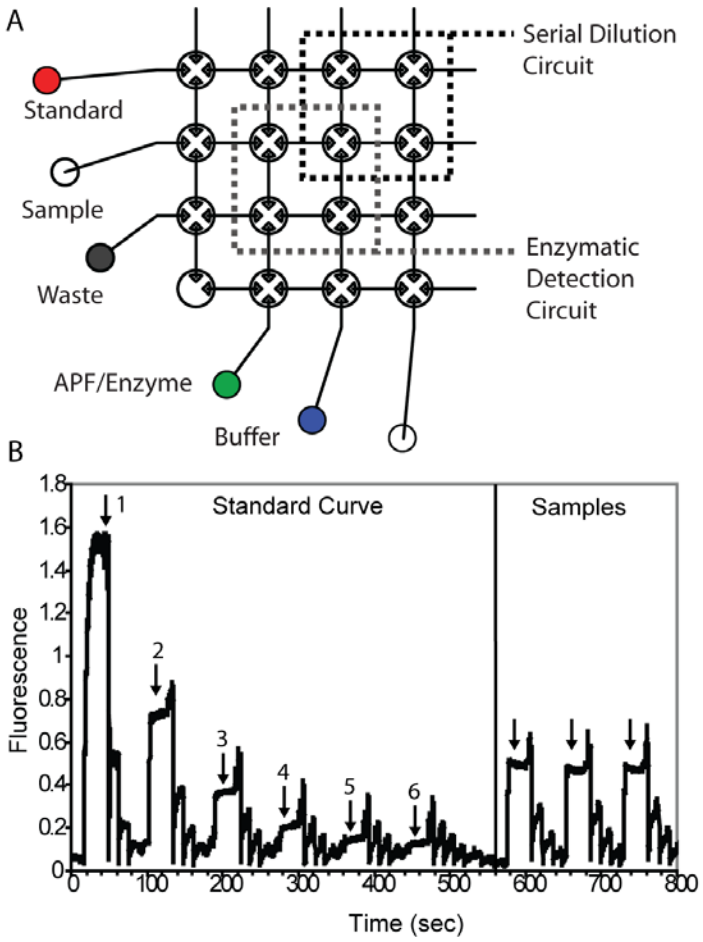

Figure 4.5 (A) Details of a fully automated assay for H_2O_2, a biomarker for oxidative stress. A H_2O_2 standard is diluted with buffer in the serial dilution circuit. A portion of the dilution is stored, and the remainder is transferred to the enzymatic detection circuit where it is mixed with aminophenyl fluorescein and horseradish peroxidase. During this phase, the aminophenyl fluorescein is oxidized to form a highly fluorescent product. After rinsing the enzymatic detection circuit, the stored H_2O_2 dilution is further diluted and the program is repeated to generate a standard curve. Finally, 120-nL samples are loaded and mixed with detection reagents for quantification. (B) Confocal fluorescence data acquired from the detection circuit during the performance of the assay. Arrows indicate the points in the assay where mixing is complete and data are collected.

We have recently enhanced the capabilities of this platform by developing procedures for inhomogeneous immunoassays. Magnetic microspheres coated with a capture antibody are loaded into specific microvalves in the array by trapping them in an external magnetic field (Fig. 4.6A). An individual capture microvalve is held continuously open while adjacent microvalves are actuated to transfer the antibody-coated microbeads from an inlet. External application of an 1/8th-in. diameter cylindrical neodymium magnet to the pneumatic wafer traps the magnetic microbeads only in the selected capture microvalve. The amount of beads loaded to the capture microvalve is adjusted based on the actuation rate and total program runtime.

To demonstrate a fluorescence enzyme-linked immunosorbent assay, we used magnetic microbeads coated with Fc-specific goat antimouse Immunoglobulin G (IgG) (Bangs Labs, BM550, Fishers, IN). Figure 4.6B illustrates the immune complex formed to detect mouse IgG. Before starting the assay, all microvalves and channels were treated with Superblock (Thermo Scientific, Waltham, MA). Approximately, 150 ng of beads were transferred to each capture microvalve as described above. Capture microvalves were held continuously opened for the duration of the assay. A total of 3 mL mouse IgG (Trevgen 4360-MC-100) in Superblock was transferred through the capture microvalve in a continuous pumping mode to a designated waste outlet. A similar program was used to rinse unbound analyte from the capture microvalves. We found that opened capture microvalves could be effectively rinsed in less than 30 s using tris-buffered saline tween-20 (Fig. 4.6C). After loading 0.8 mg/mL horseradish peroxidase-conjugated antimouse IgG (Santa Cruz Biotechnology, SC-2371, Santa Cruz, CA) and rinsing as described above, capture microvalves were filled with amplex red detection reagent (Invitrogen, A22188, Carlsbad, CA). After a 5-min incubation, the capture microvalves were imaged using epifluorescence microscopy. Figure 4.6D and E show the increase in fluorescence signal observed for a mouse IgG positive control after the 5-min incubation. These results indicate successful capture and detection of a protein target using the digital microfluidic Automaton without additional surface modification steps.

We have shown the utility of our digital microfluidic Automaton for the performance of diverse bioassay protocols on a common chip format. With the current 64-bit processor, 1.84 X 10^{19} unique states can be defined for each step of a program. This, in combination with the capabilities described above, demonstrates an unprecedented level of programmability for the automation of microfluidic bioassays. The scaling of the current device is only limited by the one-to-one correspondence between off-chip pneumatic solenoid actuators to microvalves in the array. Up to 96 solenoid valves could easily be controlled by a single USB input/output card (National Instruments, USB-6509, Austin, TX). However, we have previously shown that binary demultiplexing pneumatic circuits connected to pneumatic latching valves enable the control of $2N^{-1}$ microfluidic valves using N off-chip controllers.[58] Although the longer actuation times required for the demultiplexed latching valves (120 ms) would reduce the speed of the digital microfluidic Automaton, further design optimization of these structures may enable more rapid sample processing capabilities.

4.4 Microfluidic Emulsion Generator Array

Single-cell analysis is imperative to understanding cellular heterogeneity, which underlies mechanisms in complex biological systems and diseases, such as cancer. Monolithic membrane valve technology has enabled the development of a microfluidic platform for high-performance

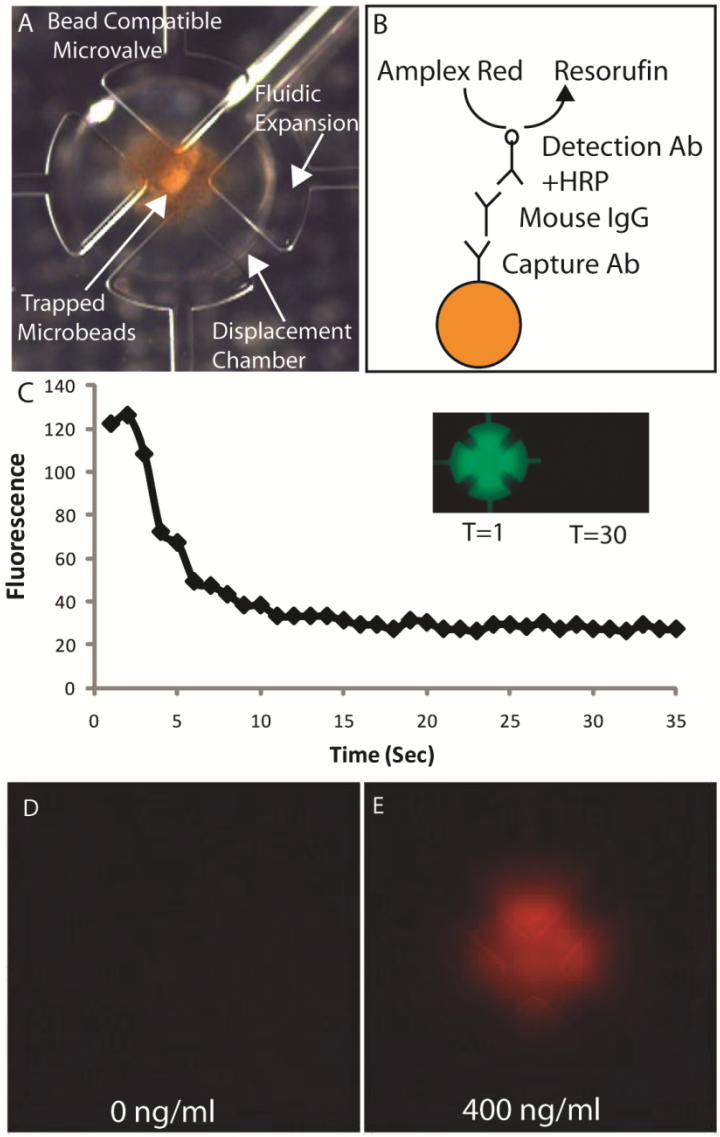

Figure 4.6 (A) Trapping microvalve loaded with approximately 120 ng of magnetic microbeads coated with antimouse IgG. The bead compatible digital microfluidic Automaton uses microvalves with larger fluidic expansions to prevent the beads from becoming trapped as they are transferred through the array. (B) Schematic of the immune complex formed in the immunoassay for mouse IgG. (C) Fluorescence profile obtained while rinsing 10 μM fluorescein dye from the trapping microvalve. The same program was used to remove unbound analyte and detection antibody after their corresponding incubations. Epifluorescence images of trapping valves after performing the assay with a negative control (D) and 400 ng/mL mouse IgG sample (E).

single-cell genetic analysis (SCGA). As illustrated in Figure 4.7A, we have devised a microfluidic emulsion generator array (MEGA) device with an integrated micropump that operates four parallel cross injectors for aqueous droplet formation.[38] The micropump consists of a serial array of three microvalves connected through a via hole to a microfabricated network enclosed between two thermally bonded glass wafers.[91] The microfluidic network is composed of symmetrically bifurcated microchannels to form four parallel crosses or droplet nozzles at the junctions. This system is used to partition individual cells within the droplets for high throughput genetic screening applications.

On-chip pumping confers the capability of on-demand generation of droplets with well-controlled frequency and droplet size. The on-chip pump drives an aqueous PCR mix into the cross injector where it is pinched by the oil flow infused from side channels (Fig. 4.7B, images 1 and 2). Because of the pulsatile nature of valve actuation, the aqueous solution is pulled back at the end of one pumping stroke, causing the release of the droplets (images 3 and 4). As a result, the frequency of droplet formation is controlled by the pump actuation frequency. In addition, the droplet size can be independently tuned by varying the actuation pressure to change the flow rate of pumped fluid. In contrast, other passive microfluidic droplet techniques, such as flow focusing, rely on the interfacial instability to form droplets, which involves complicated interplay between many parameters, including channel geometry, flow rates of two phases, and surfactant.[92,103,104] We found that the pulsatile pumping allows effective transport of large microbeads against gravity sedimentation to ensure the predictable stochastic encapsulation of single beads/cells into uniform nanoliter droplets (Fig. 4.7C). The size deviation of 3-nL droplets was found to be 3.8%, comparable to that reported by using passive microdroplet array generators (1.3-nL droplets, coefficient of variation 3.7%).[104] These results demonstrate that our technique presents a robust platform for actively controlled generation of uniform nanoliter droplets, which is crucial to achieve quantitative single-cell genetic measurement.

Our microfluidic technique is readily scalable, as the four channel array defines a basic unit for multiplexed MEGA devices. To achieve a higher density, we have designed a novel ring micropump composed of three pairs of coaxial ring-shaped valve seats connected by offset channels, and corresponding circular displacement trenches. This compact micropump permits the high-density integration of 96 T-shaped droplet generation channels on a 4-in. wafer (Fig. 4.8). A custom-made assembly module is used to deliver reagents and collect droplets from the 96-channel MEGA. The 96-channel MEGA system has a maximum droplet production rate of 3.4×10^6 droplets per hour, which greatly improves the detection limit and processing time for detection of low-frequency events.

We have used the 96-channel MEGA to perform high throughput bead-based multiplex PCR assays for single-cell genotyping. Multiplex SCGA enables the detection and quantification of both normal and mutant cells by targeting genes specific to individual cell types. In this approach, beads and cells are diluted in the PCR mix and partitioned into individual uniform reaction droplets dispersed in a carrier oil phase using a MEGA device. Statistical distribution of single beads and cells leads to a fraction of droplets containing both one bead and one or more cells. Beads are functionalized with forward primers targeting both cell types, and the PCR mix contains reverse primers each labeled with a unique fluorescent dye. Thousands of such droplets,

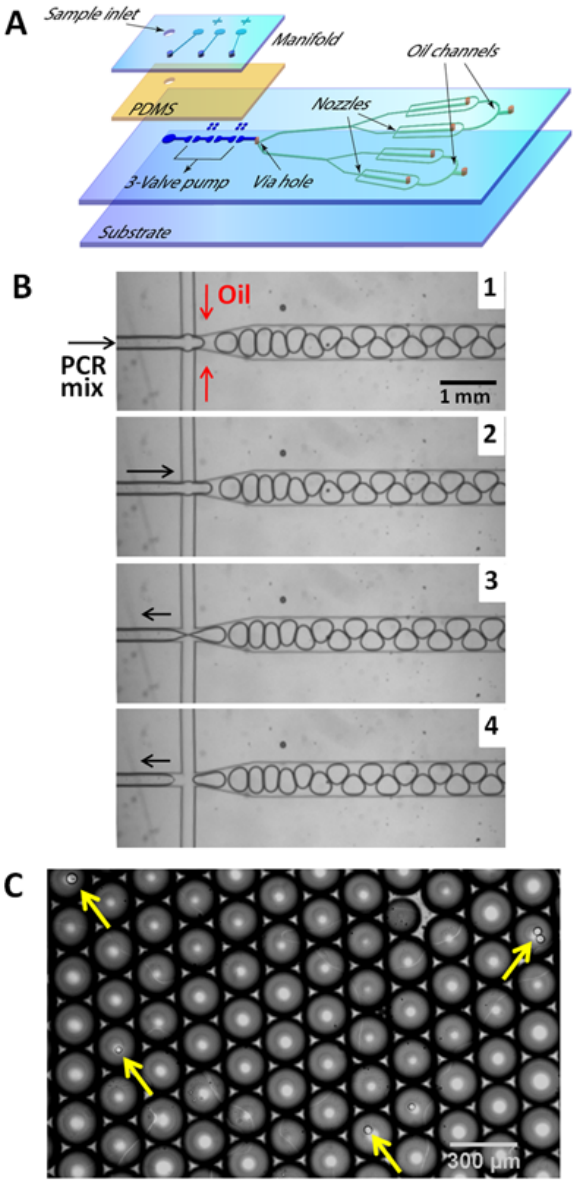

Figure 4.7 (A) Exploded view of the four-layer, four-channel MEGA device with an integrated micropump driving four parallel nozzles for droplet generation. (B) Image sequence of a cycle of droplet formation at a frequency of 5.6 Hz. PCR mix is pumped through the cross injector and pinched by the oil flow infused from side channels (images 1 and 2). The aqueous solution is pulled back at the end of each pumping cycle, which causes the release of the droplets (images 3 and 4). As a result, the droplet formation is synchronized with the pump actuation, and the droplet size is determined by the flow rate of pumped fluid. (C) Optical micrograph of highly uniform droplets generated by our method containing a predictable stochastic distribution of primer-functionalized agarose beads (~34 µm, indicated by arrows). For this experiment, the average bead concentration was 0.1 beads per 3-nL droplet.

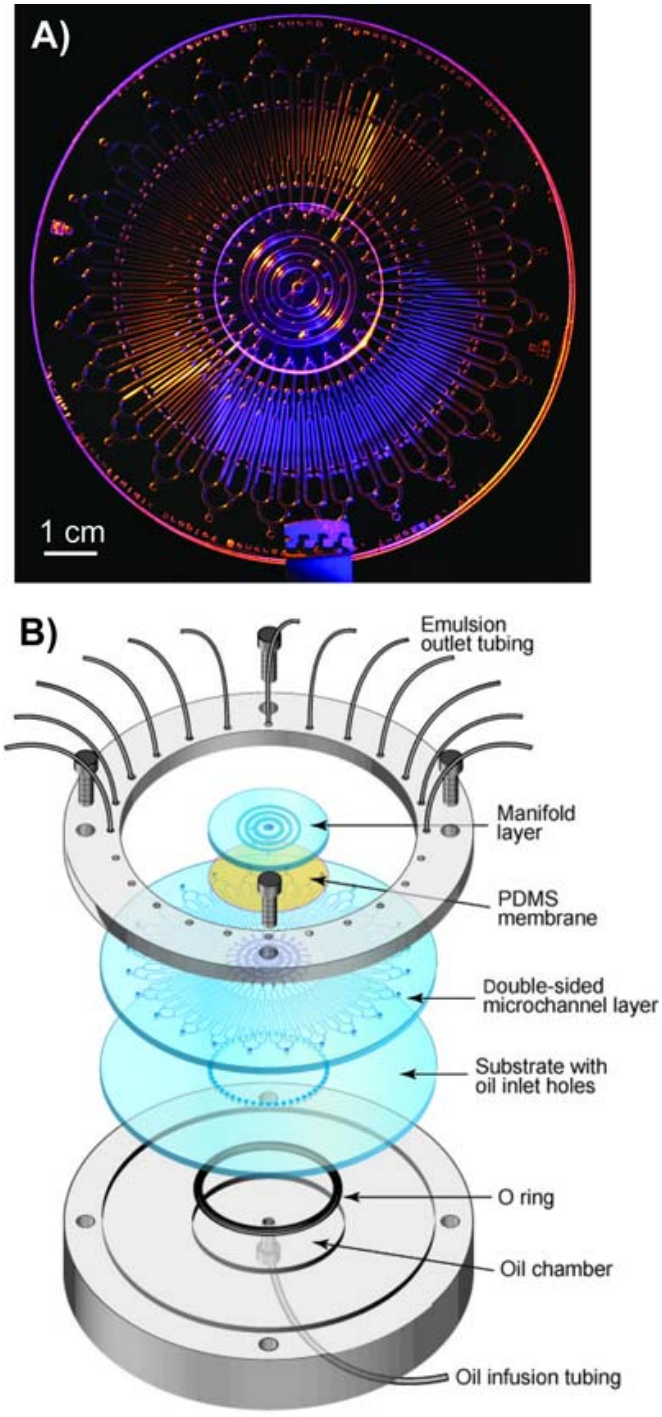

Figure 4.8 (A) Photograph of a 96-channel MEGA device. (B) Exploded view of the chip with world-to-chip interfacing manifolds used for pneumatic actuation and oil flow.

generated by MEGA chips within minutes, are collected in standard PCR tubes and thermally cycled in parallel. Post-PCR beads are recovered from the emulsion and rapidly analyzed by flow cytometry for multicolor fluorescent digital counting of each single-cell detection event. Beads coexisting with only one cell type will carry one type of dye-labeled double stranded amplicons, while beads compartmentalized with different types of target cells will be labeled with two dyes.

We have applied the MEGA devices for low-frequency detection of pathogenic Escherichia coli (E. coli) O157 bacteria in a background of nonpathogenic E. coli K12 cells (Fig. 4.9). Quantitative detection of low-frequency O157 cells can be achieved at an average cell concentration up to 100 E. coli cells per 2.5-nL droplet, which greatly increases the analysis throughput and hence the detection sensitivity, without excessively extending the droplet production time (Fig. 4.9A). This result indicates that the use of nanoliter droplets provides sufficient reagents for efficient and specific multiplex PCR amplification, and confers tolerance to PCR inhibition, as the inhibitors released from cells are significantly diluted in the large droplets. This performance would be very challenging using picoliter droplets. Compared with other droplet-format microdevices for PCR assays, such as electrowetting-on-dielectric chip[105] and SlipChip,[106] our method offers the ability of automated mixing and single bead/cell encapsulation with much higher throughput.

A detection limit of 1/105 has been achieved by screening ~10^6 cells with only 30 min of droplet generation when using the 96-channel MEGA (Fig. 4.9B). The entire procedure, including PCR thermal cycling, post-PCR cleanup, and flow cytometry takes approximately 4 h and compares favorably to standard PCR-based detection assays while providing much better sensitivity. Our quantitative digital format outperforms previously reported microsystems, which detect only one bacterial strain by PCR with detection limits ranging from a few to 10^4 bacterial cells.[79,107,108] Because our multiplex SCGA approach digitally detects single cells, the detection limit can be further improved to 1/106 or lower by extending droplet generation time to analyze more cells. Such sensitivity makes the technique a promising candidate for many applications, such as food safety, where microbial pathogen detection needs to meet a zero tolerance policy for many foods.[109] These results also indicate the feasibility of the MEGA platform for other applications, for instance, the analysis of cancer development and progression, circulating tumor cells, and stem-cell differentiation, where high-throughput genetic variation analysis of mammalian cells at the single cell level may facilitate a deeper understanding of the biological mechanisms involved.

4.5 Summary

Advances in monolithic membrane valve technology have enabled the development of robust platforms for digital microfluidic assay automation. The programmability, speed, throughput, and low-sample volume requirements conferred by these systems offer significant advantages compared with conventional benchtop robotic laboratory automation systems and specialized microfluidic processing platforms. The digital transfer of fluids between microvalves in the microfluidic Automaton platform enables the implementation of diverse serial and combinatorial sample processing operations on a common chip format. The programmability of this platform can be exploited to replace the specialized microfluidic circuits used in conventional lab-on-a chip devices. Similarly, the use of microvalve pumps in the MEGA

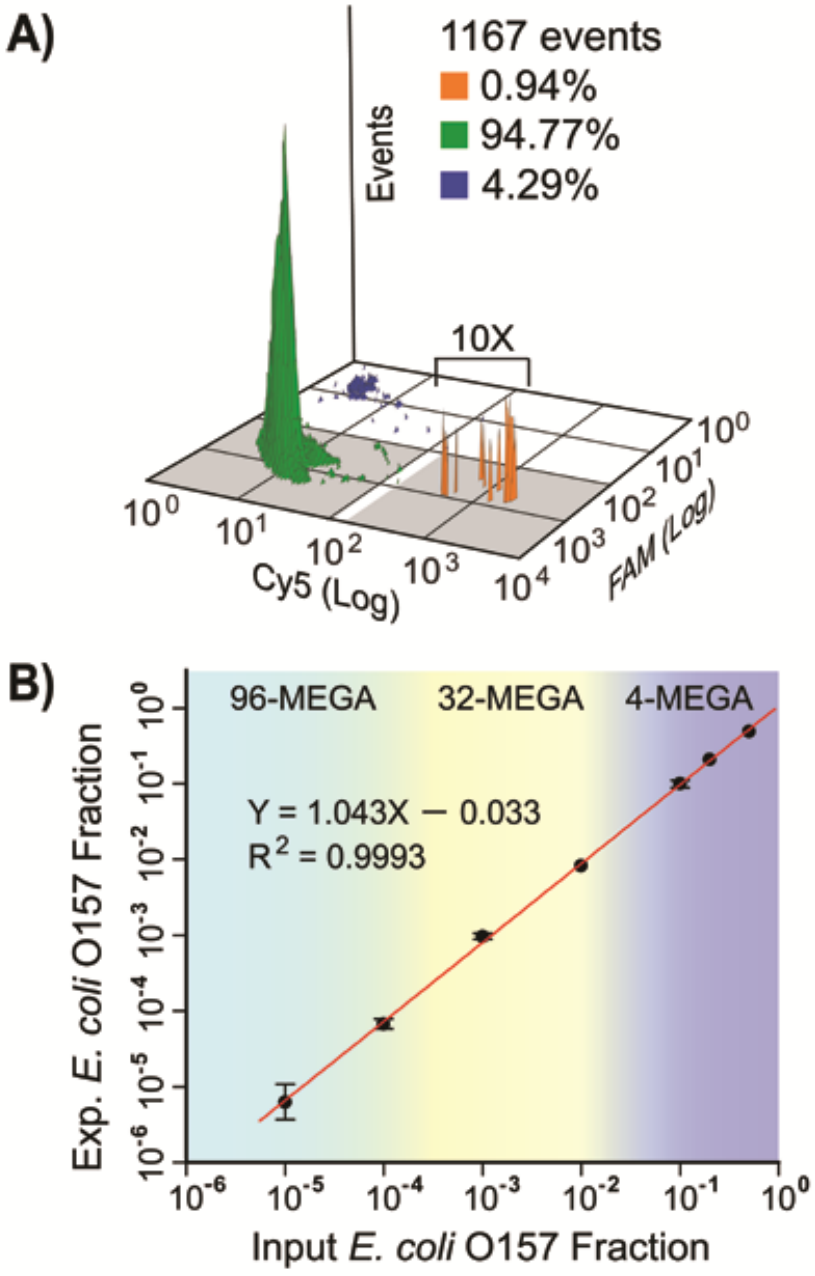

Figure 4.9 (A) Two-dimensional flow cytometry results of fluorescent amplicon beads showing detection of pathogenic E. coli O157 in a background of harmless E. coli K12 at a ratio of 10^{-4}. (B) Differently multiplexed MEGA devices enable quantitative detection of O157 frequency over five orders of magnitude with a detection limit of $1/10^5$.

platform enables high-throughput droplet generation with programmable droplet volumes and formation rates. This programmability has been instrumental for high-throughput screening of single cells for low-frequency genetic variations. These novel, digital sample-processing technologies represent significant advances in the field of microfluidic laboratory automation.

4.6 Acknowledgements

Financial support for this work was provided by grant U54ES016115 from the U.S. National Institute for Environmental Health Sciences through the trans-NIH Genes, Environment and Health Initiative. The content is solely the responsibility of the authors and does not necessarily represent the official view of the National Institute of Environmental Health Sciences or the National Institutes of Health. Additional funding was provided by Samsung Corporation. Device fabrication was performed in the UC Berkeley Microlab and Center and Biomolecular Nanotechnology Center. R.A.M. has a financial interest in IntegenX, Inc. that is commercially developing aspects of the technologies presented here.

Chapter 5: Digital Microfluidic Automaton for Multiscale Combinatorial Mixing and Sample Processing

In preparation for submission to *Lab on a Chip*. Co-authors are Thomas N. Chiesl, Amanda M. Stockton, Abhisek Bera, and Richard A. Mathies.

5.1 Abstract

A digital microfluidic Automaton consisting of a 2-dimensional array of pneumatically actuated microvalves is used to perform diverse mixing and sample processing operations. Large (μL-scale) volume processing operations are enabled by precise metering of multiple reagents within individual nL-scale valves followed by serial repetitive transfer to programmed locations in the array. A novel process is developed for rapid and complete mixing of reagents in less than 800 ms. Mixing, transfer, storage, and rinsing operations are implemented combinatorially to achieve complex assay automation protocols. The utility of this technology is demonstrated by performing automated serial dilution for quantitative analysis as well as carboxylic acid sample labeling for microchip capillary electrophoresis. A language is developed to describe how unit operations are combined to form a microfluidic program. Finally, an extension of this technology for combinatorial mixing of large sets ($> 2^6$ unique combinations) of reagents is presented. The digital microfluidic Automaton is shown to be a versatile programmable sample processor for a wide range of process volumes and analyses.

5.2 Introduction

Programmable microfluidic systems offer the unique ability to automate biomolecular assays on a common microchip format. A wide range of mechanisms have been employed for transporting and mixing nanoliter scale reagent volumes in microfluidic devices including droplet generation,[92] electrowetting,[87] and a variety of microvalve and pump technologies.[16,25] Droplet mixing and splitting operations have been used to automate diverse assays including glucose determination[88] and enzyme kinetic analysis.[89] However, these systems operate at the nanoliter scale, and often suffer from significant imprecision, limiting quantitation.[56] Multilayer soft lithography has been used to develop large reactor arrays for parallelized bioanalysis and combinatorial mixing of reagents.[25,28,93] Although these systems can address a large number of reactors in parallel, they lack programmable sample processing capabilities for large volume samples. The monolithic membrane valves developed by our group[66] have enabled automation of assay protocols including pathogen detection,[36] DNA sequencing,[39] and single nucleotide polymorphism detection.[50] While these systems offer miniaturized sample processing capabilities, each system performs only limited sets of sample processing operations and significant design modifications are required for each new application. A truly versatile, programmable microfluidic sample processing platform should provide facile automation of assays with a wide range of volumes, the ability to actively control reagent mixing, and convenient modular assembly of functional components or operations.

The ability to process large (μL scale) sample volumes is critical for many types of molecular diagnostic assays that require detection of low titer targets. For instance, HIV viral load detection typically requires several hundred μL sample volumes to achieve appropriate detection limits.[110] The standard approach to the automation of these assays utilizes slow sample handling robots that are expensive and occupy large amounts of space. Alternatively, microfluidic systems have been developed to process larger sample volumes and trap target molecules or cells within microchambers using capture probe labeled surfaces,[111,112] microspheres,[113] gels,[114] porous monoliths,[115] or other solid substrates.[116] However, these systems lack the programmable sample processing capabilities necessary to conveniently automate diverse assay protocols on the same device. There is therefore a need for a programmable microfluidic platform that can automate sample processing operations for volume scales ranging from nanoliters to milliliters.

Due to the laminar flow profiles in microfluidic systems, active mixing capabilities are critical for programmable sample processing. Microfluidic devices typically operate in the Stokes laminar flow regime so mixing only occurs via diffusion unless a mechanism to perturb the resulting laminar flow profiles is employed. Microfluidic devices for combinatorially mixing streams of reagents have been developed using passive mixing elements.[45,117] Although these systems can process large sample volumes, they are single-purpose and lack programmability. Active mixing has been demonstrated using microvalves to pump different reagents through a loop structure.[49,118] However these structures lack large volume processing capabilities and adjustable control of mixing proportions.

Programmable microfluidic systems should enable the performance of diverse sample processing operations on the same device. Modular microfluidic devices have been developed in which functional components can be rearranged to achieve different processing operations for μL-scale sample volumes.[118] However, the modifications required are labor intensive, and the devices do not permit program changes in real time. Grover et al. demonstrated a microfluidic device capable of replacing a conventional autosampler system.[35,119] This device utilized a network of bus valves to select from a set of input reagents for continuous transfer to a suspended microchannel resonance sensor. While rapid reagent switching frequencies were achieved with this device, higher dimensionality versions of this sample processor are necessary to achieve a broad range of assay automation.

We previously introduced a programmable digital microfluidic Automaton capable of automating assay protocols using nanoliter scale sample volumes.[63,120] This system utilized an 8x8 rectilinear array of pneumatically actuated monolithic membrane microvalves. Basic operations were achieved by digital transfer of fluid between microvalves in the array. Programs for reagent routing, mixing, rinsing, serial dilution, storage/retrieval were developed enabling assay automation. However, this device was not capable of processing or actively mixing larger sample volumes and an approach for programming combinatorial operations was not developed.

Here we present a novel use of the digital microfluidic Automaton that enables combinatorial processing of nanoliter to milliliter scale sample volumes. With this system, multiple reagents can be digitally mixed to generate a continuous output of processed sample. Sample storage operations utilizing external holding reservoirs are developed to enable serial processing operations for μL scale samples. The digital microfluidic array transports reagents between the holding reservoirs and can simultaneously mix reagents during the process. We present the basic rules for assay automation using this system together with an effective language to describe the automated protocols. The utility of this system for serial dilution of large volume samples, and for the automation of carboxylic acid sample labeling for capillary electrophoresis is demonstrated. Finally, an extension of this technology to enable combinatorial μL scale mixing operations for large sets of reagents is demonstrated.

5.3 Materials and Methods

Automaton fabrication and design. The digital microfluidic Automaton was fabricated as a 3-layer glass PDMS (polydimethylsiloxane) hybrid structure as previously described.[63] The pneumatically actuated 8X8 array of 4-way microvalves incorporates a rectilinear array of fluidic channels that enable discrete transfer of fluids between adjacent valves. Microvalves are actuated by vacuum (-87 kPa) and closed with an adjustable pressure applied through drilled inputs on the

pneumatic layer via computer actuated solenoid valves. Twenty-four drilled fluidic reservoirs on the perimeter of the array serve as either inputs or outputs and are connected by microchannels to the microvalves on the perimeter. To increase the volume of the reservoirs, holes were punched into 3 mm thick PDMS pieces and aligned with the drilled inlets. The Automaton device used here had fluidic features etched to a depth of 30 microns and pneumatic features etched to a depth of 70 microns.

A cross-sectional view of a microvalve array is presented in Figure 5.1A. Each monolithic membrane microvalve consists of an etched displacement chamber in one glass wafer and a discontinuous fluidic channel structure in a second glass wafer. The wafers are reversibly bonded together using a featureless 254 μm thick PDMS elastomer membrane (HT-6240, Rogers Corp.). Application of a vacuum to the displacement chamber through a control channel pulls the PDMS membrane away from the discontinuity, allowing fluid to fill the chamber and/or flow across the discontinuity in the fluid channel. The maximum volume contained by a microvalve in the array is 120 nL, corresponding to 84% of the volume of the pneumatic displacement chamber.[63]

Multiscale sample processing operations. Figure 5.1A also illustrates the mechanism of fluidic transfer within the Automaton. The basic program for the transfer of fluids between microvalves in a rectilinear array begins with a single open microvalve filled with fluid. An adjacent microvalve is opened, drawing fluid from the first valve. The first valve is then closed with an applied pneumatic pressure, forcing the remainder of the fluid into the second valve. A 120 nL bolus of fluid is thus transferred between adjacent microvalves. Reagents can be transferred from any input reservoir to any cell or output reservoir in the array, and repeated cycles enable the transfer of adjustable volumes between reservoirs.

Combining operations are performed by precisely metering multiple reagents into a single microvalve or set of adjacent microvalves in the array. This is achieved by opening a combining valve connected by open pathways to multiple inlets or filled adjacent valves. Figure 5.1B illustrates a program using a combining valve operation. In this example, reagents from reservoirs *c1* and *d2* are directed into combining valve C2 and then digitally transferred to output *b1*. The microvalves used to load the combining valve are closed prior to the transfer of the contents of the combining valve to a new location. A complete description of this program is included in Appendix C.

Figure 5.1C illustrates the language developed to efficiently describe on-chip autonomous fluidic operations. Valves are indicated by their position in matrix format, with columns designated by numbers and rows designated by letters. Reservoir inputs are labeled with the lowercase letter in italics according to the valve they are attached to. For example, an input reservoir to valve D3 is denoted *d3*. The basic operations used to automate assays are denoted by the following operators: C = combine, T = transfer, and F = flutter. The transfer operator indicates the locations between which fluid is being transferred, with the input location listed first, followed by the output location. The combining operator indicates the input locations followed by the valves in which the combining operation occurs. Both types of operations are repeated the number of times indicated after the square brackets that enclose the operation. The total volume of sample processed is adjustable based on this parameter. Fluttering operations are used to enhance mixing speed and efficiency. This is defined as repeated opening and closing of

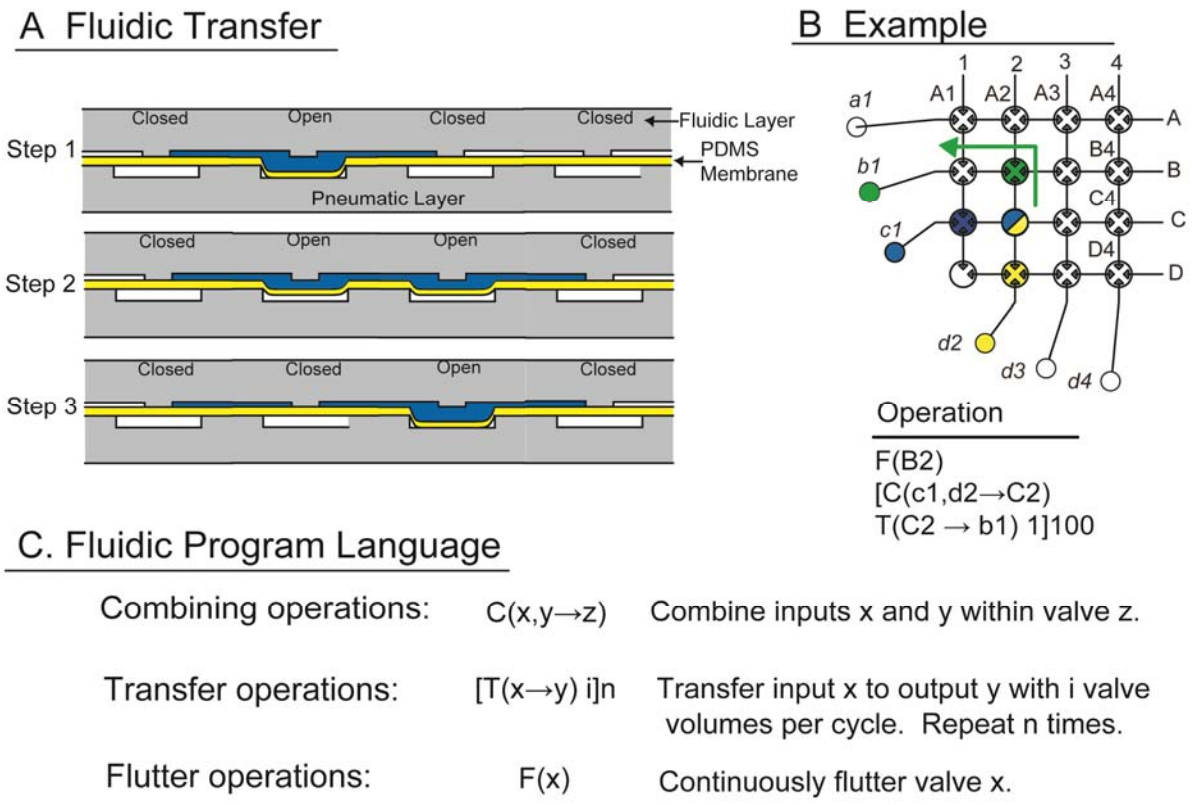

Figure 5.1 (A) Cross sectional view of a microvalve array showing the steps for transfer of fluids between microvalves. (B) Schematic of a combining operation showing labeling of valve array and inputs. Inputs from wells c1 and d2 are drawn in via valves C1 and D2, combined in valve C2, and transferred to output well b1, with a total fluidic transfer of one valve volume per cycle. The cycle is then repeated 100 times. (C) Fluidic program language. Combining operations indicate inputs (x,y…) followed by the microvalve or microvalves where combining occurs (z). Transfer operations indicate the microvalve or storage well input (x) followed by the output (y), and the number of microvalve volumes transferred per cycle (i). Operations within brackets are repeated n times. Flutter operations are performed continuously and indicate the microvalve fluttered (x).

a microvalve in a transfer pathway with 50 ms actuation times. The flutter operator defines the specific valve that is fluttered and is performed continuously throughout a program.

To characterize the operations of combining valves and complex serial processing operations including standard curve generation, fluorescent dyes including fluorescein, ROX, and Pacific Blue succinimidyl ester were loaded in different configurations on the Automaton. These dyes served as inputs to combining valves and were programmably transferred to an output reservoir. Actuation times of 250 ms were utilized for these programs unless otherwise indicated with a closing pressure of 50 kPa. Dilution factors and the proportions of reagents loaded into combining valves were determined by transferring samples from the outlet to a fluorescence plate reader (Flx800, Bio-Tek Instruments Inc.) and quantified using a standard curve. Back contamination of the inlet reservoirs was also tested by analysis of buffer in the inlets reservoirs with a fluorescence plate reader. Epifluorescence images were acquired with a Nikon Eclipse E800 using a 2X objective, 0.06 aperture and an output power at the excitation band of 4 mW.

Carboxylic acid sample labeling for capillary electrophoresis. To demonstrate the utility of the Automaton for reaction chemistry, we designed a protocol for the automation of a previously developed carboxylic acid sample labeling process for capillary electrophoresis.[59] Cascade Blue hydrazide (CB, Invitrogen) was dissolved in triply-distilled Millipore water to 10 mM. EDC (1-ethyl-3-(3-dimethylaminopropyl)carbodiimide, Sigma-Aldrich) was dissolved to 20 mM in triply-distilled acetonitrile (MeCN, Sigma-Aldrich), divided into 100 μL aliquots, evaporated to residue, and stored at -20 ^{o}C until rehydration to the appropriate concentration in 30 mM borate, pH 3. Carboxylic acid labeling was conducted by combining a carboxylic acid standard (200 μM formic acid, 400 μM each acetic, propanoic, butanoic, pentanoic, hexanoic and heptanoic acids, and 600 μM octanoic acid, Sigma Aldrich) with 4 mM CB in 30 mM borate and 10 mM EDC, all in 30 mM borate, pH 3, in a 1:1:1 ratio. In the manual control process, after a 15 min incubation, the reaction mixture was diluted 1:3 with 30 mM borate, pH 9.5 for analysis.

An on-chip automated program was also developed to 1) mix EDC, CB, and standard using combining valve technology, 2) transfer the mixture to an output for a 15 min incubation, 3) dilute the mixture 1:2 with 30 mM borate, pH 9.5 and 4) transfer the processed sample to a second output for analysis. All samples were analyzed by transferring 30 μL processed sample to the inlet reservoir on the Mars Organic Analyzer, a portable μCE analysis system described in detail elsewhere.[41,59-62,121]

Six-sample combinatorial processor. To extend the combining valve concept to larger sets of inputs, a 6-sample combinatorial processor was fabricated using a 3-layer glass-PDMS (polydimethylsiloxane)-glass hybrid structure (Figure 5.2). Etch depths were identical to those of the Automaton. In this design, a central 2 mm diameter microvalve is radially connected by microchannels to 7 check valves controlling corresponding inlet reservoirs. An additional channel extends to a series of 2 mm mixing valves. The inlet across from and in line with the mixing valves contains buffer for rinsing cycles. The contents of any subset of the 6 remaining inlets can be loaded into the combining valve by opening corresponding subsets of check valves during operation. A program was developed to cycle through all possible (64) input sets with a rinse cycle between input states. The selected inputs are indicated by a binary code. For instance,

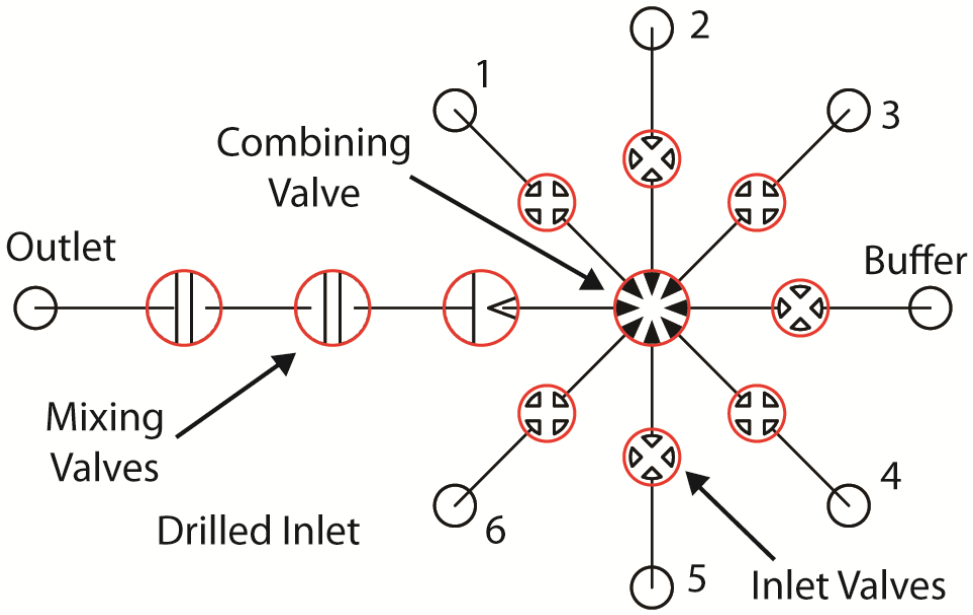

Figure 5.2 Six sample combinatorial processor. Fluidic inputs 1-6 can be precisely transferred to the combining valve and digitally transferred through a series of valves to an outlet for storage. Check valves at each fluidic input enable combinatorial selection of any subset of the reagents in a given program cycle, and prevent cross contamination of the reagents. Using this system, 2n multiscale reagent combinations are enabled by n+4 microvalves. The selected reagent sets can be represented as a binary code. For instance, selection of inlets 1, 3, and 6 is denoted by the binary string, 101001.

immediately after opening the combining valve to determine the overall flow profile of the inputs as the combining valve is filled. To determine the proportions of the inputs loaded into the selection of inputs 1, 3, and 5 is indicated by the string 101010. Sample loading and transfer operations were performed with a 250 ms valve actuation time, and a closing pressure of 50 kPa.

5.4 Results

Combining operations can be used to precisely meter multiple reagents to an individual microvalve. To explore the capabilities of combining valve operations, programs were run to combine two reagents from parallel inputs (Figure 5.3A), two reagents from orthogonal inputs (Figure 5.3B), and three reagents (Figure 5.3C). Epifluorescence images were acquired immediately after opening the combining valve to determine the overall flow profile of the inputs as the combining valve is filled. To determine the proportions of the inputs loaded into the combining valves, the programs illustrated in Figure 5.3 were performed using fluorescein dye and buffer as inputs. Outputs were quantified using a 96-well fluorescence reader, and errors were determined by performing multiple runs. The proportions for two inputs at 180^{o} are 50.3 ± 0.8% Input *d2*, and 49.7 ± 0.8% Input *d4*. The proportions for two inputs at 90^{o} are 50.6 ± 0.8% Input *d2*, and 49.4 ± 0.8% Input *c1*. The proportions loaded in the case of three reagents are 33.4 ± 0.8% Input *c1*, 37.9 ± 0.5% Input *d2*, and 28.7 ± 0.5% Input *d4*. The differences in proportions of the three inputs are due to different fluidic resistances in pathways from the inlets to the combining valve.

The rate at which processed sample is generated depends on the volume of microvalve displacement chambers, the valve actuation rate, the number of microvalve volumes transferred per cycle, and the fluidic resistance of microchannel connections. While smaller microchannels reduce the dead volume between microvalves, they increase the time necessary for complete transfer of the contents of one microvalve to the next. The rate at which sample is processed can be increased by decreasing the actuation times of the microvalves. With valve actuation times as low as 50 ms, the proportions of reagents loaded into a combining valve are not significantly affected by the processing speed.

The contents of a combining valve are partially mixed as they are transferred through a series of microvalves to an output. The mixing efficiency can be significantly enhanced by continuously fluttering one of the microvalves (with 50 ms actuation times) in the transfer pathway from the combining valve to the output. To visually evaluate the mixing efficiency, 10 μM fluorescein and 10 μM ROX were loaded into *d4* and *d2* respectively and the following program (Program 1 in Figure 5.4) was run:

F(A3)	Flutter valve A3
[C(*d2*,*d4* → C3)	Combine fluorescein and ROX in C3
T((C3 → *a1*)1]250	Transfer to a1 and repeat 250 times

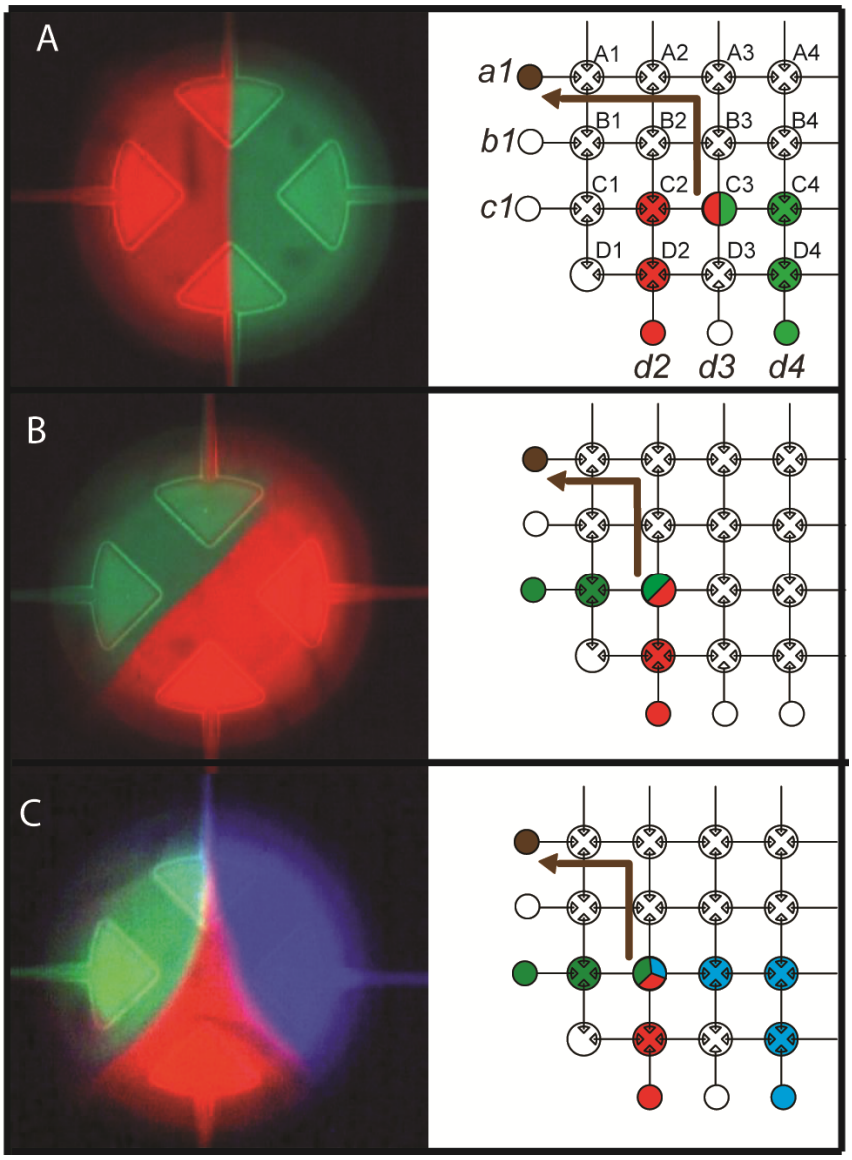

Figure 5.3 Epifluorescence images of loaded combining valves and schematics of multiscale sample processing operations on the digital microfluidic Automaton. (A) Combining valve C3 is loaded with of two fluorescent dyes from parallel input channels. The contents of C3 are then digitally transferred between B3-A1 to a1 in this example. (B) Combining valves loaded with two reagents from orthogonal inputs, and (C) with fluorescent dyes from three different inputs. The contents of a combining valve can be transferred to any microvalve or output in the array.

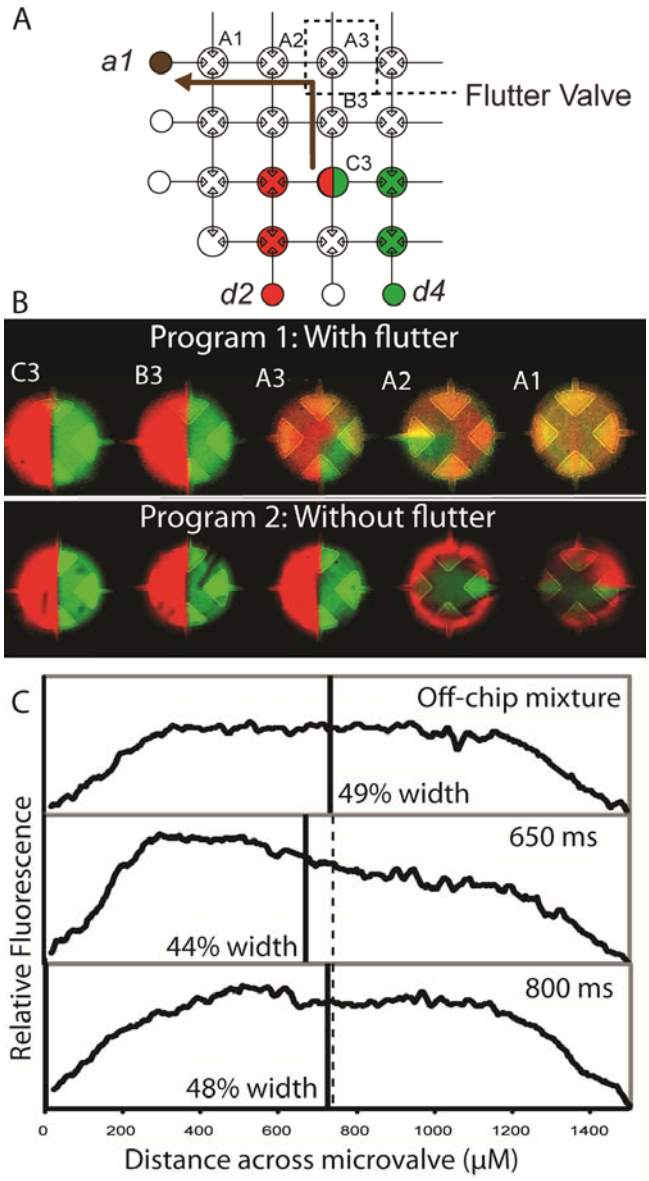

Figure 5.4 (A) Illustration of the program for continuous digital mixing of two reagents. ROX and fluorescein dyes are drawn into combining valve C3 and then digitally transferred through valves B3-A1 to an output well. (B) Epifluorescence images of each step of two different mixing programs. Program 1 includes continuous fluttering (repeated opening and closing of A3 with 50 ms cycles) throughout the program, while Program 2 is run without fluttering. (C) Fluorescence line profiles obtained across valve A1 intersecting the direction of flow during the performance of Program 1 with fluorescein and pure buffer inputs. The vertical lines indicate the location of the first moment of the fluorescence distribution; a sample mixed off chip results in a center at 49 ± 1% of the microvalve width. With a 200 ms valve actuation time, complete mixing occurs within 800 ms during transfer from B3 to A1.

Figure 5.4B presents epifluorescence images of the dye solutions as they are loaded into combining valve C3, and then transferred between microvalves to output *a1* in a single cycle of the program. Program 1 results in complete mixing of the two dyes by the time they reach A1. Program 2, which did not include fluttering, results in significantly less mixing of the two dyes in each cycle of the program, as illustrated by distinct green and red fluorescence regions in the valve A1 and A2 images. Microvalve fluttering is therefore an effective approach to enhancing mixing speed and efficiency for large volume processing operations on the Automaton.

To quantify the efficiency of mixing, Program 1 was performed using 10 μM fluorescein and 1X TTE Buffer pH 8.3 as inputs. Fluorescence line profiles were acquired across valve A1 intersecting the direction of flow when fully opened (Figure 5.4C). The first moment for each profile was calculated to measure the symmetry of the distribution of the fluorescence across the microvalve. Complete mixing is indicated by a distribution centered at 50% of the microvalve width. The mixing time was defined as the time required for complete transfer of the reagents from microvalve B3 to A1, and was adjusted by varying the microvalve actuation time. With an 800 ms mixing time, the fluorescence distribution center (48 ± 1% microvalve width) was virtually identical to that of a mixture prepared off chip and run through the same program (49 ± 1% microvalve width). The fluttering step included in Program 1 therefore results in complete mixing of reagents in less than 800 ms for each cycle of the program.

The speed of mixing for this program compares favorably to other microfluidic mixing approaches. For instance, we previously demonstrated a program to cyclically transfer two reagents within a loop of four microvalves in the array, requiring 2.5 seconds to achieve complete mixing.[63] Traditional microfluidic loop mixers require even longer times (<10 seconds) to achieve complete mixing.[49] Our approach to rapid, on-chip mixing may be useful for a broad range of applications that require complete mixing of reagents on-chip on either the nanofluidic (nL) or microfluidic (μL) volume scales.

Multiscale serial dilution program. Since the output of a step in a fluidic program can be used as an input for a subsequent program step, multiscale serial processing operations can be performed on the Automaton. As an example, we demonstrate the serial dilution of fluorescein to generate a 5-level standard curve (Figure 5.5A) with adjustable output volumes. Fluorescein (10 μM) and TE buffer (10 mM Tris, 1 mM EDTA) pH 8.3 were loaded into *c1* and *d2,* respectively. In the first step of the program, fluorescein and buffer are combined in both C2 and B2 for improved processing speed, and transferred to reservoir *b1* to produce *Out1*. Each subsequent standard curve level (Out2-Out4) was generated by combining one valve volume of fluorescein sample with one valve volume of buffer and transferring to the designated output. The following program was used to perform the overall process:

Out 1: [C(*c1*, *d2* → B2, C2), T(B2,C2 → *b1*)2]60 Combine dye and buffer to produce *Out1*

Out 2: [C(*b1*, *d2* → B2, C2), T(B2,C2 → *a1*)2]60 Combine *Out1* and buffer to produce *Out2*

Out 3: [C(*a1*, *d2* → B2, B3), T(B2,B3 → *d3*)2]6 Combine *Out2* and buffer to produce *Out3*

Out 4: [C(*d3*, *d2* → B3, B4), T(B3,B4 → *d3*)2]60 Combine *Out3* and buffer to produce *Out4*

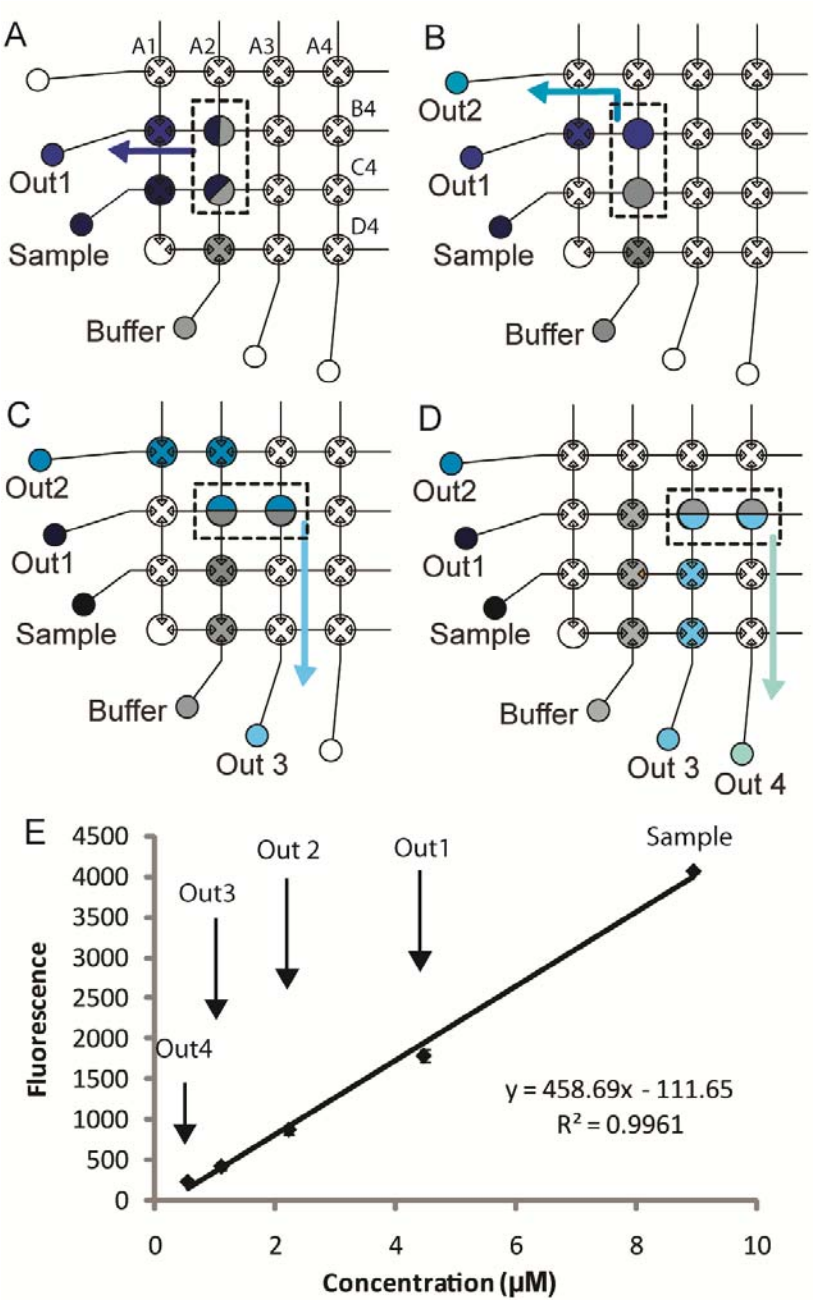

Figure 5.5 Multiscale serial dilution program implemented on the Automaton. (A) The first dilution is achieved by combining sample and buffer in two microvalves (dashed box). The contents of two microvalves are then transferred to Out1 at each cycle, resulting in faster generation of large volumes. Each subsequent standard concentration level (B-D) is generated by combining sample from the previous standard curve level and buffer in the two indicated microvalves. (E) Results of the standard curve program generating 6 µL of each concentration level within a total runtime of 7 minutes. Error is estimated based on four separate runs. An R^2 of 0.9961 is achieved with a predicted dilution factor of 2 for each level.

Six µl of each standard level was generated with a total runtime of 7 minutes. Based on the predicted dilution factor of 2 for each level, a highly linear standard curve was generated (R^2 = 0.9961). Each standard curve level was quantified using a standard curve prepared off-chip. The actual dilution factors produced were 2.27 ± 0.10, 2.02 ± 0.11, 1.96 ± 0.15, and 1.93 ± 0.14 for levels Out1-Out4, respectively. The error was estimated based on four separate runs and was within the range previously reported for operations on the Automaton.[63] Although each of the standard levels uses two microvalves for combining operations, the different input configurations and geometries affect the final proportions of the two inputs loaded. For instance, to produce Out1, buffer and dye are simultaneously loaded into C2, and then B2 is opened drawing fluid from the two input reservoirs. A larger volume of buffer is drawn into the combining valves due to the asymmetry of the pathways between the two inputs and B2, resulting in a dilution factor slightly greater than two. Further modeling of microvalve flow should enable precise prediction of these dilution factors. These results demonstrate the utility of our system for generating adjustable volumes of serially diluted sample for quantitative chemical and biochemical analysis.

Cascade Blue labeling of EDC-activated carboxylic acids. Cascade Blue labeling of carboxylic acids was performed with an automated program on the Automaton and analyzed on a µCE microchip with the MOA. The Automaton program depicted in Figure 5.6A combines CB from reservoir *c1,* carboxylic acid standard from reservoir *d2,* and EDC from reservoir *d4* in combining valve C2. The combined fluids are mixed by serial transfer via B2, A2, and A1 to the reservoir *a1* where it undergoes a 15 minute incubation. After the 15 minute incubation, the contents of reservoir *a1* are diluted by combining with pH 9 borate buffer in combining valves B3 and B2, and then transferred to reservoir *b1*. This program step is alternated with transfer of one microvalve volume of buffer to reservoir *b1* to achieve a dilution factor of 3.

The following program was utilized to automate this process:

[C(*c1*,*d2*,*d4*→ C2)	Combine EDC, Cascade Blue, and sample.
T((C2 → *a1*)1]250	Transfer to Output 1.
Store 15 min	
[C(*a1*,*d2*→ B2,B3)	Combine one unit buffer and one unit reacted product.
T(B2,B3 → *b1*)2	Transfer to Output 2.
T(*d3*→*b1*)1]250	Transfer 1 unit buffer to Output 2.

The assay was performed by transferring 30 µL of the output of reservoir *b1* to the CE microdevice and separated as described previously.[59] An electropherogram of autonomous on-chip carboxylic acid labeling and dilution is compared to a fully manual protocol in Figure 5.6B. The processing conditions were evaluated by comparing reaction efficiency as quantified by the peak areas and separation quality as quantified by the peak efficiencies. The peak areas obtained by on-chip reaction are 40-50% larger than those obtained by a similar manual off-chip reaction with a run-to-run error of less than 5%. The reaction efficiency variation is likely due to a difference in mean reaction time. While the manual reaction was allowed to run for precisely 15 min, the automated reaction time varied from 15 min to 25 min because of the 10 min transfer time. Since it has previously been demonstrated that EDC-activated CB labeling of carboxylic acids requires > 8 hr to proceed to completion,[59] the observed peak areas are expected to increase with increased reaction times. The autonomously labeled samples exhibited only a 1% difference

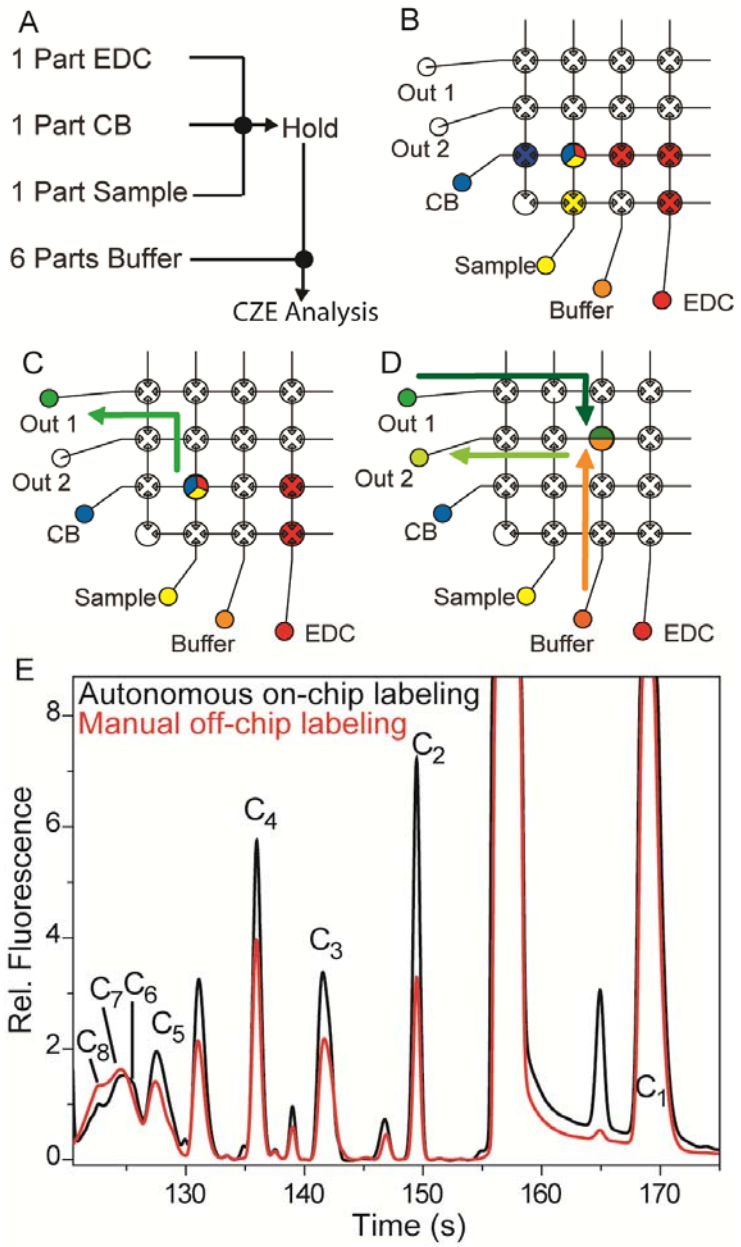

Figure 5.6 (A) Schematic of the program for labeling carboxylic acids performed on the Automaton. (B) Sample containing a standard set of carboxylic acids is loaded into a combining microvalve with Cascade Blue (CB) and 1-Ethyl-3-(3-dimethylaminopropyl) carbodiimide (EDC). (C) At each cycle, the contents of the combining valve are transferred to Out1 with an output rate of 0.06 uL/sec. (D) After a 15 minute incubation, the contents of Out1 are combined with 30 mM borate buffer, pH 9.5 for dilution and transferred to Out2. Approximately 30 µL of labeled sample is generated for analysis by microcapillary electrophoresis. The standard contains 200 µM formic acid, 400 µM each acetic, propanoic, butanoic, pentanoic, hexanoic, and heptanoic acids, and 600 µM octanoic acid.

in peak efficiency compared to the manual process, which is within the normal run-to-run variation.

Evaluation of 6-input combinatorial processor. A program was utilized to generate all possible combinations of reagents using the 6-input combinatorial processor. Figure 5.7 illustrates combining valve operations for all possible permutations of 6 inputs dyes. For each case, all of the selected input dyes are precisely metered into a single combining valve. The proportions loaded for each input configuration were quantified by running the program described above with fluorescein dye and buffer as inputs and analyzing the outputs on a fluorescence plate reader (Appendix C). In cases where only two inputs are selected, the results are similar to the two-input combining valve operations on the Automaton. Among these cases, the average dilution factor is 2.0 ± 0.2. For larger sets of reagents, the proportions loaded are more highly dependent on the configuration of inputs. Further modeling of the fluid flow within microvalves should enable precise prediction and adjustment of the loading proportions. These results demonstrate that reagent sets larger than 4 can be controlled and combinatorially processed within a digital microvalve array by increasing the number of fluidic connections or inputs to the combining valves.

5.5 Discussion

The digital microfluidic Automaton presented here is a versatile platform for combinatorial sample processing operations and automation of diverse protocols that require from nanoliter to microliter scale sample volumes. The compact design of this microchip processor should enable significant miniaturization of laboratory automation robots that perform similar functions. Such systems typically require minimum sample volumes of a few microliters and the use of costly disposable pipettes tips. Our platform can precisely process sample volumes ranging from a few nanoliters to the milliliter range, without the requirement for expensive disposables. Acoustic droplet ejection systems have been developed for transfer of nanoliter to microliter scale sample volumes into microtiter plates,[122] however they lack the serial processing capabilities demonstrated here.

The large volume serial processing operations of the digital microfluidic Automaton are enabled by the use of combining valve technology. No back contamination of reagents was observed during experiments performed herein. Combining valves are therefore a valuable alternative to bus valves, which have been used in previous work for contamination-free reagent delivery.[42,50] The extension of combining valve technology to larger sets of inputs enables the integration of operations of greater complexity involving large reagent sets on smaller digital microvalve arrays.

Design modifications can be implemented to improve processing speed in cases where faster sample processing is necessary. The volume transferred between microvalves can be increased by modification of the diameter of the microvalves or the microvalve etch depths.[66] For instance, doubling the etch depth and diameter would result in microvalve displacement chamber volumes greater than 1 μL and processing speeds up to eight times faster than demonstrated here.

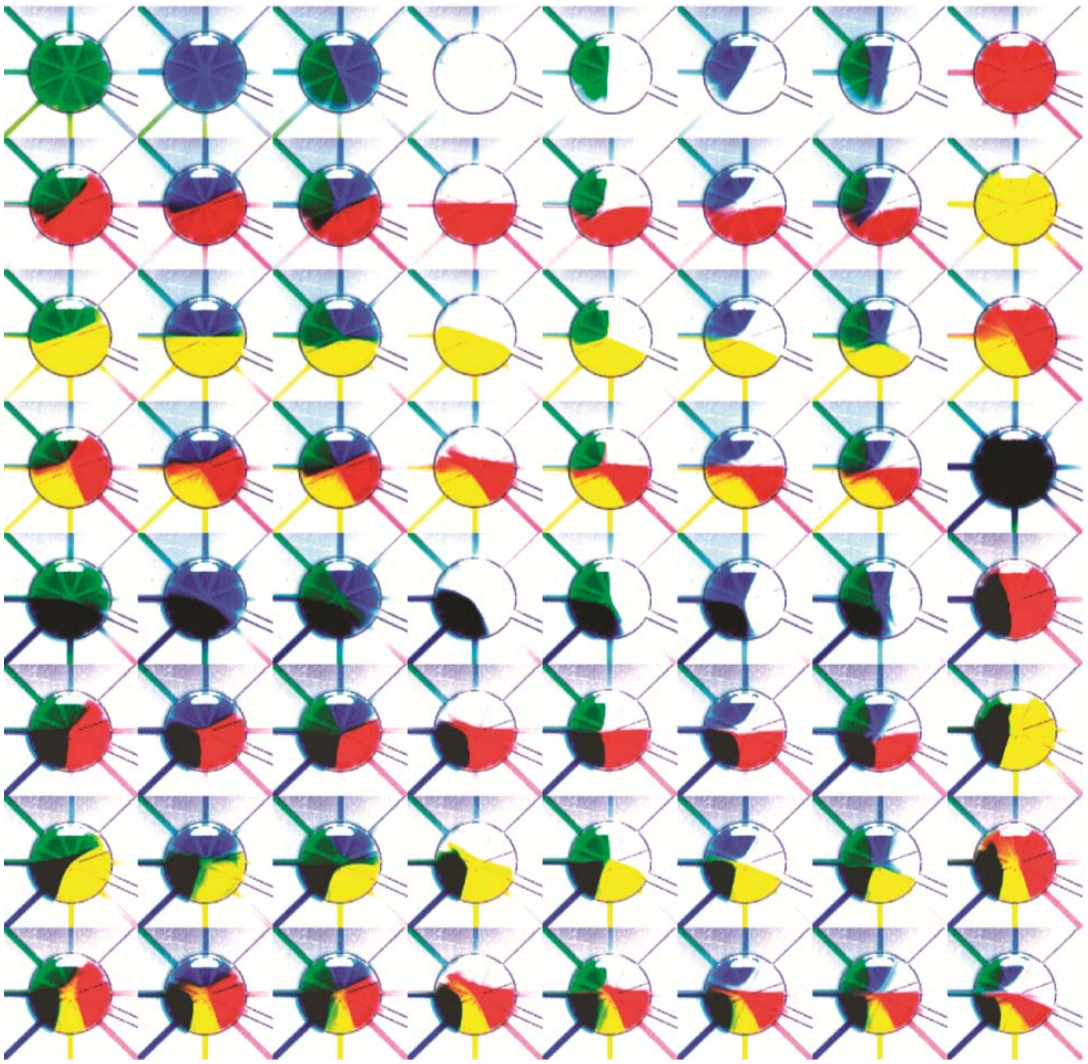

Figure 5.7 Bright field images of all possible reagent subsets loaded into the combining valve of the 6-bit combinatorial mixing device. Green, blue, clear, red, yellow, and black dyes were loaded into reservoirs 1,2,3,4,5,6 respectively.

The proportions of reagents loaded into a combining valve are significantly affected by the fluidic resistance of the inputs. For instance, in the three input case (Figure 5.3C), significantly less fluid from *d4* was loaded in the combining valve compared to reagent from *c1*. This can be explained by the longer pathway and correspondingly higher resistance between input *d4* and the combining valve. Modeling the fluidic resistance and flow profiles of these circuits should enable prediction of the reagent proportions resulting from combining operations and rebalancing through design or operational changes.

The ability to process large sample volumes on the digital microfluidic Automaton will enable the coupling of this system to a wide range of analytical testing devices. We previously demonstrated automated concentration of target biomolecules on derivatized magnetic microspheres using the Automaton.[120] This platform could therefore be coupled to particle detections systems such as flow cytometers. Grover et al. previously demonstrated the efficiency of coupling the autosampler device to downstream analysis systems using the PEEK tubing method.[26] In addition, PEEK tubing interconnections have been used for automated sample loading onto the Mars Organic Analyzer.[41] PEEK tubing interconnections between the drilled outputs of the Automaton and the inputs of other analytical devices should enable programmable processing and delivery of samples to a wide range of analytical systems such as mass spectrometers, surface plasmon resonance detectors, or DNA microarrays (Figure 5.8).

5.6 Acknowledgements

This work was supported by the trans-NIH Genes, Environment and Health Initiative, Biological Response Indicators of Environmental Systems Center grant U54 ES016115-01. Additional funding was provided by Samsung Corporation. The Automaton was fabricated in the UC Berkeley Biomolecular Nanotechnology Center.

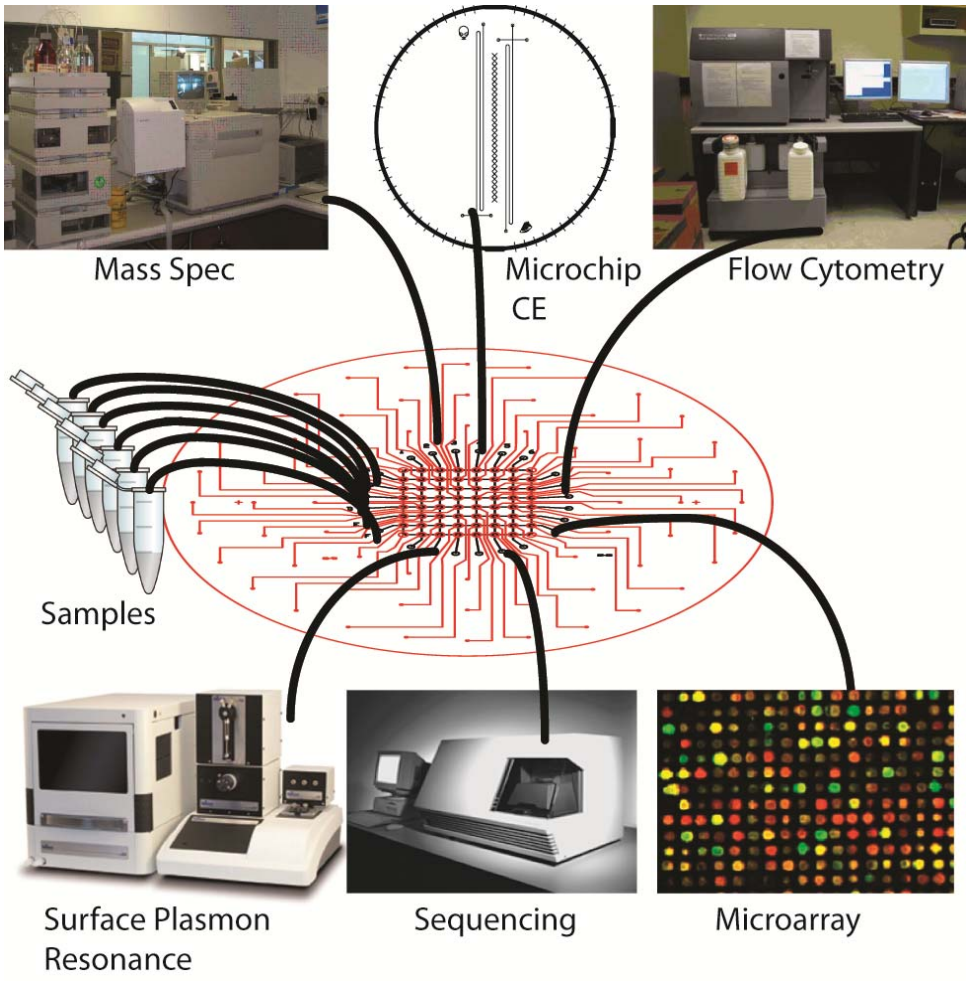

Figure 5.8 Schematic illustration of systems that could be coupled to the digital microfluidic Automaton. Large volume sample processing capabilities enable the coupling of the Automaton to a broad range of detection systems using simple PEEK tubing interconnections.

Chapter 6: Prospects

All physical systems can be thought of as registering and processing information, and how one wishes to define computation will determine your view of what computation consists of.

- Seth Loyd

The intersection between theoretical computer science, molecular biology, and mechanical engineering offers extraordinary new opportunities for the miniaturization and automation of molecular diagnostic systems. The preceding chapters have focused on the development of universal digital processing architectures for both micropneumatic and microfluidic logical operations. The micropneumatic logic architecture utilizes standard Boolean operators to integrate logical operations on a microfluidic chip. The digital microfluidic Automaton is a first step towards precise, generic microfluidic processing and analysis systems. This processing platform enables basic storage and retrieval operations similar to those of memory registries in conventional computers. Additionally, a range of new operations including transfer, mixing, rinsing, and serial dilution were required for the automation of biochemical analyses. The Automaton platform enables the performance of these operations and the assembly of the basic operations into complex automation routines. The development of a simple pseudocode for the description of arbitrary programs illustrates the natural connection between symbolic logic and biochemical assays. The unprecedented level of *programmability* of this system has enabled the total automation of quantitative homogeneous biomarker assays, inhomogeneous immunoassays, and sample processing operations for capillary electrophoresis of carbonaceous biomarkers.

6.1 Demultiplexed Automaton Control

The development of micropneumatic latching circuits and demultiplexers described in Chapter 1 suggests the possibility of combining digital micropneumatics with digital microfluidics to enable far more powerful processors. With such integration, an 8X8 Automaton array could be controlled using only six pnuematic inputs. Exponentially larger arrays could be controlled with a linear increase in control inputs,[58] enabling dramatic increases in processing power.

The initial characterization of demultiplexed valve control by Grover et al. focused on the actuation of individual valves that were not connected in a fluidic array.[58] In a normal pumping procedure, all of the valves that are closed during a particular step are held closed with an applied closing pressure. Since a demultiplexing circuit can only address one valve at a time, this type of parallel control is not possible. Initial attempts to control the Automaton with a demultiplexer and vacuum latching circuits resulted in significant leakage between microvalves during basic fluidic operations. This is due to the large closing pressure (40 kPa) required to pressurize the vacuum latching circuit and the resulting fluid pressure that is applied to the adjacent microvalves. Using existing pressure latching circuits is not a feasible solution since they only remain closed against pressure heads up to 17 kPa. Additionally, fabrication of standard latching circuits is cumbersome due to the need for via holes in the PDMS layer for each circuit.

To address these issues, I developed a single microvalve latching circuit that can be closed with an adjustable pressure and that eliminates via holes in the design. Figure 6.1 illustrates the layout of a linear array of single-valve latching circuits with demultiplexed control.

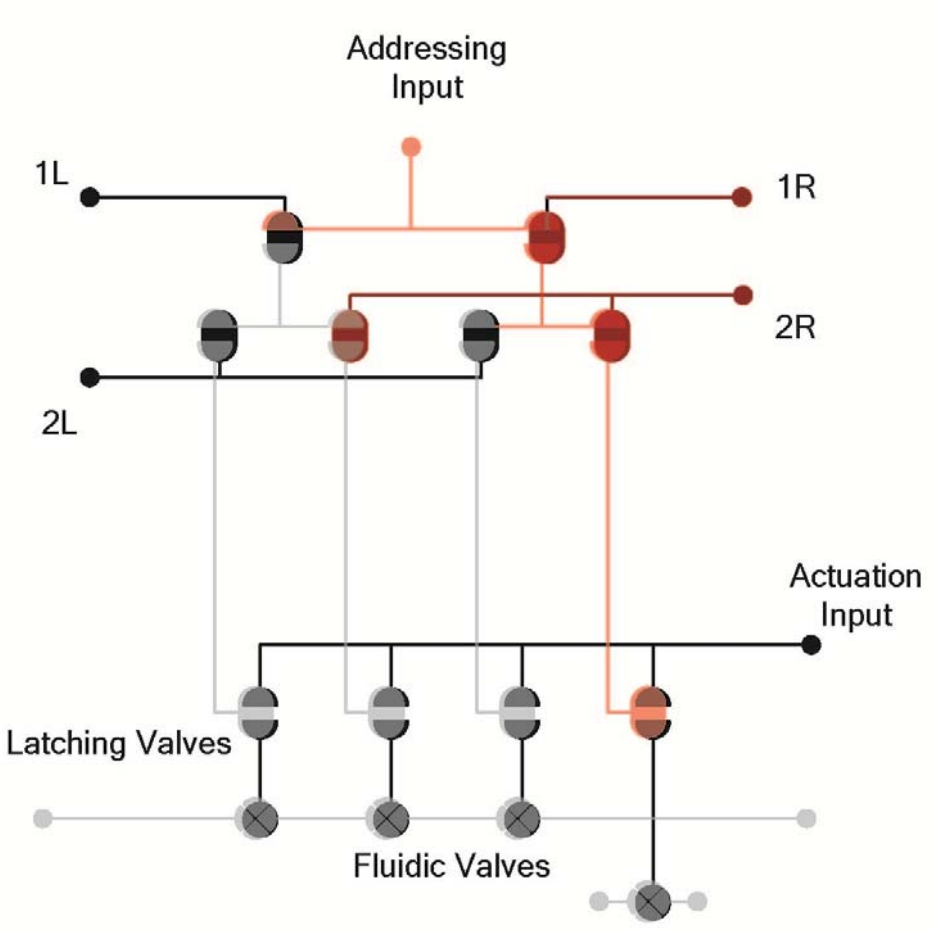

Figure 6.1 Demultiplexed latching system in which the addressing signal is decoupled from the actuation signal. To address a particular output valve, demultiplexer control valves are actuated and vacuum (pink) is applied to the Addressing Input. Application of vacuum to the Actuation Input opens the selected output valve, and subsequent pressurization of the Addressing Input latches the selected output microvalve in the open state. To close an output valve, vacuum is transmitted through the Addressing Input, and an adjustable closing pressure is applied to the Actuation Input (0-50 kPa).

When a vacuum is applied to the addressing and actuation inputs of a single-valve latching circuit, it opens temporarily and then closes after the output reaches 98% of the vacuum magnitude applied to the control channel. At this point, the vacuum can be removed from the addressing input and the slightly weaker vacuum remains latched in the output channel if there is no connection between the output channel and atmospheric pressure. Each of the single-valve latching circuits in this design share a common actuation input that can be switched between vacuum and an adjustable closing pressure. For closing operations, this configuration is identical to a series of micropneumatic NOT gates with control inputs actuated in parallel (Chapter 2).

Figure 6.2 shows the current design of the demultiplexed Automaton. The 6-bit demultiplexing system has a radial layout along the perimeter of the chip, addressing 64 latching circuits toward the center of the device. These latching circuits, in turn, set arbitrary patterns of valve actuations within the central rectilinear array of microvalves. With the current device, 400 ms pulses of vacuum (-87 kPa) and pressure (0-50 kPa) can reliably open and close microvalves in the rectilinear array. In addition, high fidelity digital fluidic operations have been achieved using this system. Figure 6.3 shows images from a basic program in which a bolus of fluid is transferred through a series of microvalves in the demultiplexed Automaton.

The basic transfer operations demonstrated with the demultiplexed Automaton can be extended to more complex operations, and further design optimization may improve processing speed. The nanoliter scale mixing program presented in Chapter 3 utilizes 50 ms valve actuations and results in the complete mixing of two reagents in approximately 3 sec.[63] Approximately 24 sec is required for the demultiplexed Automaton to achieve the same result due to the longer microvalve actuation times. Although this is significantly slower, it is slightly less than the amount of time required for mixing two reagents using conventional microfluidic loop mixers.[49] The current device could therefore be used for the practical automation of microfluidic bioassay procedures. The response time of the addressing system is affected by the cross sectional area of addressing channels within the demultiplexer. Larger channel cross-sectional area results in decreased resistance to airflow and corresponding improvements in response time. Additional optimization of the latching structures could enable high-speed and large scale digital microfluidic arrays for sample processing and analysis.

6.2 Autonomous Sample Processing for the Mars Organic Analyzer

In Chapter 5, effective Automaton protocols were demonstrated for processing larger sample volumes and automating the labeling of carboxylic acids with Cascade Blue for analysis on the Mars Organic Analyzer (MOA), a portable μCE system. Since this work, an effective approach to coupling the Automaton with the Mars Organic Analyzer has been developed to enable fully autonomous sample labeling and loading. Preliminary results for the analysis of amino acids and carboxylic acids are presented here.

The Automaton and the MOA were coupled via a PEEK tubing interface for fluidic transfer. The PEEK tubing (30 cm long, 50 μm I.D.) was attached to an Automaton fluidic output through a 3 mm thick PDMS gasket with a tightfitting punched hole. Gel Slick (BioWhittaker Molecular Applications) was applied to both the Automaton glass surface and the PDMS gasket surface to ensure good PDMS-glass adhesion. The output end of the PEEK tubing was permitted to hang freely just inside the drilled hole of the sample well of the microchip capillary electrophoresis device. This interface is shown in Figures 6.4 and 6.5.

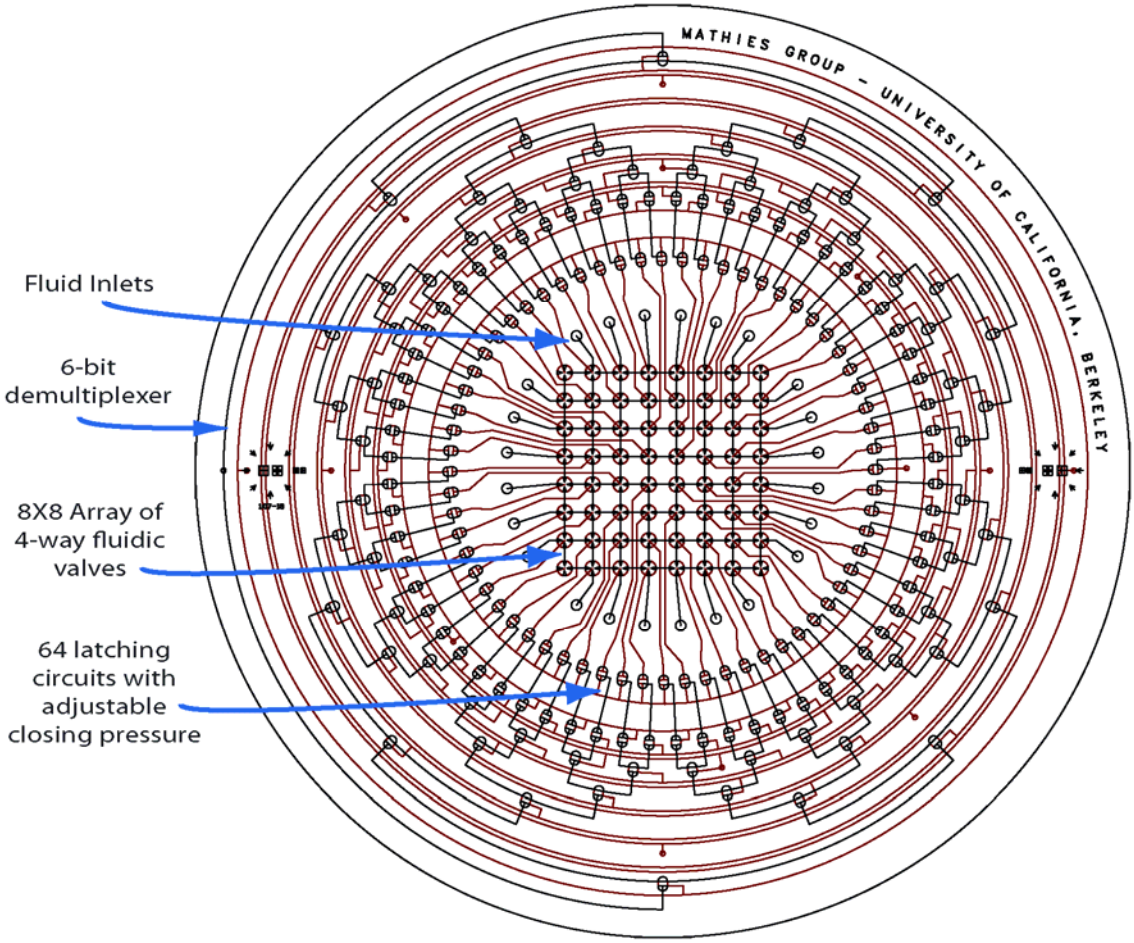

Figure 6.2 Layout of the demultiplexed Automaton. Red and black lines represent features on two different layers of the device.

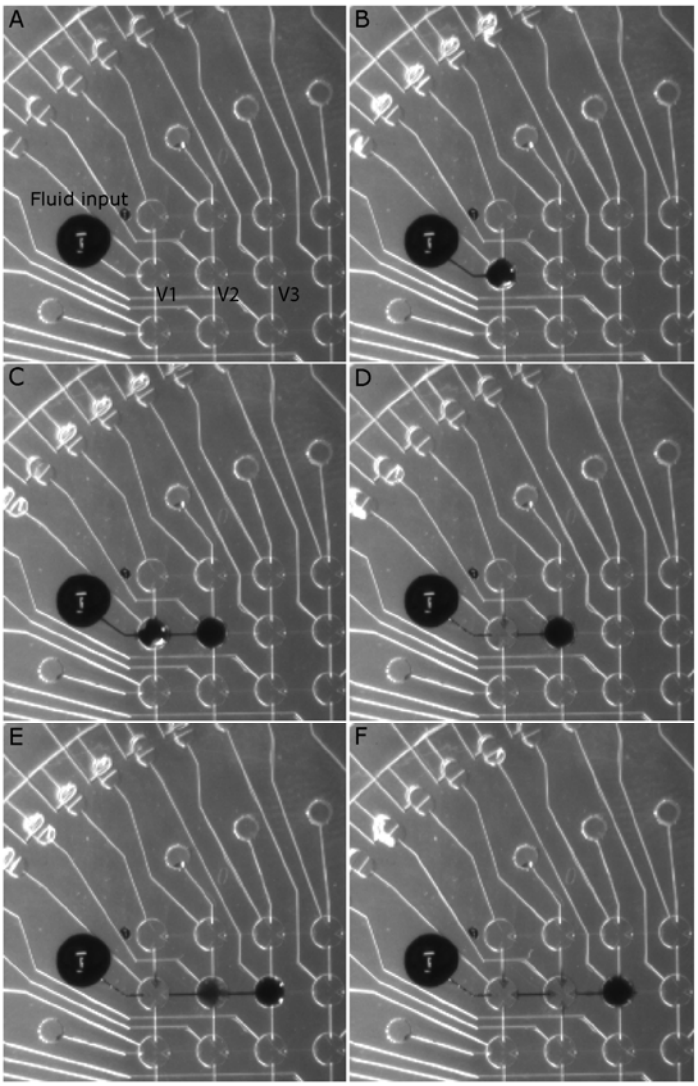

Figure 6.3 High-fidelity fluidic operations in the digital microfluidic platform. In (A), dye was applied to the drilled fluidic reservoir connected to latching valve V1. In (B), latching valve V1 is actuated drawing fluid into the valve. In (C), V2 is actuated and V1 remains latched open, drawing fluid through V1 into V2. In (D), V1 is closed and its contents are transferred backwards into the fluidic reservoir. In (E), V3 is actuated and a portion of the fluid in V2 is transferred to V3. In (F), V2 is closed resulting in the completion of the fluid transfer from V2 to V3.

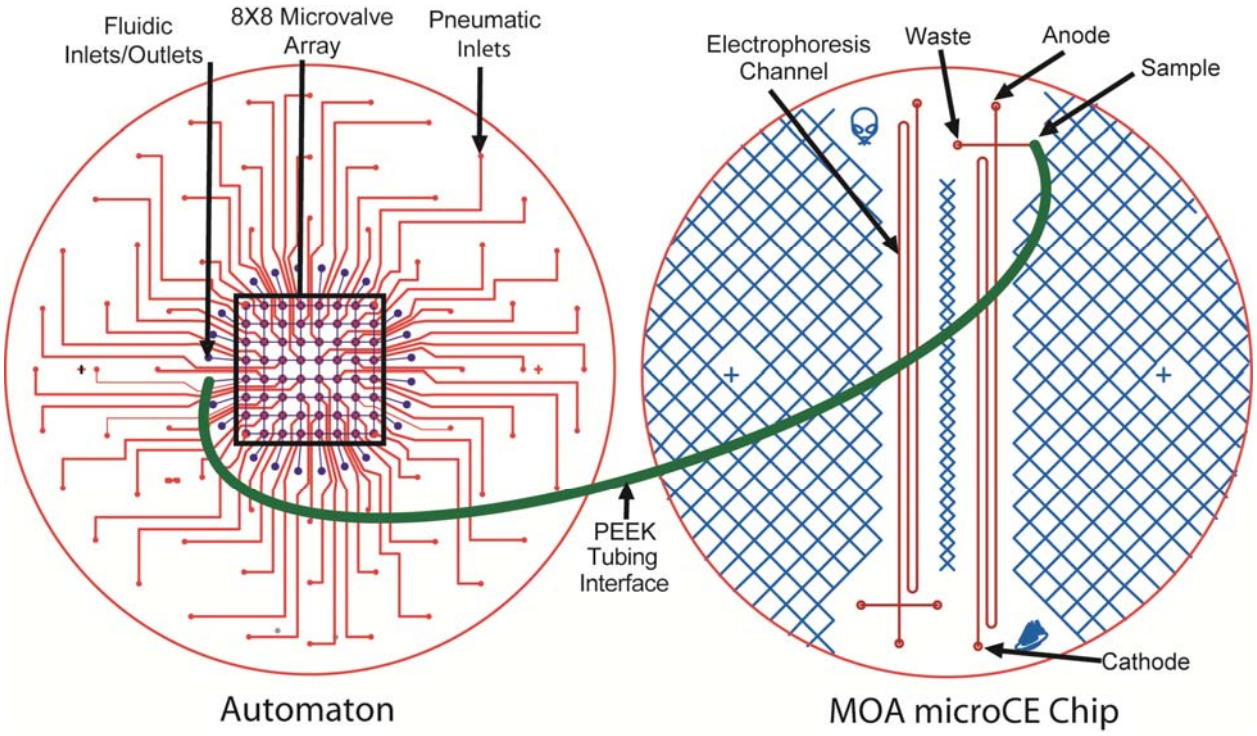

Figure 6.4 Schematic of coupling the Automaton device (left) and the MOA μCE chip (right). The Automaton pneumatic features are shown in red, the fluidic features in blue. The MOA μCE channels are shown in red, channel identifiers and bonding lines in blue.

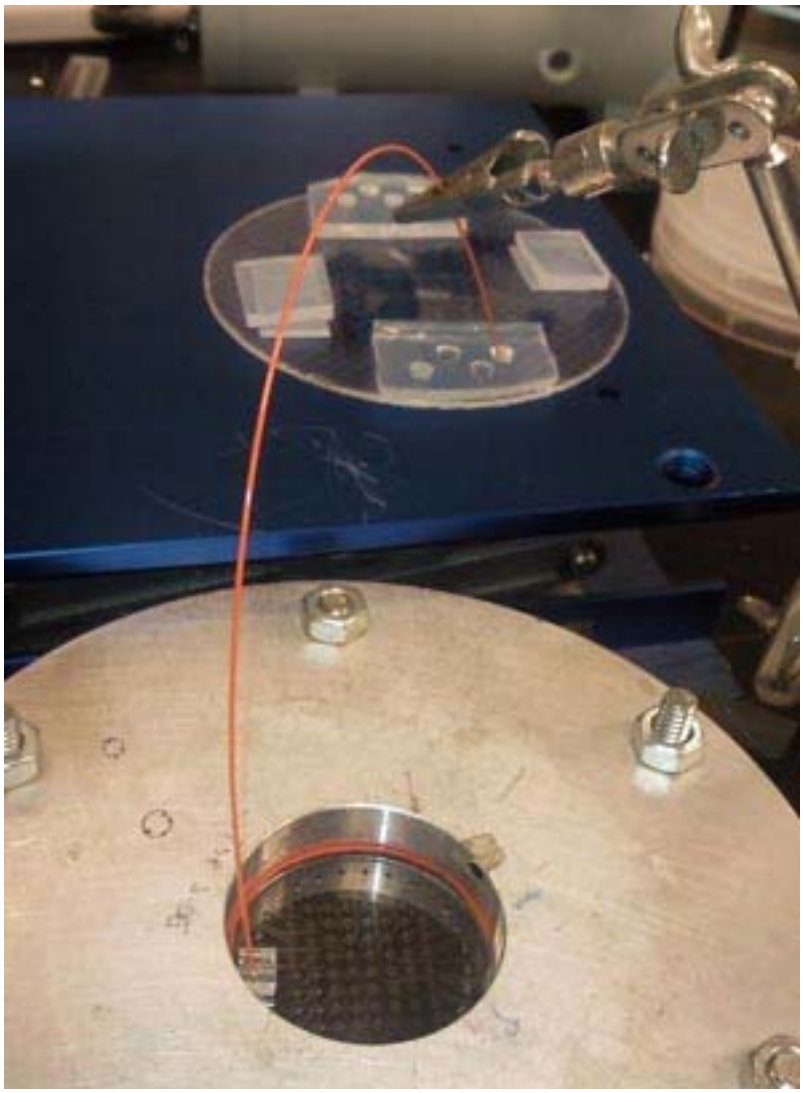

Figure 6.5 The Automaton device (bottom), an 8x8 rectilinear array of valves, and its interface to the Mars Organic Analyzer microchip CE device (top). The 30 cm long, 50 μm internal diameter PEEK tubing interface attaches to the Automaton fluidic outlet via a snug-fitting PDMS gasket, and is freestanding in the 3 mm wide 40 μL capacity well formed by a similar PDMS gasket over the MOA CE chip sample well.

Pacific Blue succinimidyl ester (PB) labeling of amino acids. PB labeling of amino acids was conducted on the Automaton device with automatic transfer to the sample well of the CE microchip as well as manually. The Automaton program depicted in Figure 6.6A combines PB from reservoir *c1* and an amino acid standard from reservoir *d2*. The combined fluid is mixed through serial transfer and sent to the MOA for analysis through output b1. The fluidic travel time from the Automaton to the MOA was ~ 10 min, and an additional ~ 10 min were required to fill the MOA reservoir. The manual reaction was allowed to proceed for 15 min before manual loading and separation.

The resulting electropherograms using the two labeling methods are shown in Figure 6.6B. Autonomous on-chip labeling provided approximately 70% (± 20%) the peak areas of manual off-chip labeling. Autonomous sample transfer results in peak efficiencies that are 30% of those resulting from manual transfer. Reduced peak efficiencies are also obtained when the sample is manually labeled and loaded and then analyzed 10-15 min later. This indicates that the cause of the decreased separation quality is due primarily to diffusion of sample from the sample well into the injection arm during the 10 min sample transfer and is not inherent to autonomous labeling. A more detailed description and analysis of these experiments can be found elsewhere.[123]

Cascade Blue hydrazide (CB) labeling of amino acids. The program used to label carboxylic acid standards described in Chapter 5 was also used for autonomous loading of the MOA (Figure 6.7). Faster processing operations reduced the transfer time and improved separation qualities from 30% of manual loading for the slower program (PB-labeling) to 97% of manual loading for the faster program (CB-EDC labeling). However, the tailing of the later peaks in this separation indicates that further optimization of processing speed is necessary.

The resulting electropherograms using the two labeling methods are shown in Figure 6.6B. Autonomous on-chip labeling provided approximately 70% (± 20%) the peak areas of manual off-chip labeling. Autonomous sample transfer results in peak efficiencies that are 30% of those resulting from manual transfer. Reduced peak efficiencies are also obtained when the sample is manually labeled and loaded and then analyzed 10-15 min later. This indicates that the cause of the decreased separation quality is due primarily to diffusion of sample from the sample well into the injection arm during the 10 min sample transfer and is not inherent to autonomous labeling. A more detailed description and analysis of these experiments can be found elsewhere.[123]

Cascade Blue hydrazide (CB) labeling of amino acids. The program used to label carboxylic acid standards described in Chapter 5 was also used for autonomous loading of the MOA (Figure 6.7). Faster processing operations reduced the transfer time and improved separation qualities from 30% of manual loading for the slower program (PB-labeling) to 97% of manual loading for the faster program (CB-EDC labeling). However, the tailing of the later peaks in this separation indicates that further optimization of processing speed is necessary.

The separation quality of autonomously loaded samples can be increased in a number of

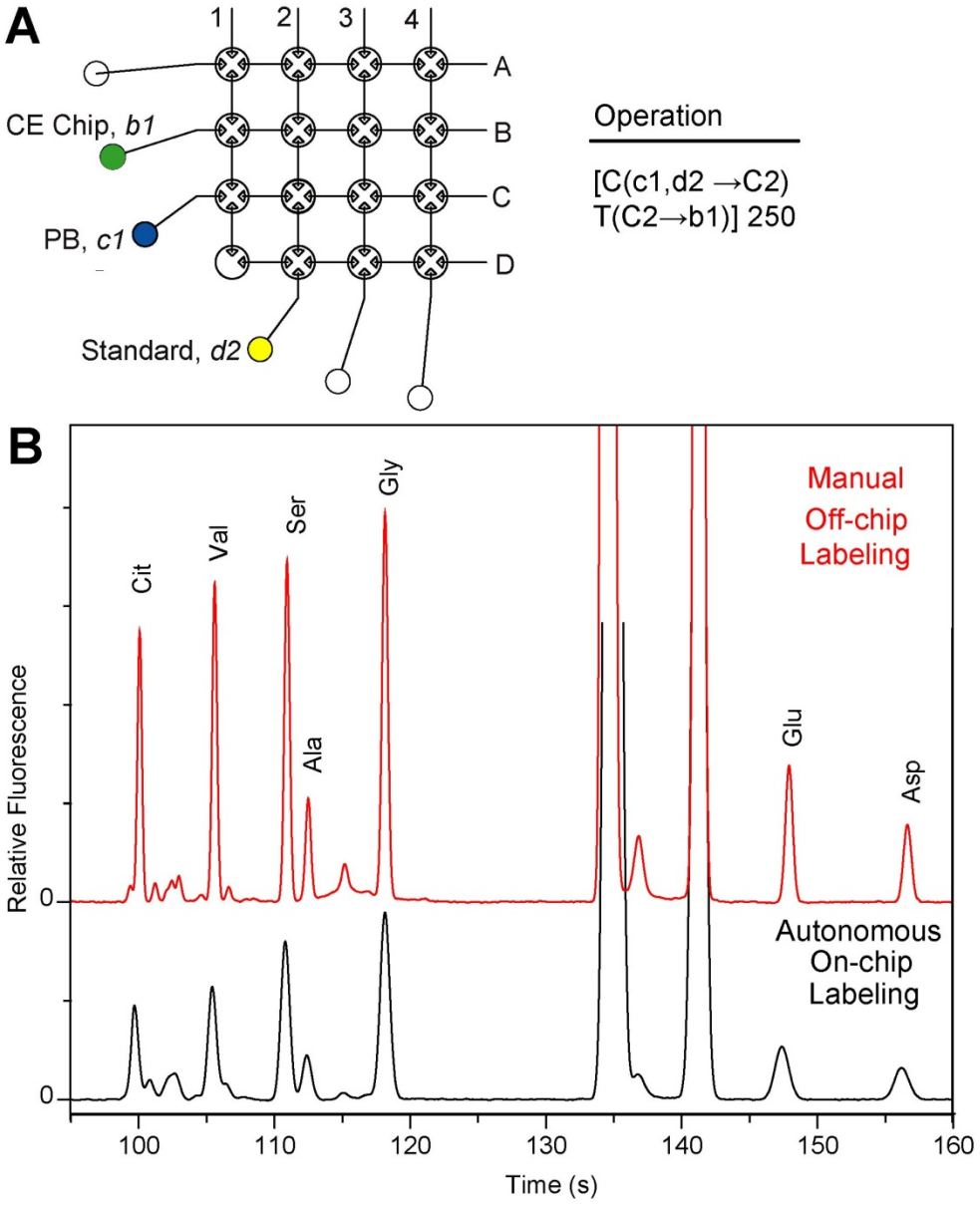

Figure 6.6 Autonomous and manual Pacific Blue succinimidyl ester (PB) labeling of an amino acid standard.(A) A depiction of the Automaton delineating reservoir use and the fluidic program executed here, and (B) electropherograms of autonomous on-chip sample labeling and transfer (bottom) and manual sample labeling and transfer (top). Labeling is conducted by combining equal volumes of 40 μM PB in 30 mM borate, pH 5-6 with an amino acid standard in 30 mM borate, pH 9.5. The standard contains 2 μM each citrulline (Cit), valine (Val), serine (Ser), alanine(Ala), and glycine (Gly) and 8 μM each aspartic acid (Asp) and glutamic acid (Glu).

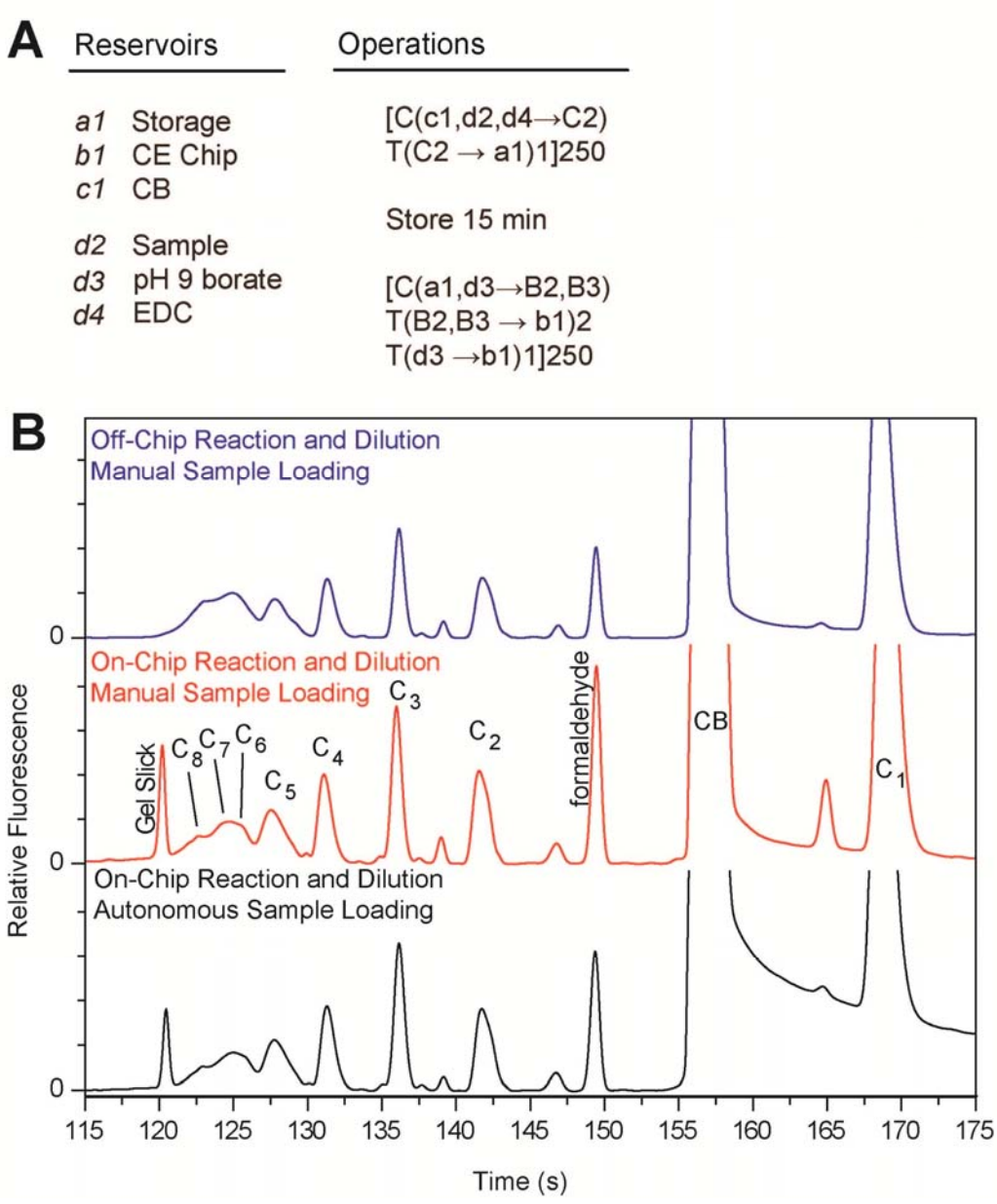

Figure 6.7 Autonomous and manual Cascade Blue hydrazide (CB) labeling of a carboxylic acid standard with 1-ethyl-3-(3-dimethylaminopropyl)carbodiimide (EDC) activation. (A) Reservoir designations and fluidic program for the operations conducted here, and (B) electropherograms of autonomous on-chip sample labeling, dilution, and transfer (bottom) autonomous on-chip sample labeling and dilution with manual transfer (middle) and manual sample labeling, dilution, and transfer (top). Labeling is conducted as described in Chapter 5. The standard contains 3.2 mM total carboxylic acid content: 200 μM formic acid, 400 μM each acetic, propanoic, butanoic, pentanoic, hexanoic, and heptanoic acids, and 600 μM octanoic acid.

ways: the Automaton protocols can be modified to achieve greater transfer rates, smaller fluidic reservoirs can be used for the CE microchip, larger microvalves can be used to increase the volume processed per cycle, and the electrophoretic injection program can be modified to include a "push-back" step, where EOF drives fluid from all arms of the chip back into the sample well for several seconds before the usual injection procedure. With these improvements, we expect future versions will have autonomous peak efficiencies similar to those obtained manually. The preliminary experiments described in this chapter demonstrate the feasibility of high-quality MOA separations for multiple analytes using the Automaton for programmable sample processing and loading.

6.3 Total Automation of the Mars Organic Analyzer

The programmability and large volume sample processing capabilities of the Automaton make it ideal for automating diverse sample labeling and analysis procedures for the MOA. A wide range of operations can be performed on the Automaton and can be combined into programs for totally automated analysis of unknown samples for amines, amino acids, aldehydes, ketones, and carboxylic acids. For instance, operations such as dilutions prior to labeling, sample derivatization, spiking with a standard, dilutions post-labeling, spiking post-reaction with a pre-labeled standard, and loading buffers and samples into the electrophoresis column can all be achieved with previously demonstrated Automaton operations. A flow chart of a CZE sample analysis for amines, amino acids, aldehydes, ketones, and carboxylic acids and MEKC[121] for amines and amino acids is shown in Figure 6.8. After loading sample for analysis, different subroutines are selected based on the type of analyte that will be labeled. These subroutines enable spiking with standard for peak identification, labeling of sample, serial dilution for quantification, and a choice between CZE or MEKC analysis. Additional subroutines enable processing high salt concentration samples to increase the flexibility for sample types. Finally, sample is autonomously transferred to the Mars Organic Analyzer sample well. To date, no system has been demonstrated with this level of programmability for CZE sample processing. However, all of the operations could easily be performed using the Automaton.

Future work and program optimization should enable implementation of all operational steps shown in Figure 6.8 using the Automaton platform. Although devices have been demonstrated that can automate small portions of these procedures, no system has been demonstrated for fully autonomous chip-based sample processing for a general purpose CZE analyzer. Such an achievement would represent a significant advancement in the miniaturization and automation of chemical and biological analysis systems.

6.4 Nucleic Acid Analysis

The detection of specific nucleic acid sequences typically requires a target amplification method such as PCR, or signal amplification method such as branched DNA.[124] Since each microvalve of the Automaton platform can be loaded as a discrete volume, it should be possible to perform nucleic acid amplifications within a single microvalve reactor. Initial efforts focused on PCR thermal cycling using externally applied Minco heaters for temperature control. However difficulties were encountered due to high temperature required for the denaturation step (95°C). Microvalves are held open with an applied vacuum, and the permeability of PDMS to gases results in a decreased pressure inside of the reactor region. This decreased pressure significantly reduces the boiling point of water (74°C with an applied vacuum of -87 kPa).

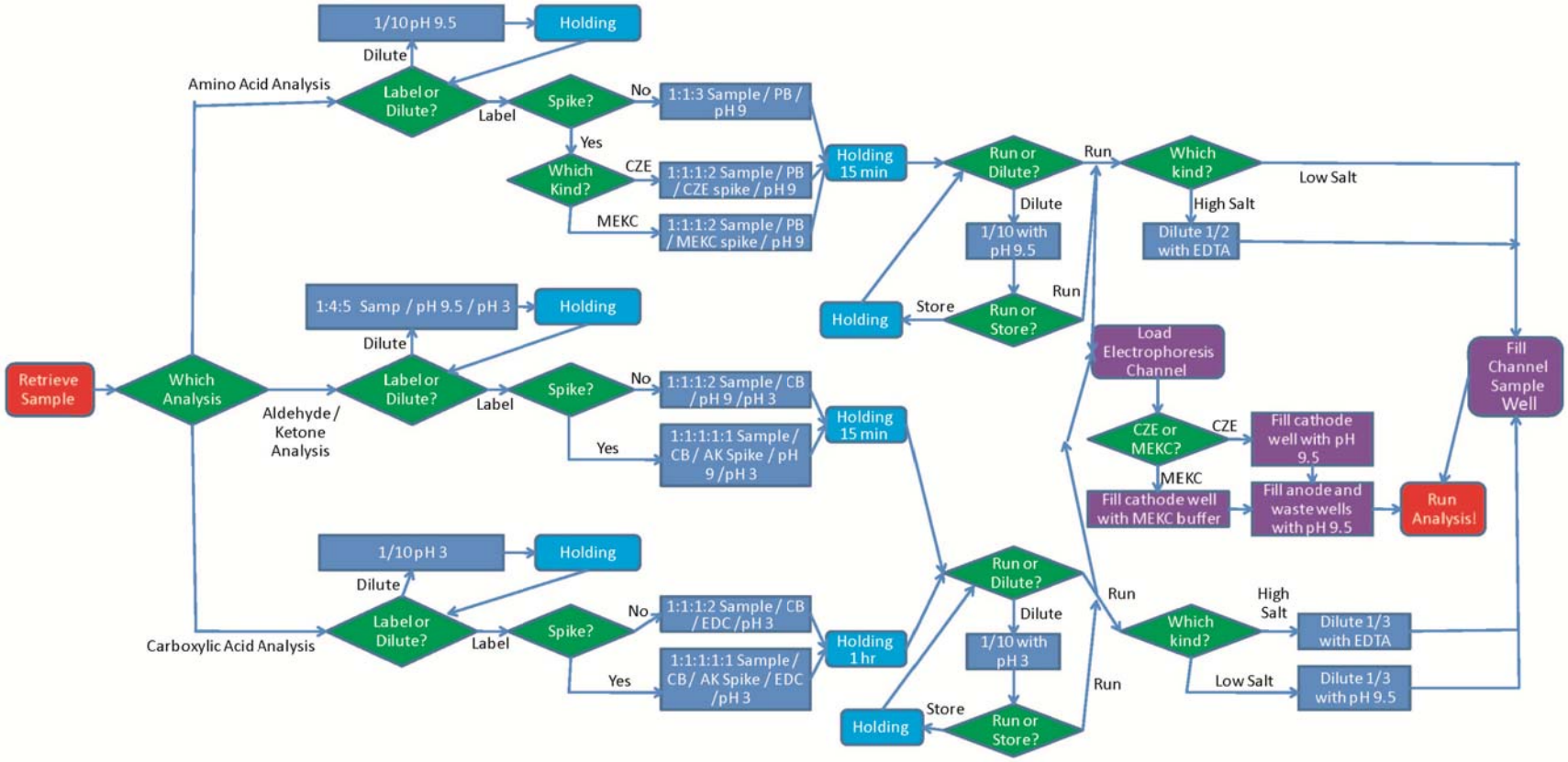

Figure 6.8 Flow chart depicting the full analysis of an unknown sample using CZE for amines, amino acids, aldehydes, ketones, and carboxylic acids, and MEKC for amines and amino acids

Although this property prevents PCR within an open microvalve, it could be useful for other applications such as lyophilization of reagents within individual microvalves for on-chip storage.

Helicase dependent amplification (HDA) is an alternative to PCR for nucleic acid amplification that is performed isothermally at 65° C.[125] With this system, helicases are used to denature DNA instead of elevated temperature. To evaluate the feasibility of performing HDA on the Automaton platform, reagents, primers, and control template were acquired from the IsoAmp II Universal tHDA Kit (Biohelix Corp., Beverly, MA). A mastermix was prepared for the real time HDA protocol according to the manufacturer instructions. Individual microvalves were loaded with mastermix containing 0.02 ng/uL control template, and a negative control. An external Minco heater was used to adjust the reaction temperature to 65° C. Figure 6.9 shows a schematic of the external heating system and epifluoresence images of the positive and negative control microvalve reactors after 30 minutes. A significant increase in fluorescence indicates successful target amplification in the reactor containing template. Further characterization and optimization of these procedures should enable simple protocols for nucleic acid amplification and analysis using the Automaton platform.

Our group has developed high-throughput and portable microfluidic PCR analysis systems for sequencing,[39] pathogen detection,[36,126] forensic applications,[127] and single cell genetic expression analysis.[128] Although these systems have enabled robust detection of nucleic acid biomarkers in the field, complex fabrication and control systems are required, and a variety of device designs are necessary for different applications. The ability to perform HDA amplifications on the Automaton could enable a common sample processing architecture for each of these applications. Furthermore, the reduction in fabrication complexity enabled by isothermal amplification could reduce costs and increase the portability of microfluidic genetic analysis systems.

6.5 Sample Processing for Low Titer Protein Biomarkers

As our understanding of disease mechanisms continues to evolve, the need for high-sensitivity protein biomarker detection is increasing. For example, interleukin-13 (IL-13) has been implicated in the pathophysiology of asthma.[129] However, standard ELISA assays lack the sensitivity necessary to detect baseline levels in healthy subjects (approximately 0.25 pg/mL). Since IL-13 is a potential therapeutic target, more sensitive tests are necessary for evaluation of drug efficacy. As another example, the HIV p24 antigen is present in infected individuals well before anti-HIV antibodies can be detected.[130] However, the plasma titer during early stages is lower than the limit of detection for standard p24 assays.

Ledger et al.[131] demonstrated sufficient sensitivity for baseline IL-13 levels using paramagnetic particles as a solid phase, and a fluorescence detection system that counts single molecules as they flow through an interrogation space in a capillary. The use of magnetic microbeads as a solid phase offers much higher surface area for target capture and faster binding kinetics than standard ELISA in a 96-well plate. With this approach, capture antibody labeled beads are incubated with sample followed by a fluorescently labeled detection antibody. After rinsing unbound detection antibody, the detection antibody is detached from the beads using an elution buffer. The fluorescently labeled antibodies are then detected as described above using a flow-through fluorescence detector.[132]

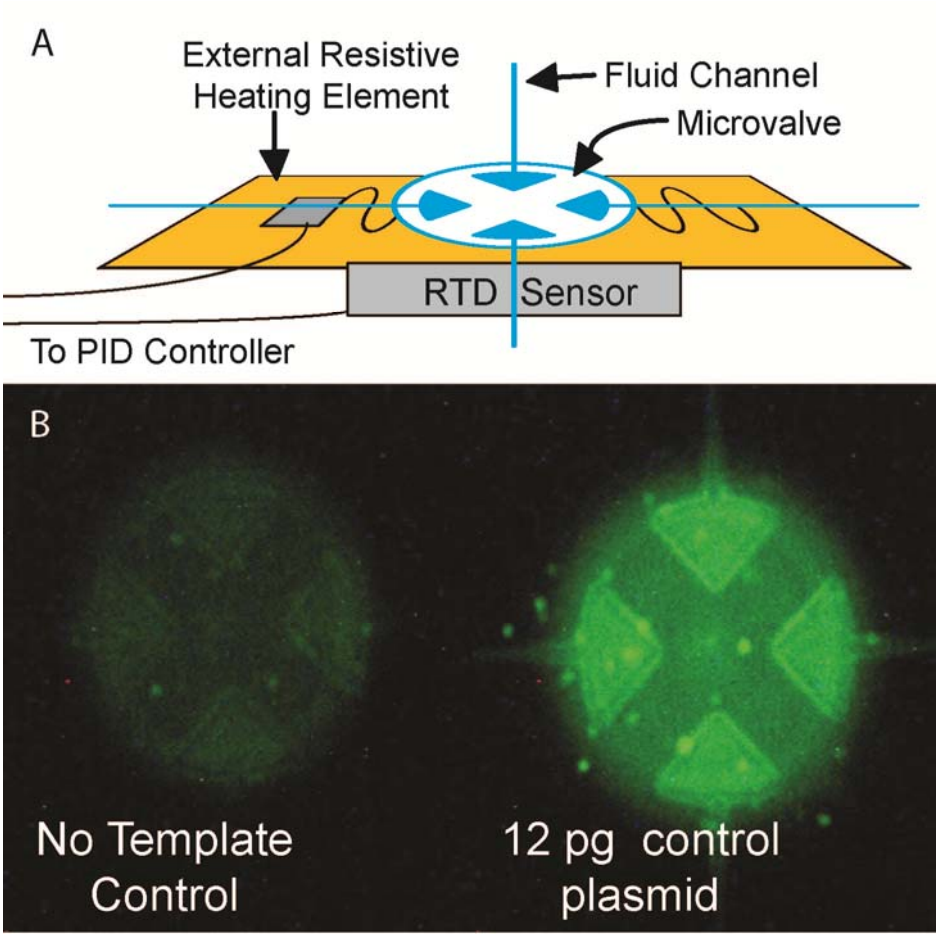

Figure 6.9 (A) Schematic of external heating system for isothermal HDA amplification of nucleic acids. A resistive heating element is externally affixed to the pneumatic layer and an RTD sensor is used to monitor temperature of the heater. (B) Epifluorescence images of HDA reactions containing no template (left) and 12 pg of a control plasmid (right) after 30 min incubations at 65° C. Signal from the Eva green intercalating dye is significantly higher in the positive control, indicating successful target amplification.

The programmable sample processing capabilities of the microfluidic Automaton make it ideally suited for automation of high-sensitivity immunoassay procedures. Figure 6.10 illustrates a proposed automation protocol. In Chapter 4, a procedure for trapping antibody labeled magnetic particles within individual microvalves was demonstrated. Furthermore, protocols for perfusion of the beads with μL scale volumes were demonstrated to capture a protein target and perform rinsing of unbound materials. Similar procedures can be used to load beads, deliver sample, deliver detection antibody, and perform rinsing operations in this procedure (Figure 6.10A-6.10C). In the next step, a single microvalve is loaded with magnetic microbeads and an elution buffer to remove the detection antibody (Figure 6.10D). It is important note that the beads can be treated with a single microvalve volume of elution buffer resulting in the release of the detection antibodies into only 120 nL (or less depending on microvalve design). This should result in a significant concentrating effect since the beads can be used to process microliters of sample. The final step of this procedure requires transfer of the elution buffer to a flow-through fluorescence detector (Figure 6.10E). This process could be automated using a simple PEEK tubing interconnection between the detection system and the Automaton as demonstrated in this chapter and using protocols described in Chapter 5. The successful automation of these sample processing procedures would enable miniaturized, high-sensitivity immunoassays for protein targets that would be of tremendous value for point-of-care applications. Nucleic acid targets could also be concentrated and analyzed using sequence specific oligonucleotide capture probes and elevated temperature for target release.

6.6 Conclusion

The objective of this dissertation was to develop generic microfluidic sample processors with sufficient programmability to perform a broad range of molecular diagnostic assays. In the preceding chapters, the digital microfluidic Automaton was used to automate quantitative homogeneous assays for metabolites, inhomogeneous assays for protein biomarkers, and target amplification procedures for nucleic acids. Currently, no commercially available miniaturized analysis systems have this range of capabilities. The combinatorial mixing and serial processing capabilities of the Automaton at multiple volume scales enables emulation of most of the operations performed by conventional robotic sample handling systems. So far, only a small fraction of possible operations have been evaluated with this system. It is the hope of the author that this work will inspire continued research in the development of programmable microfluidic systems for miniaturized and automated molecular diagnostic applications.

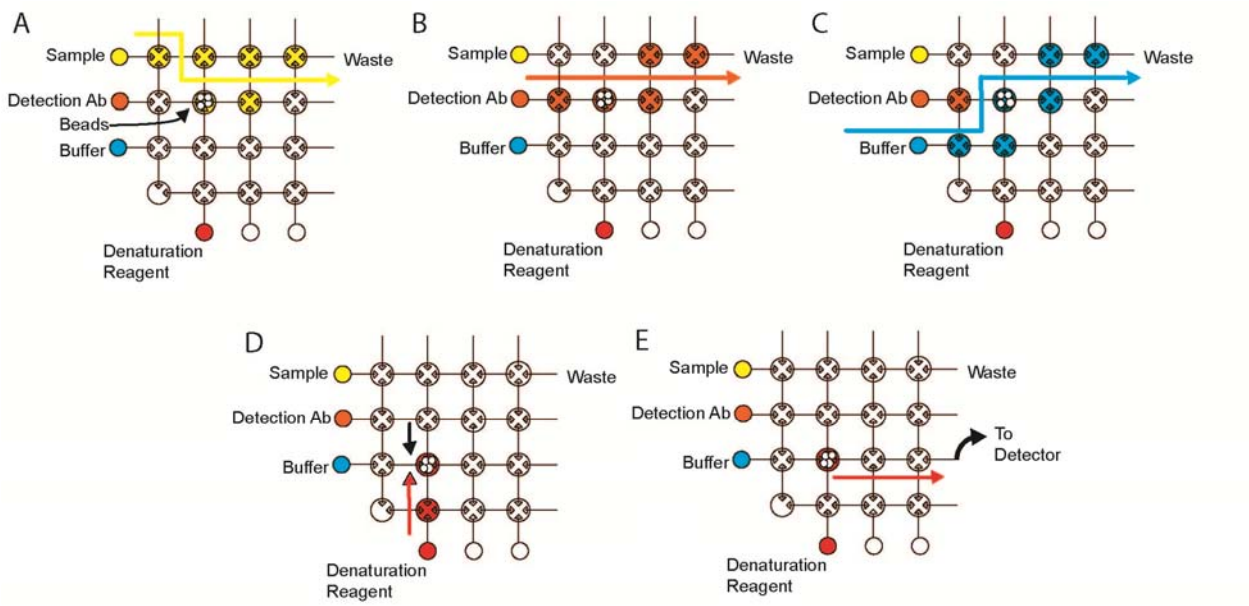

Figure 6.10 Proposed Automaton program for high-sensitivity immunoassays using magnetic microparticles. (A) Sample is continuously transferred through a microvalve containing magnetic capture beads. (B) Detection antibody is loaded through the microbead reactor valve. (C) Unbound detection antibody is rinsed from the beads. (D) 120 nL elution buffer is loaded to the beads to release the detection antibody. (E) The elution buffer is transferred to a fluorescence detection system through a PEEK tubing interconnection.

Appendix A: Supplemental Information for Chapter 2

A.1 Pneumatic Logic Truth Tables and Dynamic Response Times

As described in Chapter 2, propagation times and output magnitudes for each individual logic gate were characterized on a single fabricated device. Separate pumps were used to supply logic high (-87 kPa) and logic low (6 kPa) pressures to the off-chip solenoid valves. For each logic gate, operand and control inputs were actuated simultaneously, and output pressure was measured with a strain gauge pressure transducer (PM 100D, World Precision Instruments). Each logic gate generated output vacuum magnitudes in the expected ranges for all possible combinations of input magnitudes. In each case, logic high output magnitudes were significantly higher than the upper bound of valve actuation threshold (-32 kPa). Logic low output magnitudes were significantly below the lower bound for valve actuation (-20 kPa). Response times were determined using CCD camera videography.

NOT Gate

A	NOT(A)
6	-87
-87	-6

AND Gate

A	B	AND
6	-86	0
-86	-86	-82
6	6	0
-86	6	0

OR Gate

A	B	OR
6	6	0
-86	6	-82
6	-86	-83
-86	-86	-82

XOR Gate

A	B	XOR
6	6	0
-86	6	-63
6	-86	-64
-86	-86	0

NAND Gate

A	B	NAND
6	6	-85
-86	6	-85
6	-86	-85
-86	-86	-6

Dynamic response times

NOT	45 ms
AND	175 ms
OR	125 ms
XOR	250 ms
NAND	45 ms

A.2 Transfer Characteristics of the Pneumatic Inverter

The transfer characteristics of individual microvalves were determined by varying operand input pressure and measuring equilibrium output pressure with a strain gauge pressure transducer. A family of curves was collected by repeating the analysis for several gate control input channel pressures (-15 – -87 kPa). Sharp threshold transitions between high and low output were observed for a each of the gate control input pressures. Inverter thresholds depend on gate control input pressures for reasons similar to those described in section 2.4 for individual microvalves. As this data demonstrates, actuation of the inverter microvalve opens a low resistance path between the output and a drilled hole to atmosphere, resulting in a highly effective reduction of output vacuum magnitude to subthreshold levels.

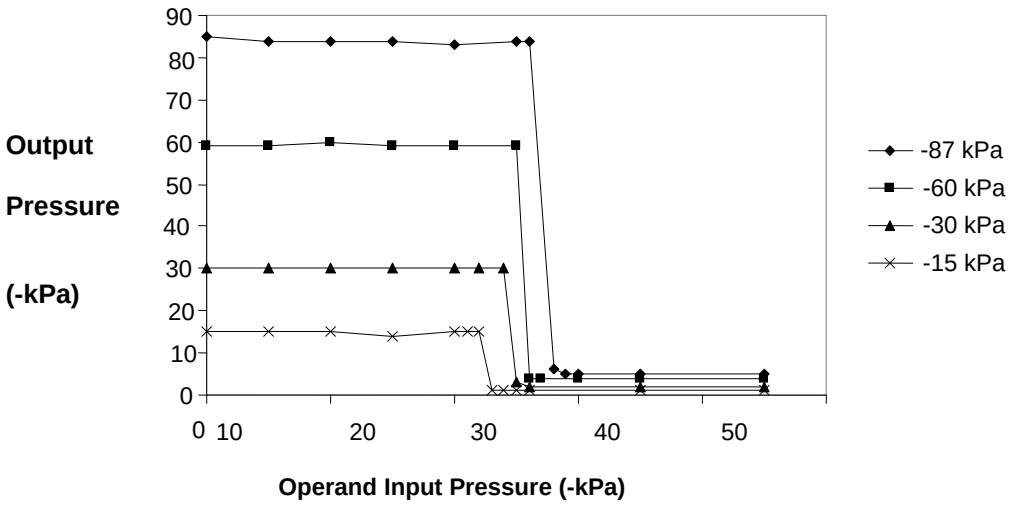

Figure A.1. Transfer characteristics of the micropneumatic inverter.

A.3 Adder Closing Procedure

In an *n*-bit, pneumatic ripple carry adder, two binary numbers are added:

$$A_n A_{n-1} \ldots A_1 \quad \text{and} \quad B_n B_{n-1} \ldots B_1$$

A_1 and B_1 represent least significant bits, whereas A_n and B_n represent most significant bits.

The closing procedure shown below removes latched vacuum from the circuitry of a pneumatic 8-bit ripple carry adder. The "Open" instruction results in the application of a -87 kPa vacuum to the corresponding inputs, the "Close" instruction results in the application of a 6 kPa pressure, and the "Wait" instruction results in a 250 ms delay before the program continues to the next step.

Close{Ctrl C, Ctrl S, B}
Wait
Close{Ctrl X2} AND Open{Ctrl C, $A_1A_2 \ldots A_n$, Ctrl X1}
Wait
Close{Ctrl X1} AND Open{ $B_1B_2 \ldots B_{n-1}$}
Wait
Close{Ctrl C, $A_1A_2 \ldots A_n$, B_1 }
Wait
Open{$A_1A_2 \ldots A_n$, $B_1B_2 \ldots B_n$, Ctrl X1, Ctrl X1X2 }
Wait
Close{$B_1B_2 \ldots B_n$, Ctrl X1X2}
Wait
Close{Ctrl X1}
Wait
Close{$A_1A_2 \ldots A_n$}
Wait

A.4 Videos

Videos of the micropneumatic 8-bit binary adder are available online at:
http://ieeexplore.ieee.org/xpl/multimedia.jsp?arnumber=4380307&isnumber=4389159

A.5 Further Developments and Applications of Micropneumatic Logic

In 2009, Rhee et al.[133] demonstrated enhancements of the micropneumatic logic structures presented in Chapter 2. Normally closed microvalves were fabricated using multilayer soft lithography. These two-layer structures consisted of a discontinuity in PDMS microchannels bonded to a diaphragm membrane in a PDMS manifold layer. The anisotropic nature of PDMS microchannel formation enables precise control of the resistance to airflow by adjusting channel widths. Figure A.2 illustrates the design of an inverter structure developed using this system. This structure is virtually identical to the inverter structure presented in Chapter 2, however a high-resistance microchannel is incorporated between the output and the control vacuum input. The inclusion of a high-resistance microchannel reduces static current of airflow when the not gate is in the off-state. Similar principles were utilized to develop a variety of high-efficiency logic gates and assemble them into complex digital logic structures including flip-flops and clock signal generators. These developments demonstrate the potential of this technology for advanced pneumatic microprocessing systems. It may therefore be possible to construct serial single-ended computer bus systems similar to I^2C circuits. Such systems enable the addressing of a large number of outputs using only two control inputs. This would offer significant advantages over demultiplexers for scaled control of large microvalve arrays.

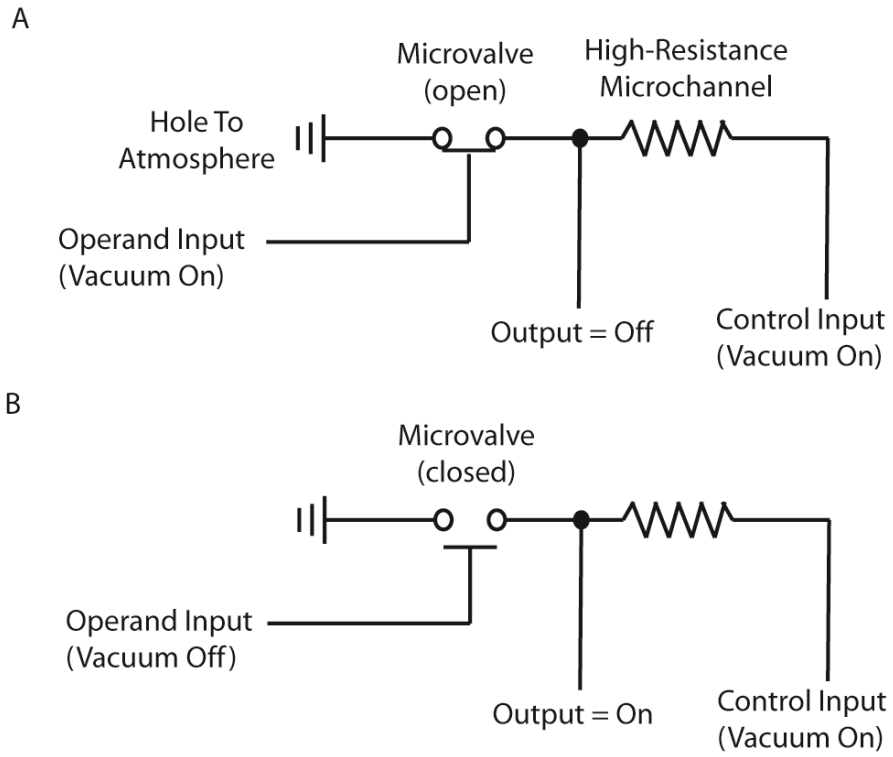

Figure A.2 Electrical representations of the pneumatic inverter with high-resistance channel developed by Rhee et al.[133] (A) When vacuum is applied to the operand input, a connection is formed between the hole to atomosphere and the output, resulting in a significant increase in pressure at the output. Since most of the resistance is on the control input side, the output is close to atmospheric pressure. (B) When vacuum is removed from the operand input, the valve closes, and the full magnitude of vacuum from the control input is transmitted to the output.

Appendix B: Supplemental Information for Chapter 3

B.1 Automaton Manifold Assembly

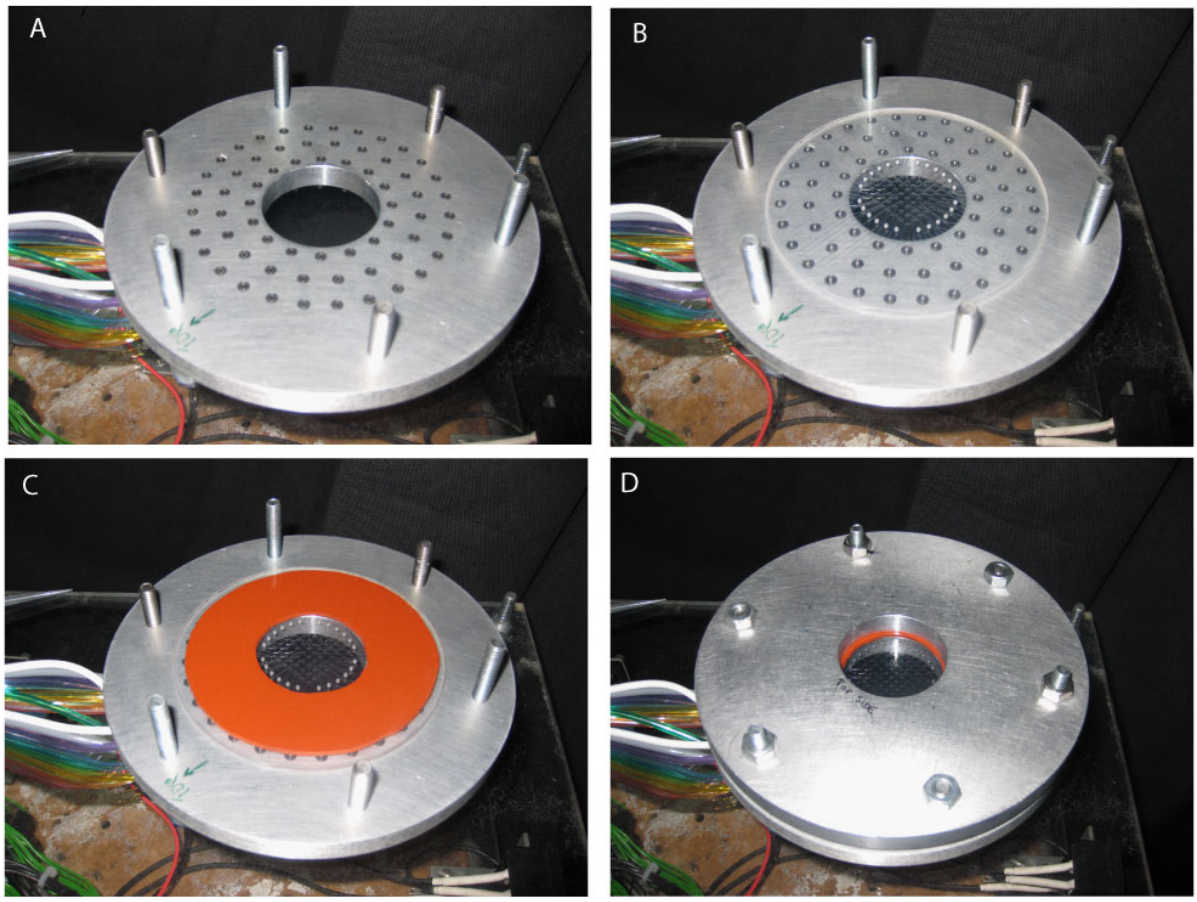

Figure B.1 Manifold for pneumatic control of the microfluidic Automaton. (A) 3/8” Aluminum plate with embedded O-rings ports. Pneumatic tubing (rainbow colored) addresses each port on the opposite side. (B) Microfluidic Automaton with drilled pneumatic inputs facing each of the pneumatic ports on the manifold. (C) A silicon rubber gasket is placed on the top surface of the Automaton. (D) An additional 3/8” aluminum manifold is screwed in place using six ¼” bolts to complete the assembly. Fluidic inlets and outlets can be accessed through a central hole in the top manifold layer.

B.2 Program Details for Automaton Fluid Transfer

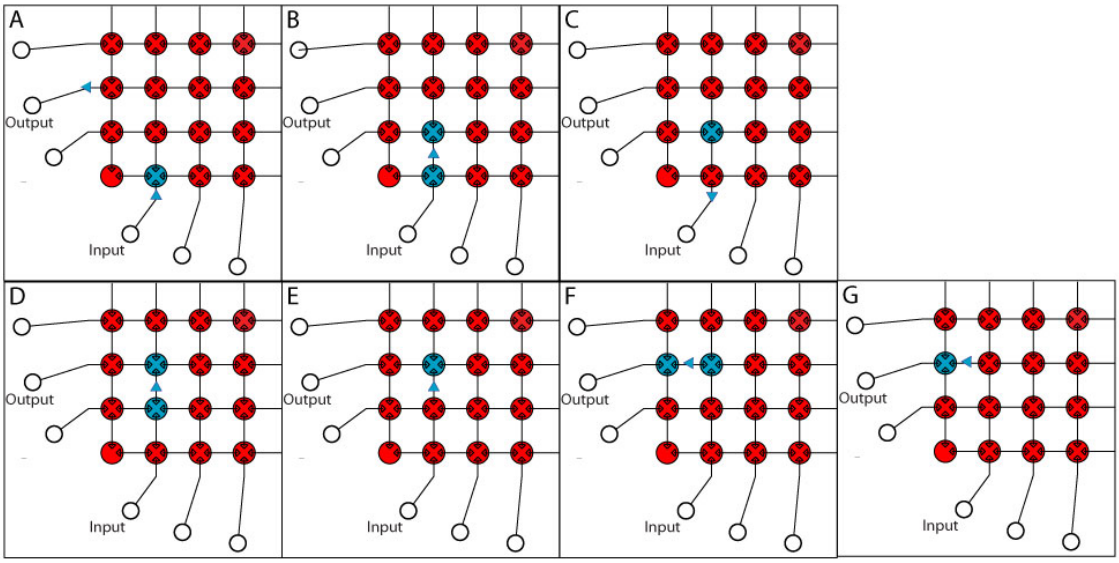

Figure B.2 Schematic of the 4-valve pumping program used to evaluate fluidic transfer efficiency between microvalves. The blue arrow indicates the direction of fluid flow at each step. A closing pressure of 25 kPa was applied to all valves in the closed state (red). Switching individual microvalves to the open state (blue) is achieved by applying a -87 kPa opening pressure and holding for a specified actuation time before proceeding to the next step. Switching to the closed state is achieved by applying the same 25 kPa closing pressure to an open microvalve and holding for the same actuation time. With this program (steps A-E), the volume of one open microvalve is transferred from the input to the output per 7-step cycle.

B.3 Automaton Dead Volume Specifications

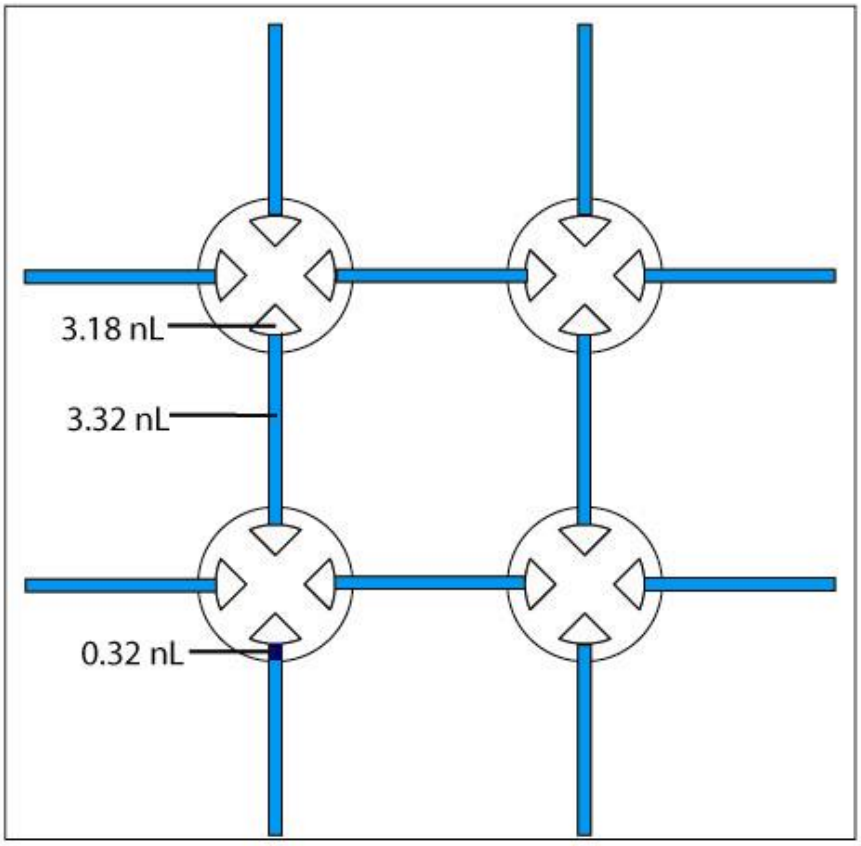

Figure B.3 Specification of dead volumes in fluidic channels with closed microvalves. The dead volumes in a 4-valve mixing loop are calculated as follows: D = (16 * 3.18) + (4*3.32) + (8 * 0.320) = 66.7 nL

B.4 Video

A video of the Automaton mixing procedure is available online at:

http://www.rsc.org/suppdata/lc/b9/b920124f/Automaton_mix.mov

Appendix C: Supplemental Information for Chapter 5

C.1 Full Program for Figure 5.1B

```
main
call cycle 100
end

cycle
open(C1)
open(D1)
call wait
open(C2)
call wait
close(C1)
close(D1)
call wait
open(B1)
call wait
close(C2)
call wait
close(B1)
end

wait
w250
end
```

B2 is fluttered continuously in a separate program that runs simultaneously.

C.2 Proportions Loaded to the Combining Valve in the 6-bit Combinatorial Mixing Device for Inputs A-C

Binary Sequence	%A Input	%B Input	%C Input	Binary Sequence	%A Input	%B Input	%C Input
100000	100	0	0	100001	52	0	0
010000	0	100	0	010001	0	56	0
110000	48	52	0	110001	32	32	0
001000	0	0	100	001001	0	0	54
101000	49	0	50	101001	35	0	16
011000	0	52	47	011001	0	38	31
111000	33	34	30	111001	22	24	22
000100	0	0	0	000101	0	0	0
100100	38	0	0	100101	32	0	0
010100	0	54	0	010101	0	39	0
110100	22	33	0	110101	28	25	0
001100	0	0	38	001101	27	0	0
101100	22	0	20	101101	30	0	25
011100	0	39	24	011101	0	38	21
111100	22	30	20	111101	21	22	12
000010	0	0	0	000011	0	0	0
100010	48	0	0	100011	27	0	0
010010	0	63	0	010011	0	36	0
110001	30	43	0	110011	21	22	0
001010	0	0	35	001011	0	0	40
101010	36	0	24	101011	23	0	15
011010	0	53	28	011011	0	38	21
111010	16	40	16	111011	20	20	11
000110	0	0	0	000111	0	0	0
100110	32	0	0	100111	26	0	0
010110	0	47	0	010111	0	36	0
110110	28	29	0	110111	24	21	0
001110	0	0	32	001111	0	0	25
101110	28	0	24	101111	23	0	17
011110	0	38	21	011111	0	33	20
111110	20	18	12	111111	19	25	11
000001	0	0	0	000000	0	0	0

References

(1) Winston, B. *Media technology and society: a history : from the telegraph to the Internet*; Routeledge: London, 1998.

(2) Poste, G. *Expert Rev. Mol. Diagn.* **2001**, *1*, 1.

(3) Bearinger, J. P.; Dugan, L. C.; Baker, B. R.; Hall, S. B.; Ebert, K.; Mioulet, V.; Madi, M.; King, D. P. *IEEE Trans. Biomed. Eng.* **2011**, *58*, 805.

(4) Tomar, R. *Clin. Diagn. Lab. Immunol.* **1999**, *6*, 293.

(5) Rodrigues Ribeiro Teles, F. S.; Pires de Tavora Tavira, L. A.; Pina da Fonseca, L. J. *Crit. Rev. Clin. Lab. Sci.* **2010**, *47*, 139.

(6) Steinfelder-Visscher, J.; Teerenstra, S.; Gunnewiek, J. M.; Weerwind, P. W. *J. Extra Corpor. Technol.* **2008**, *40*, 57.

(7) Bruls, D. M.; Evers, T. H.; Kahlman, J. A. H.; van Lankvelt, P. J. W.; Ovsyanko, M.; Pelssers, E. G. M.; Schleipen, J.; de Theije, F. K.; Verschuren, C. A.; van der Wijk, T.; van Zon, J. B. A.; Dittmer, W. U.; Immink, A. H. J.; Nieuwenhuis, J. H.; Prins, M. W. J. *Lab Chip* **2009**, *9*, 3504.

(8) Brenwald, N. P.; Baker, N.; Oppenheim, B. *J. Hosp.Infect.* **2010**, *74*, 245.

(9) Skeggs, L. T. *Am. J.Clin. Path.* **1957**, *28*, 311.

(10) Mathies, J. C. *Clin. Chem.* **1974**, *20*, 1573.

(11) Squires, T. M.; Quake, S. R. *Rev.Mod. Phys.* **2005**, *77*, 977.

(12) Briem, S.; Martinsson, S.; Bueters, T.; Skoglund, E. *Rapid Commun. Mass. Spectrom.* **2007**, *21*, 1965.

(13) Chang, H.; Yeo, L. *Electrokinetically driven microfluidics and nanofluidics*; Cambridge University Press: Cambridge, 2010.

(14) Fair, R. B. *Microfluid. Nanofluid.* **2007**, *3*, 245.

(15) Haeberle, S.; Zengerle, R. *Lab Chip* **2007**, *7*, 1094.

(16) Oh, K. W.; Ahn, C. H. *Journal of Micromechanics and Microengineering* **2006**, *16*, R13.

(17) Daniels, R. *Delmar's Guide to Laboratory and Diagnostic Tests*; Delmar: Albany, NY, 2002.

(18) Grover, W. H.; Mathies, R. A. *Lab-on-a-Chip Technology: Vol. 1,Fabrication and Microfluidics*; Caister Academic Press: Norfolk, 2009.

(19) Kovacs, G. T. A. *Micromachined transducers sourcebook.*; McGraw-Hill: New York, 1998.

(20) Zdeblick, M.; Anderson, R.; Jankowski, J.; Kline-Schoder, B.; Christel, L.; Miles, R.; Weber, W. In *Solid-State Sensor and Actuator Workshop* Hilton Head,SC, 1994, p 251.

(21) Anderson, R. C.; Bogdan, G. J.; Barniv, Z.; Dawes, T. D.; Winkler, J.; Roy, K. In *International Conference on Solid-State Sensors and Actuators (Transducers 97)*; IEEE: Chicago, Il, 1997, p 477.

(22) Lagally, E. T.; Medintz, I.; Mathies, R. A. *Anal. Chem.* **2001**, *73*, 565.

(23) Unger, M. A.; Chou, H. P.; Thorsen, T.; Scherer, A.; Quake, S. R. *Science* **2000**, *288*, 113.

(24) Duffy, D. C.; McDonald, J. C.; Schueller, O. J. A.; Whitesides, G. M. *Anal. Chem.* **1998**, *70*, 4974.

(25) Thorsen, T.; Maerkl, S. J.; Quake, S. R. *Science* **2002**, *298*, 580.

(26) Hansen, C. L.; Sommer, M. O.; Quake, S. R. *Proc. Natl. Acad. Sci. U. S. A.* **2004**, *101*, 14431.

(27) Hansen, C. L.; Classen, S.; Berger, J. M.; Quake, S. R. *J. Am. Chem. Soc.* **2006**, *128*, 3142.

(28) Liu, J.; Hansen, C.; Quake, S. R. *Anal. Chem.* **2003**, *75*, 4718.

(29) Lee, C. C.; Sui, G.; Elizarov, A.; Shu, C. J.; Shin, Y. S.; Dooley, A. N.; Huang, J.; Daridon, A.; Wyatt, P.; Stout, D.; Kolb, H. C.; Witte, O. N.; Satyamurthy, N.; Heath, J. R.; Phelps, M. E.; Quake, S. R.; Tseng, H. R. *Science* **2005**, *310*, 1793.

(30) Wang, J.; Sui, G.; Mocharla, V. P.; Lin, R. J.; Phelps, M. E.; Kolb, H. C.; Tseng, H. R. *Angew. Chem. Int. Ed. Engl.* **2006**, *45*, 5276.

(31) Marcus, J. S.; Anderson, W. F.; Quake, S. R. *Anal. Chem.* **2006**, *78*, 3084.

(32) Lee, J. N.; Park, C.; Whitesides, G. M. *Anal. Chem.* **2003**, *75*, 6544.

(33) Grover, W. H.; Skelley, A. M.; Liu, C. N.; Lagally, E. T.; Mathies, R. A. *Sensors and Actuators B-Chemical* **2003**, *89*, 315.

(34) Zhang, W.; Lin, S.; Wang, C.; Hu, J.; Li, C.; Zhuang, Z.; Zhou, Y.; Mathies, R. A.; Yang, C. J. *Lab Chip* **2009**, *9*, 3088.

(35) Grover, W. H.; von Muhlen, M. G.; Manalis, S. R. *Lab Chip* **2008**, *8*, 913.

(36) Beyor, N.; Yi, L.; Seo, T. S.; Mathies, R. A. *Anal. Chem.* **2009**, *81*, 3523.

(37) Easley, C. J.; Karlinsey, J. M.; Bienvenue, J. M.; Legendre, L. A.; Roper, M. G.; Feldman, S. H.; Hughes, M. A.; Hewlett, E. L.; Merkel, T. J.; Ferrance, J. P.; Landers, J. P. *Proc Natl Acad Sci U S A* **2006**, *103*, 19272.

(38) Zeng, Y.; Novak, R.; Shuga, J.; Smith, M. T.; Mathies, R. A. *Anal. Chem.* **2010**, *82*, 3183.

(39) Blazej, R. G.; Kumaresan, P.; Mathies, R. A. *Proc. Natl. Acad. Sci. U. S. A.* **2006**, *103*, 7240.

(40) Paegel, B. M.; Joyce, G. F. *PLoS Biol.* **2008**, *6*, e85.

(41) Skelley, A. M.; Scherer, J. R.; Aubrey, A. D.; Grover, W. H.; Ivester, R. H.; Ehrenfreund, P.; Grunthaner, F. J.; Bada, J. L.; Mathies, R. A. *Proc. Natl. Acad. Sci. U. S. A.* **2005**, *102*, 1041.

(42) Benhabib, M.; Chiesl, T. N.; Stockton, A. M.; Scherer, J. R.; Mathies, R. A. *Anal. Chem.* **2010**, *82*, 2372.

(43) Easley, C. J.; Karlinsey, J. M.; Bienvenue, J. M.; Legendre, L. A.; Roper, M. G.; Feldman, S. H.; Hughes, M. A.; Hewlett, E. L.; Merkel, T. J.; Ferrance, J. P.; Landers, J. P. *Proc. Natl. Acad. Sci. U. S. A.* **2006**, *103*, 19272.

(44) Whitesides, G. M. *Nature* **2006**, *442*, 368.

(45) Neils, C.; Tyree, Z.; Finlayson, B.; Folch, A. *Lab Chip* **2004**, *4*, 342.

(46) Kee, S. P.; Gavriilidis, A. *Chem. Eng. J.* **2008**, *142*, 109.

(47) Hong, J. W.; Chen, Y.; Anderson, W. F.; Quake, S. R. *Journal of Physics-Condensed Matter* **2006**, *18*, S691.

(48) Chou, H. P.; Unger, M. A.; Quake, S. R. *Biomed. Microdev.* **2001**, *3*, 323.

(49) Paegel, B. M.; Grover, W. H.; Skelley, A. M.; Mathies, R. A.; Joyce, G. F. *Anal. Chem.* **2006**, *78*, 7522.

(50) Grover, W. H.; Mathies, R. A. *Lab Chip* **2005**, *5*, 1033.

(51) Mugele, F.; Duits, M.; van den Ende, D. *Adv. Colloid. Interface. Sci.* **2010**, *161*, 115.

(52) Mark, D.; Haeberle, S.; Roth, G.; von Stetten, F.; Zengerle, R. *Chem. Soc. Rev.* **2010**, *39*, 1153.

(53) Srinivasan, V.; Pamula, V. K.; Fair, R. B. *Lab Chip* **2004**, *4*, 310.

(54) Schaller, V.; Sanz-Velasco, A.; Kalabukhov, A.; Schneiderman, J. F.; Oisjoen, F.; Jesorka, A.; Astalan, A. P.; Krozer, A.; Rusu, C.; Enoksson, P.; Winkler, D. *Lab Chip* **2009**, *9*, 3433.

(55) Welch, E. R.; Lin, Y. Y.; Madison, A.; Fair, R. B. *Biotechnol. J.* **2011**, *6*, 165.

(56) Urbanski, J. P.; Thies, W.; Rhodes, C.; Amarasinghe, S.; Thorsen, T. *Lab Chip* **2006**, *6*, 96.

(57) Melin, J.; Quake, S. R. *Annu. Rev. Biophys. Biomol. Struct.* **2007**, *36*, 213.

(58) Grover, W. H.; Ivester, R. H.; Jensen, E. C.; Mathies, R. A. *Lab Chip* **2006**, *6*, 623.

(59) Stockton, A. M.; Chandra Tjin, C.; Huang, G. L.; Benhabib, M.; Chiesl, T.; Mathies, R. A. *Electrophoresis* **2011**, *Submitted*.

(60) Stockton, A. M.; Tjin, C. C.; Huang, G. L.; Benhabib, M.; Chiesl, T. N.; Mathies, R. A. *Electrophoresis* **2010**, *31*, 3642.

(61) Stockton, A. M.; Chiesl, T. N.; Scherer, J. R.; Mathies, R. A. *Anal. Chem.* **2009**, *81*, 790.

(62) Stockton, A. M.; Chiesl, T. N.; Huang, G. L.; Tjin, C. C.; Turkia, H.; Paasikallio, T.; Pitkanen, J. P.; Mathies, R. A. *J. Chromatogr. B* **2011**, *In Preparation*.

(63) Jensen, E. C.; Bhat, B. P.; Mathies, R. A. *Lab Chip* **2010**, *10*, 685.

(64) Lagally, E. T.; Mathies, R. A. *J. Phys: D: Appl. Phys.* **2004**, *37*, R245.

(65) Dittrich, P. S.; Tachikawa, K.; Manz, A. *Anal. Chem.* **2006**, *78*, 3887.

(66) Grover, W. H.; Skelley, A. M.; Liu, C. N.; Lagally, E. T.; Mathies, R. A. *Sens. Act. B Chem.* **2003**, *89*, 315.

(67) Hua, Z. S.; Xia, Y. M.; Srivannavit, O.; Rouillard, J. M.; Zhou, X. C.; Gao, X. L.; Gulari, E. *Journal of Micromechanics and Microengineering* **2006**, *16*, 1433.

(68) Jensen, D. F.; Mueller, H. R.; Schaffer, R. R. *Pneumatic diaphragm logic*; Amer. Soc. Mech. Eng.: New York, 1967.

(69) Holbrook, E. L. *Control Engineering* **1961**, *8*, 104.

(70) Wojtecki, R. *Air logic controls for automated systems*; CRC Press: Bocca Raton, Fl, 1999.

(71) Schneider, R. T. *Hydraul. Pneum.* **1995**, *48*, 59.

(72) Takao, H.; Ishida, M.; Sawada, K. *J. Microelectromech. Sys.* **2002**, *11*, 421.

(73) Takao, H.; Ishida, M. *J. Microelectromech. Sys.* **2003**, *12*, 497.

(74) Henning, A. K. In *Proc. Int. Mech. Eng. Congr. RD Expo.* Anaheim, CA, 2004, p 1.

(75) Reyes, D. R.; Ghanem, M. M.; Whitesides, G. M.; Manz, A. *Lab Chip* **2002**, *2*, 113.

(76) Simpson, P. C.; Roach, D.; Woolley, A. T.; Thorsen, T.; Johnston, R.; Sensabaugh, G. F.; Mathies, R. A. *Proc. Natl. Acad. Sci. U. S. A.* **1998**, *95*, 2256.

(77) Ayers, J. E. *Digital Integrated Circuits*; CRC Press: Boca Raton, FL, 2004.

(78) Omandi, A. R. *Computer Arithmetic Systems: Algorithms, Architecture, and Implementation*; Prentice-Hall: New York, 1994.

(79) Lagally, E. T.; Scherer, J. R.; Blazej, R. G.; Toriello, N. M.; Diep, B. A.; Ramchandani, M.; Sensabaugh, G. F.; Riley, L. W.; Mathies, R. A. *Anal. Chem.* **2004**, *76*, 3162.

(80) Liu, C. N.; Toriello, N. M.; Mathies, R. A. *Anal. Chem.* **2006**, *78*, 5474.

(81) Harrison, T. J. *Control Engineering* **1967**, *14*, 74.

(82) Butefisch, S.; Seidemann, V.; Buttgenbach, S. *Sens. Act. A Phys.* **2002**, *97-8*, 638.

(83) Fatikow, S.; Rembold, U. *Microsystem Technology and Microrobotics*; Springer-Verlag: Berlin, 1997.

(84) Morgan, D. *A Handbook for EMC Testing and Measurement*; Perenginus: London, U.K., 1994.

(85) Messenger, G. C.; Ash, M. S. *The Effects of Radiation on Electronic Systems*; Van Nostrand: New York, 1992.

(86) Jensen, E. C.; Grover, W. H.; Mathies, R. A. *J. Microelectromech.Sys.* **2007**, *16*, 1378.

(87) Teh, S. Y.; Lin, R.; Hung, L. H.; Lee, A. P. *Lab Chip* **2008**, *8*, 198.

(88) Srinivasan, V.; Pamula, V. K.; Fair, R. B. *Anal. Chim. Acta.* **2004**, *507*, 145.

(89) Miller, E. M.; Wheeler, A. R. *Anal. Chem.* **2008**, *80*, 1614.

(90) Li, L.; Mustafi, D.; Fu, Q.; Tereshko, V.; Chen, D. L. L.; Tice, J. D.; Ismagilov, R. F. *Proc. Natl. Acad. Sci. U. S. A.* **2006**, *103*, 19243.

(91) Kumaresan, P.; Yang, C. J.; Cronier, S. A.; Blazej, R. G.; Mathies, R. A. *Anal. Chem.* **2008**, *80*, 3522.

(92) Song, H.; Chen, D. L.; Ismagilov, R. F. *Angew. Chem. Int. Ed. Engl.* **2006**, *45*, 7336.

(93) Schudel, B. R.; Choi, C. J.; Cunningham, B. T.; Kenis, P. J. A. *Lab Chip* **2009**, *9*, 1676.

(94) Hong, J. W.; Chen, Y.; Anderson, W. F.; Quake, S. R. *J. Phys. Condens. Mat.* **2006**, *18*, S691.

(95) Jambovane, S.; Duin, E. C.; Kirn, S. K.; Hong, J. W. *Anal. Chem.* **2009**, *81*, 3239.

(96) Djamali, A.; Sadowski, E. A.; Muehrer, R. J.; Reese, S.; Smavatkul, C.; Vidyasagar, A.; Fain, S. B.; Lipscomb, R. C.; Hullett, D. H.; Samaniego-Picota, M.; Grist, T. M.; Becker, B. N. *Am. J. Physiol. Renal. Physiol.* **2007**, *292*, F513.

(97) Bao, L.; Avshalumov, M. V.; Patel, J. C.; Lee, C. R.; Miller, E. W.; Chang, C. J.; Rice, M. E. *J. Neurosci.* **2009**, *29*, 9002.

(98) Dunford, B. H. *Heme Peroxidases*; John Wiley & Sons, Inc.: New York, NY, 1999.

(99) Setsukinai, K.; Urano, Y.; Kakinuma, K.; Majima, H. J.; Nagano, T. *J. Biol. Chem.* **2003**, *278*, 3170.

(100) Emrich, C. A.; Medintz, I. L.; Chu, W. K.; Mathies, R. A. *Anal. Chem.* **2007**, *79*, 7360.

(101) Holden, M. A.; Jung, S. Y.; Cremer, P. S. *Anal. Chem.* **2004**, *76*, 1838.

(102) Sista, R. S.; Eckhardt, A. E.; Srinivasan, V.; Pollack, M. G.; Palanki, S.; Pamula, V. K. *Lab Chip* **2008**, *8*, 2188.

(103) Christopher, G. F.; Anna, S. L. *J. Phys. D: Appl. Phys.* **2007**, *40*, R319.

(104) Nisisako, T.; Torii, T. *Lab Chip* **2008**, *8*, 287.

(105) Chang, Y. H.; Lee, G. B.; Huang, F. C.; Chen, Y. Y.; Lin, J. L. *Biomed. Microdev.* **2006**, *8*, 215.

(106) Shen, F.; Du, W. B.; Davydova, E. K.; Karymov, M. A.; Pandey, J.; Ismagilov, R. F. *Anal. Chem.* **2010**, *82*, 4606.

(107) Liu, R. H.; Yang, J. N.; Lenigk, R.; Bonanno, J.; Grodzinski, P. *Anal. Chem.* **2004**, *76*, 1824.

(108) Cady, N. C.; Stelick, S.; Kunnavakkam, M. V.; Batt, C. A. *Sens. Act. B Chem.* **2005**, *107*, 332.

(109) Batt, C. A. *Science* **2007**, *316*, 1579.

(110) Bourlet, T.; Signori-Schmuck, A.; Roche, L.; Icard, V.; Saoudin, H.; Trabaud, M. A.; Tardy, J. C.; Morand, P.; Pozzetto, B.; Ecochard, R.; Andre, P. *J. Clin. Microbiol.* **2011**, *49*, 292.

(111) Goluch, E. D.; Nam, J. M.; Georganopoulou, D. G.; Chiesl, T. N.; Shaikh, K. A.; Ryu, K. S.; Barron, A. E.; Mirkin, C. A.; Liu, C. *Lab Chip* **2006**, *6*, 1293.

(112) Douglas, E. S.; Hsiao, S. C.; Onoe, H.; Bertozzi, C. R.; Francis, M. B.; Mathies, R. A. *Lab Chip* **2009**, *9*, 2010.

(113) Beyor, N.; Seo, T. S.; Liu, P.; Mathies, R. A. *Biomed. Microdev.* **2008**, *10*, 909.

(114) Toriello, N. M.; Liu, C. N.; Blazej, R. G.; Thaitrong, N.; Mathies, R. A. *Anal. Chem.* **2007**, *79*, 8549.

(115) Stachowiak, T. B.; Rohr, T.; Hilder, E. F.; Peterson, D. S.; Yi, M.; Svec, F.; Frechet, J. M. *Electrophoresis* **2003**, *24*, 3689.

(116) Reedy, C. R.; Hagan, K. A.; Strachan, B. C.; Higginson, J. J.; Bienvenue, J. M.; Greenspoon, S. A.; Ferrance, J. P.; Landers, J. P. *Anal. Chem.* **2010**, *82*, 5669.

(117) Smith, R. L.; Demers, C. J.; Collins, S. D. *Microfluid. Nanofluid.* **2010**, *9*, 613.

(118) Yuen, P. K. *Lab Chip* **2008**, *8*, 1374.

(119) Grover, W. H.; Weng, Y. C.; Manalis, S. R. In *Eleventh Conference on Miniaturized Systems for Chemistry and Life Sciences (MicroTAS)* Paris, France, 2007.

(120) Jensen, E. C.; Zeng, Y.; Kim, J.; Mathies, R. A. *J. Assoc. Lab. Auto.* **2010**, *15*, 455.

(121) Chiesl, T. N.; Chu, W. K.; Stockton, A. M.; Amashukeli, X.; Grunthaner, F.; Mathies, R. A. *Anal. Chem.* **2009**, *81*, 2537.

(122) Grant, R. J.; Roberts, K.; Pointon, C.; Hodgson, C.; Womersley, L.; Jones, D. C.; Tang, E. *J. Biomol. Screen.* **2009**, *14*, 452.

(123) Stockton, A. M., University of California, 2010.

(124) Church, D.; Gregson, D.; Lloyd, T.; Klein, M.; Beckthold, B.; Laupland, K.; Gill, M. J. *J. Clin. Microbiol.* **2011**, *49*, 118.

(125) Li, Y.; Jortani, S. A.; Ramey-Hartung, B.; Hudson, E.; Lemieux, B.; Kong, H. *Clin. Chim. Acta.* **2011**, *412*, 79.

(126) Thaitrong, N.; Toriello, N. M.; Del Bueno, N.; Mathies, R. A. *Anal. Chem.* **2009**, *81*, 1371.

(127) Liu, P.; Li, X.; Greenspoon, S. A.; Scherer, J. R.; Mathies, R. A. *Lab Chip* **2011**, *11*, 1041.

(128) Toriello, N. M.; Douglas, E. S.; Thaitrong, N.; Hsiao, S. C.; Francis, M. B.; Bertozzi, C. R.; Mathies, R. A. *Proc. Natl. Acad. Sc.i U. S. A.* **2008**, *105*, 20173.

(129) Lloyd, C. M.; Hessel, E. M. *Nat. Rev. Immunol.* **2010**, *10*, 838.

(130) Schupbach, J. *Int. Arch. Allergy. Immunol.* **2003**, *132*, 196.

(131) St Ledger, K.; Agee, S. J.; Kasaian, M. T.; Forlow, S. B.; Durn, B. L.; Minyard, J.; Lu, Q. A.; Todd, J.; Vesterqvist, O.; Burczynski, M. E. *J. Immunol. Methods.* **2009**, *350*, 161.

(132) Todd, J.; Freese, B.; Lu, A.; Held, D.; Morey, J.; Livingston, R.; Goix, P. *Clin. Chem.* **2007**, *53*, 1990.

(133) Rhee, M.; Burns, M. A. *Lab Chip* **2009**, *9*, 3131.